TECHNICAL REPORT

ISO/ASTM TR 52905

First edition
2023-06

Additive manufacturing of metals — Non-destructive testing and evaluation — Defect detection in parts

Fabrication additive de métaux — Essais et évaluation non destructifs — Détection de défauts dans les pièces

Reference number
ISO/ASTM TR 52905:2023(E)

ISO copyright office
CP 401 • Ch. de Blandonnet 8
CH-1214 Vernier, Geneva
Phone: +41 22 749 01 11

Email: copyright@iso.org
Website: www.iso.org

ASTM International
100 Barr Harbor Drive, PO Box C700
West Conshohocken, PA 19428-2959, USA
Phone: +610 832 9634
Fax: +610 832 9635
Email: khooper@astm.org
Website: www.astm.org

Published in Switzerland

Contents

Page

Foreword

ISO (the International Organization for Standardization) is a worldwide federation of national standards bodies (ISO member bodies). The work of preparing International Standards is normally carried out through ISO technical committees. Each member body interested in a subject for which a technical committee has been established has the right to be represented on that committee. International organizations, governmental and non-governmental, in liaison with ISO, also take part in the work. ISO collaborates closely with the International Electrotechnical Commission (IEC) on all matters of electrotechnical standardization.

The procedures used to develop this document and those intended for its further maintenance are described in the ISO/IEC Directives, Part 1. In particular, the different approval criteria needed for the different types of ISO documents should be noted. This document was drafted in accordance with the editorial rules of the ISO/IEC Directives, Part 2 (see www.iso.org/directives).

Attention is drawn to the possibility that some of the elements of this document may be the subject of patent rights. ISO shall not be held responsible for identifying any or all such patent rights. Details of any patent rights identified during the development of the document will be in the Introduction and/or on the ISO list of patent declarations received (see www.iso.org/patents).

Any trade name used in this document is information given for the convenience of users and does not constitute an endorsement.

For an explanation of the voluntary nature of standards, the meaning of ISO specific terms and expressions related to conformity assessment, as well as information about ISO's adherence to the World Trade Organization (WTO) principles in the Technical Barriers to Trade (TBT), see www.iso.org/iso/foreword.html.

The committee responsible for this document is ISO/TC 261, *Additive manufacturing*, in cooperation with ASTM Committee F42, *Additive manufacturing technologies*, on the basis of a partnership agreement between ISO and ASTM International with the aim to create a common set of ISO/ASTM standards on additive manufacturing, in collaboration with the European Committee for Standardization (CEN) Technical Committee CEN/TC 438, *Additive manufacturing,* in accordance with the Agreement on technical cooperation between ISO and CEN (Vienna Agreement).

Any feedback or questions on this document should be directed to the user's national standards body. A complete listing of these bodies can be found at www.iso.org/members.html.

Introduction

In response to the urgent need for standards for Additive Manufacturing (AM), this document initially indicates Non-Destructive Testing (NDT) methods with potential to detect defects and determine residual strain distribution that are generated in AM processes. A number of these methods were verified. The strategy adopted was to review existing NDT standards for matured manufacturing processes which are similar to AM, namely casting and welding. This potentially reduces the number of standards required to comprehensively cover the defects in AM. For identified AM unique defects, this document proposes a two-level NDT approach: a star artefact as an Initial Quality Indicator (IQI) and *à la carte* artefact where an example shows the specific steps to follow for the very specific unique AM part to be built, paving the way for a structured and comprehensive framework.

Most metal inspection methods in NDT use ultrasound or X-rays, but these techniques cannot always cope with the complicated shapes typically produced by AM. In most circumstances X-ray computed tomography (CT) is a more suitable method, but it also has limitations and room for improvement or adaptation to AM, on top of being a costly method both in time and money.

This document includes post-process non-destructive testing of additive manufacturing (AM) of metallic parts with a comprehensive approach. It covers several sectors and a similar framework can be applied to other materials (e.g. ceramics, polymers, etc.). In-process NDT and metrology standards are referenced as they are being developed. This document presents current standards capability to detect which of the Additive Manufacturing (AM) flaw types and which flaws require new standards, using a standard selection tool. NDT methods with the highest potential will be tested.

Additive manufacturing of metals — Non-destructive testing and evaluation — Defect detection in parts

1 Scope

This document categorises additive manufacturing (AM) defects in DED and PBF laser and electron beam category of processes, provides a review of relevant current NDT standards, details NDT methods that are specific to AM and complex 3D geometries and outlines existing non-destructive testing techniques that are applicable to some AM types of defects.

This document is aimed at users and producers of AM processes and it applies, in particular, to the following:

— safety critical AM applications;

— assured confidence in AM;

— reverse engineered products manufactured by AM;

— test bodies wishing to compare requested and actual geometries.

2 Normative references

The following documents are referred to in the text in such a way that some or all of their content constitutes requirements of this document. For dated references, only the edition cited applies. For undated references, the latest edition of the referenced document (including any amendments) applies.

ISO 11484, *Steel products — Employer's qualification system for non-destructive testing (NDT) personnel*

ISO/ASTM 52900, *Additive manufacturing — General principles — Fundamentals and vocabulary*

ASTM E1316, *Terminology for Nondestructive Testing*

EN 1330-2, *Non-destructive testing — Terminology — Part 2: Terms common to the non-destructive testing methods*

3 Terms and definitions

For the purposes of this document, the terms and definitions given in ISO/ASTM 52900, ASTM E1316, EN 1330-2, ISO 11484, and the following apply.

ISO and IEC maintain terminological databases for use in standardization at the following addresses:

— ISO Online browsing platform: available at https://www.iso.org/obp

— IEC Electropedia: available at https://www.electropedia.org/

3.1
flaw type
identifiable features that defines a specific flaw

Note 1 to entry: defect term, this word is used when a flaw that does not meet specified acceptance criteria and is rejectable.

Note 2 to entry: Flaw term, an imperfection or discontinuity that is not necessarily rejectable

3.2
lack of fusion
LOF
type of process-induced porosity, in which the powder or wire feedstock is not fully melted or fused onto the previously deposited substrate

Note 1 to entry: In PBF, this type of flaw can be an empty cavity, or contain unmelted or partially fused powder, referred to as unconsolidated powder.

Note 2 to entry: LOF typically occurs in the bulk, making its detection difficult.

Note 3 to entry: Like voids, LOF can occur on the build layer plane (layer/horizontal LOF) or across multiple build layers (cross layer/vertical LOF).

3.3
unconsolidated powder
unmelted powder that due to process failure was not melted and became trapped internally

3.4
layer shift
<E beam> when it is disturbed by a magnetic field a layer or a number of layers are shifted away from the other build layers

Note 1 to entry: see stop/start for PBF laser/E beam.

3.5
trapped powder
unmelted powder that is not intended for the part but is trapped within internal part cavities

3.6
porosity
presence of small voids in a part making it less than fully dense

Note 1 to entry: Porosity may be quantified as a ratio, expressed as a percentage of the volume of voids to the total volume of the part.

[SOURCE: ISO/ASTM 52900:2019, 3.11.8]

4 NDT potential for authentication and/or identification

Some of the NDT methods in this technical report have the additional potential to extract authentication and/or identification apparatus or design embedded in the design of the AM part. Such a potential clearly depends on the material(s), geometry and process selected to fabricate the part, however the design information and AM data file can embed in its geometry or texture ad-hoc devices that potentially could be extracted by NDT techniques. ISO/TC 292 specifies and maintains a number of standards supporting such devices within the ISO referential, and are fully applicable to AM digital information. The specific requirements of design techniques, materials, processes, NDT modalities and applications, however, still require careful evaluation, selection and classification.

5 List of abbreviated terms

AM	additive manufacturing
BAE	British Aerospace and Engineering Systems
EB-PBF	electron beam powder bed fusion
ESFR	European Synchrotron Research Facility
EWI	Edison Welding Institute
FMC	full matrix capture
GE-PD	general electric powder division
HZB	Helmholtz Zentrum Berlin
ILL	Institute Laue-Langevin
IR	infrared
IRT	infrared thermography
J & J	Johnson & Johnson
LNE	laboratoire national de métrologie et d'essais
PBF-LB	laser powder bed fusion
DED-LB	laser directed energy deposition
MTC	The Manufacturing Technology Centre
ND	neutron diffraction
NDE	non-destructive evaluation
NDT	non-destructive testing
NI	neutron Imaging
NIST	National Institute of Standards and Technology
NLA	non-linear acoustic testing
NLR	non-linear resonance testing
PAUT	phase array ultrasound testing
PCRT	process compensated resonance testing
PT	pulse thermography
RAM	resonance acoustic method
ROI	Region of interest
SX	X-ray synchrotron
SHT	step heating thermography

TFM	total focusing method
TMS	the modal shop
UoB	university of bath
XCT	X-ray computed tomography

6 Typical flaws/defects in AM

6.1 Flaw origins/causes

The causes of defects across different types of AM processes can be quite different, but the defects that they generate can be remarkably similar. Detecting the defects also does not depend on the cause, and in general only the size and geometry (and potentially morphology) of the defect matters for detection.

The causes and effects of a number of AM flaws have been reported in the European project AMAZE[21]. Table A.1 and Table A.2 give explanations of the mechanisms by which these flaws are generated and those mechanisms are linked to the process parameters selected and the resulting processing conditions, see ISO 11484. Understanding the conditions under which flaws are generated and simplifying the terminology used to describe these flaws will aid the drive for quality improvement required for widespread implementation of the technology.

The flowchart displayed in Figure 1 gives an idea of the complexity of flaw generation within the PBF process. As can be seen, the generation of one flaw type can result in an anomalous processing condition, which in turn generates a second flaw. For example, the presence of a thick layer or low laser (or electron beam) power can lead to under-melting, which in turn can lead to unconsolidated powder. Coupled with the tendency of the power source to decrease the surface energy of unconsolidated powder under the action of surface tension, ensuing ball formation may arise due to shrinkage and worsened wetting, leading to pitting, an uneven build surface, or an increase in surface roughness; see EN 1330-2.

Therefore, even when there are multiple causes, a single flaw type or conditions can be generated (excessive surface roughness) causing failure by a single failure mode (surface cracking leading to reduced fatigue properties). Alternatively, it is also conceivable that a single flaw type or condition can cause failure by several different failure modes.

6.2 Flaw/defects classification

Post-built AM flaws have been identified based on a report from the FP7 European AMAZE project. Potential flaws in directed energy deposition (DED) and powder bed fusion (PBF) are listed in Table 1 and Table 2 respectively. A brief description for each flaw type is also given in the tables.

Due to the similarity in manufacturing, defects from welding and casting bear some resemblance to defects from AM processes such as PBF and DED. Defects in post-built PBF and DED parts are identified and listed in EN 1330-2, ASTM E1316 and References [22]. As noted in Table 1 and Table 2, both technologies have common defects such as porosity, inclusions, undercuts, geometry, LOF, and a rough surface texture. However, the mechanisms for PBF and DED defect generation are very different, and more importantly, the relative abundance of each defect type will be very different due to the melting and solidification mechanisms involved (and the significantly higher thermal gradients present in DED). DED involves imparting a momentum into the melt pool rather than melting the powder that is already present. The important difference between the two methods is that of timescales.

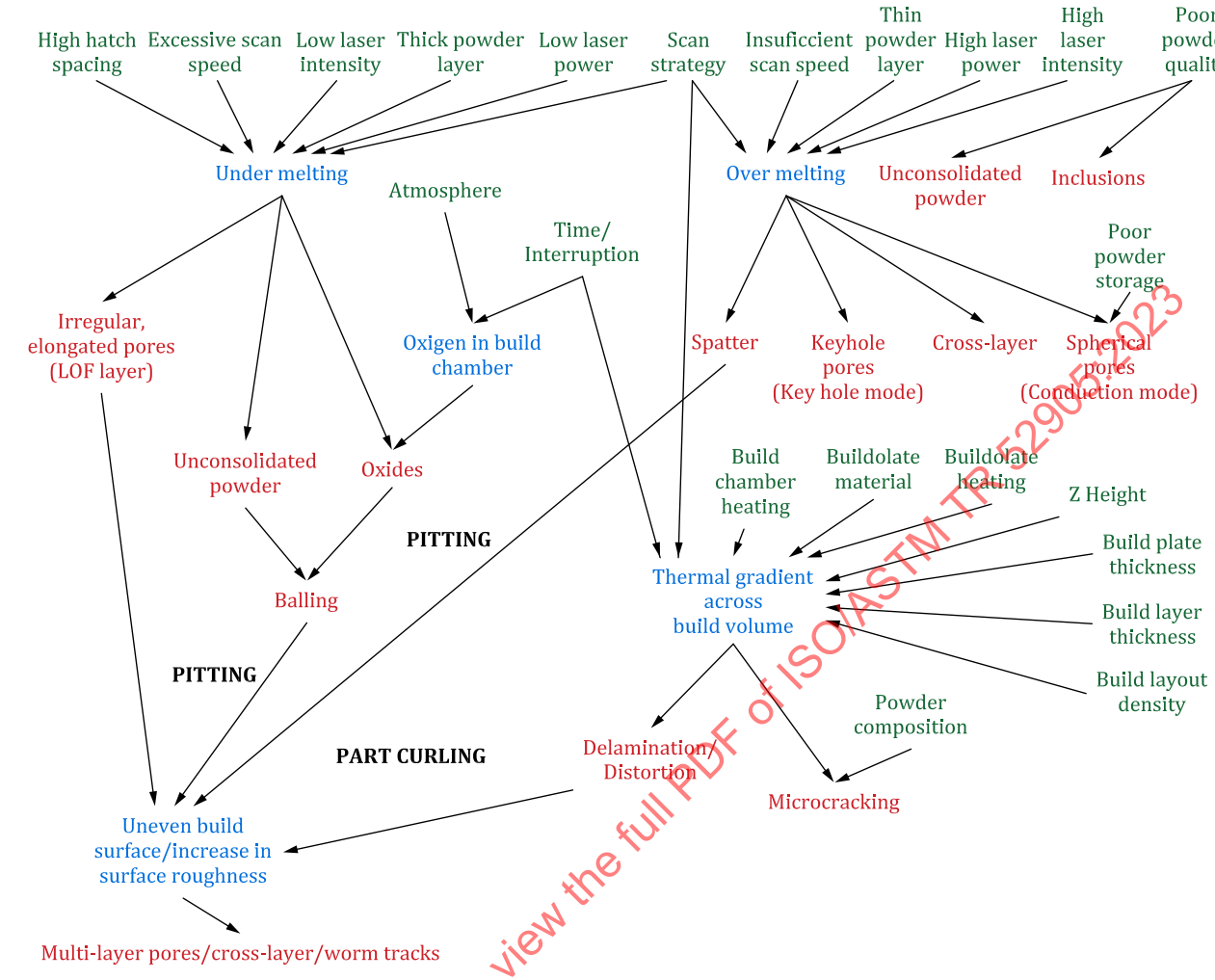

Figure 1 — Causes, mode of failures and defect formation in PBF AM (see ISO/ASTM 52900)

In PBF there is a balance of timescales between melting and re-solidification. If the melt rate is too low, then the melt pool can become unstable and break into multiple pools. If the melt rate is too high, powder partially melts in front of the melt pool, which can cause defects or heat affected zones. In DED, this balance is not relevant, but the powder (or wire) that is fed into the melt pool can melt sufficiently quickly. The issue of adding cold material (with a given momentum) to a melt pool is not well understood, but has a large effect on the Marangoni convection direction and thermal gradients present. It is likely that the melt pool depth will be much shallower (which may reduce powder surrounding the melt pool) and that the thermal gradients less severe (which cause a flatter melt pool), though this depends on the wetting between substrate (which has no surrounding powder) and the melt pool. This difference in the melt pool dynamics impacts its shape.

This has two important consequences, grain growth and bubble dynamics. Internal defects are attributable to cracking, pores, or lack of material. Cracking has many causes, but is generally related to the grain boundary (apart from solidification cracking). Note that the issue of “spattering” that is

believed to be prominent in DED (or indeed welding) is still a significant issue in PBF. For L-PBF the issue is that of ablation at the surface of the melt pool caused by the large thermal gradients. For EB-PBF the problem occurs from two mechanisms; ablation and charging of the powder.

Table 1 — Typical flaws in directed energy deposition

Flaw type	Description
Poor surface finish	The surface roughness on the part does not meet the target specification for the part. Measurement of the surface roughness is considered out-of-scope for NDT however, visual examination can be included. 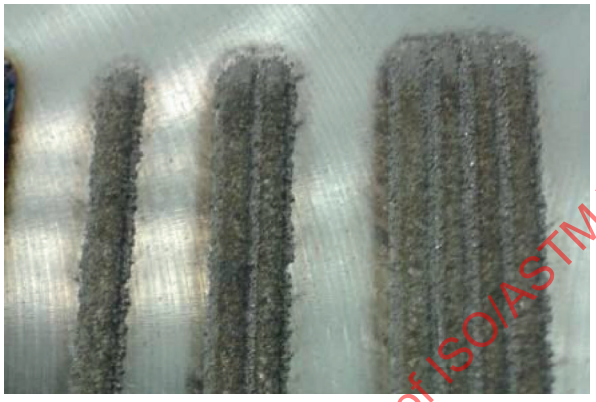
Porosity	Typically spherical in shape and contains gas. Porosities can grow in a line to form a chain or elongated porosity. 
Incomplete fusion	Fusion between the entire base metal surfaces and between adjoining welds are not complete. This occurs when new material has been used and the build parameters have not been optimised. Typically, this flaw is eliminated as the process improved when all parameters have been optimised. 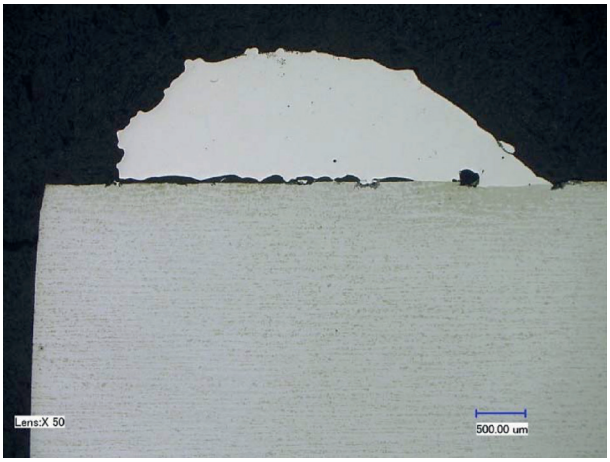
Undercuts at the toe of the welds between adjoining weld beads	A groove melted into the base metal adjacent to the weld toe or weld face and left unfilled by weld metal.

Table 1 *(continued)*

Flaw type	Description
Non-uniform weld bead and fusion characteristic	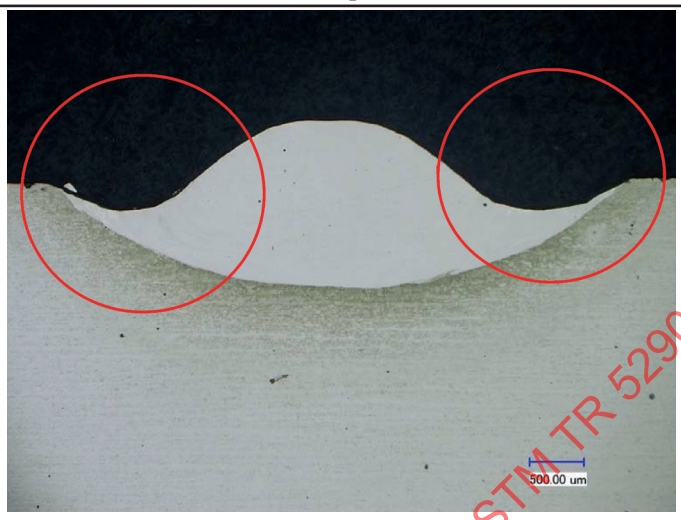 These indicate errors in the process which can risk integrity of the build. Internal flaws caused by this can be void, porosity, or incomplete fusion.
Hole or void	Typically occurs internally in the built part as shown in the micrograph below. It is difficult to detect by physical examination of the part. 
Non-metallic inclusions	Inclusions can come from the powder or the wire feedstock. Some inclusions are intentionally added to the powder to improve the process (e.g. for oxidation) but they could also be caused by contaminates in the process.
Cracking	Cracking can develop from internal holes or voids which then grows to the external surface. 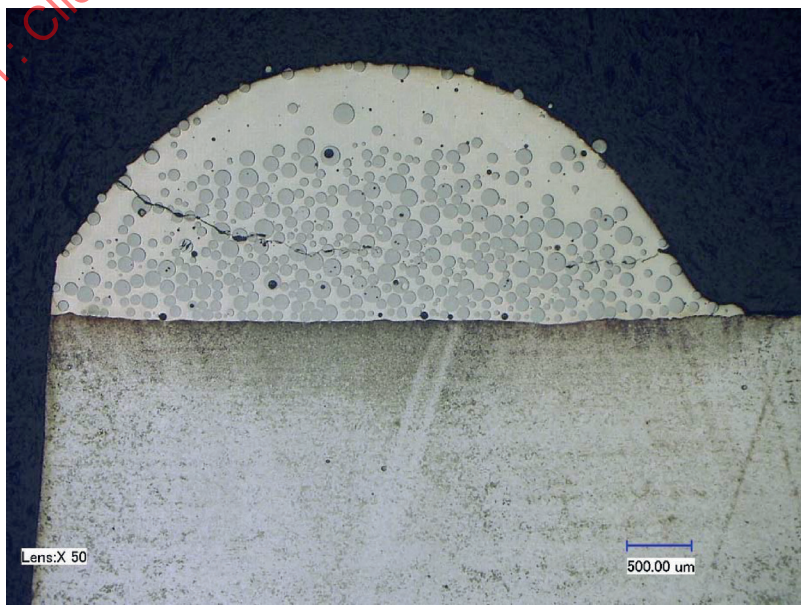
Lack of geometrical accuracy/steps in the part	Variation of the part dimension from the CAD model will not be currently part of the review. Nevertheless, steps and gross variation which can be detected by visual examination are included.

Table 2 — Typical flaws in powder bed fusion

Flaw type	Description
Unconsolidated powder	Unconsolidated powder leading to porosity or voids. The morphology is different to gas generated pores, but the geometry and size are not dissimilar. The image below is an example taken from RASCAL project. 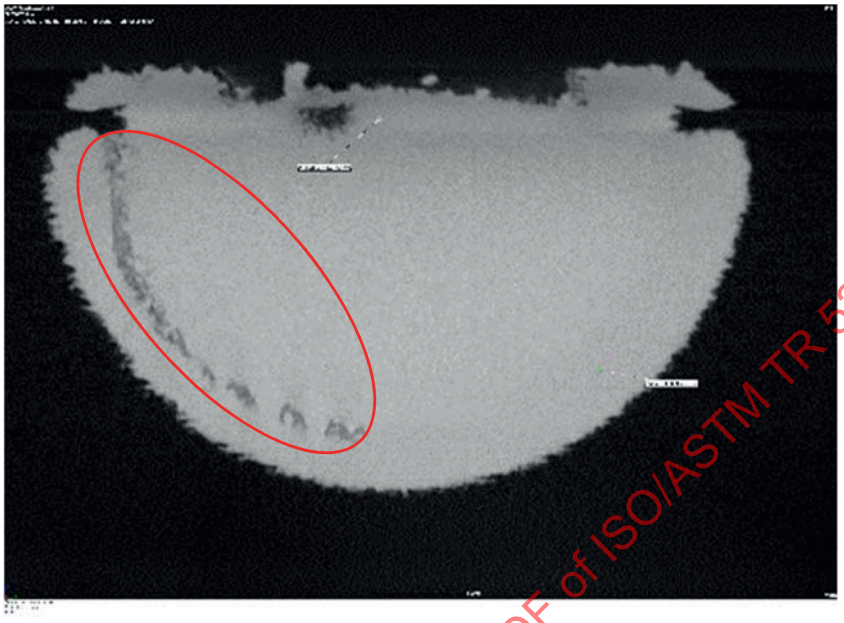
Trapped powder	Unmelted powder that is not intended for the part is trapped within part cavities. 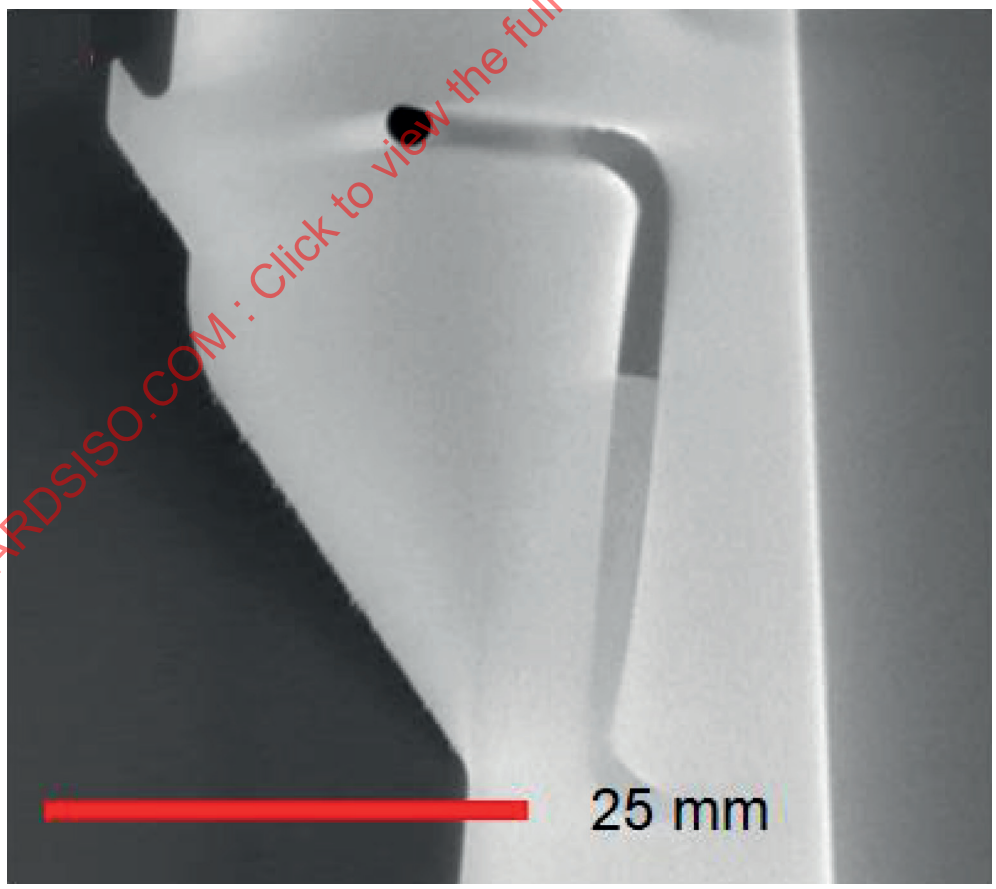
Layer defect (Horizontal lack of fusion)	Void or porosity with or without unconsolidated powder that grows on the build layer plane in a connected or semi-connected manner. The image below is a vertical slice of an X-ray computed tomography scan.

Table 2 *(continued)*

Flaw type	Description
	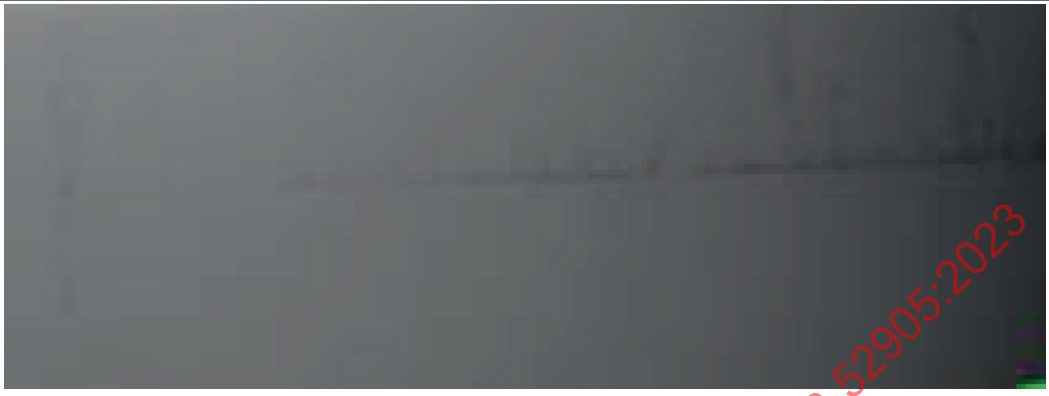
Cross layer (Vertical lack of fusion)	Void or porosity with or without unconsolidated powder that grows along the build axis in a connected or semi-connected manner. The images below show vertical and horizontal slices from an X-ray computed tomography scan. Vertical slice view. 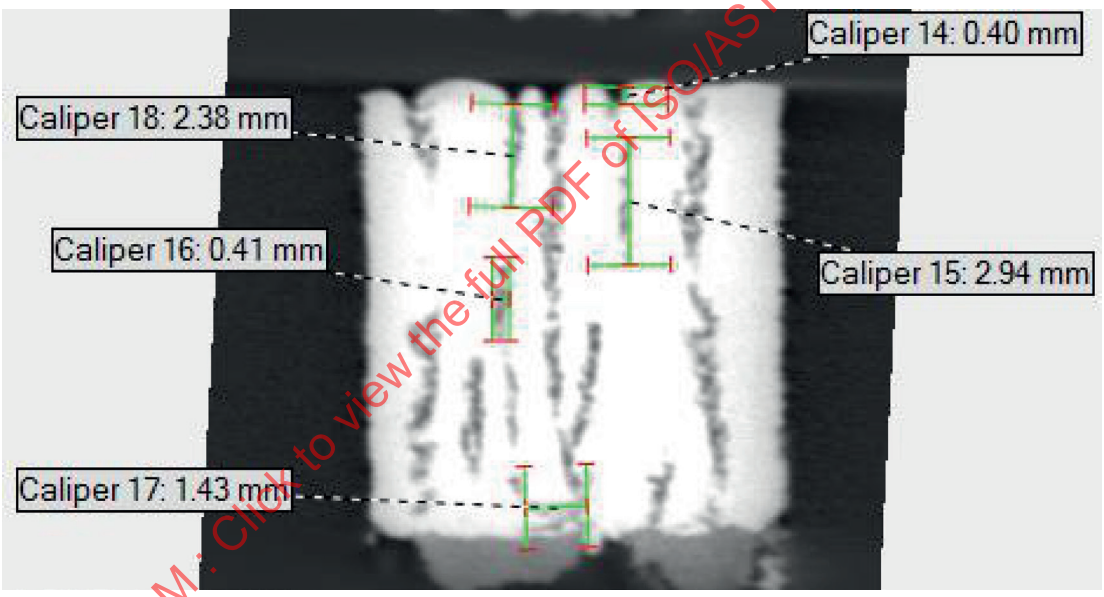
	Top slice view.

Table 2 *(continued)*

Flaw type	Description
	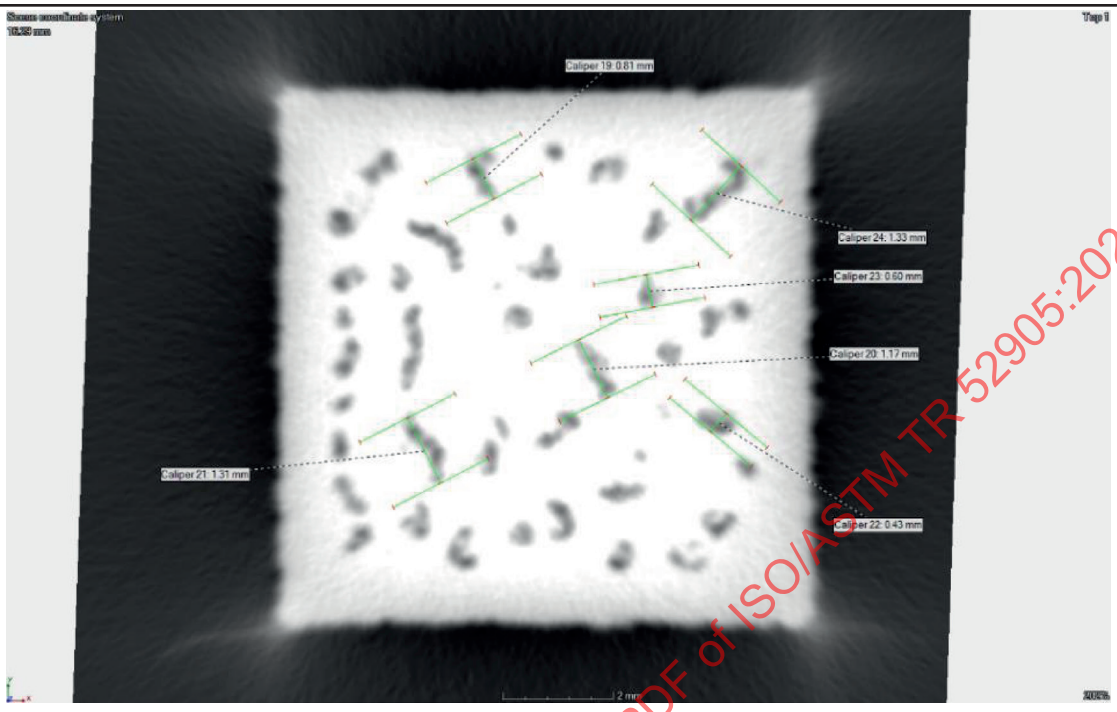
Porosity	Typically spherical in shape and contains gas. Porosities can grow in a line to form a chain or elongated porosity. The image below is a horizontal slice of an X-ray computed tomography scan. 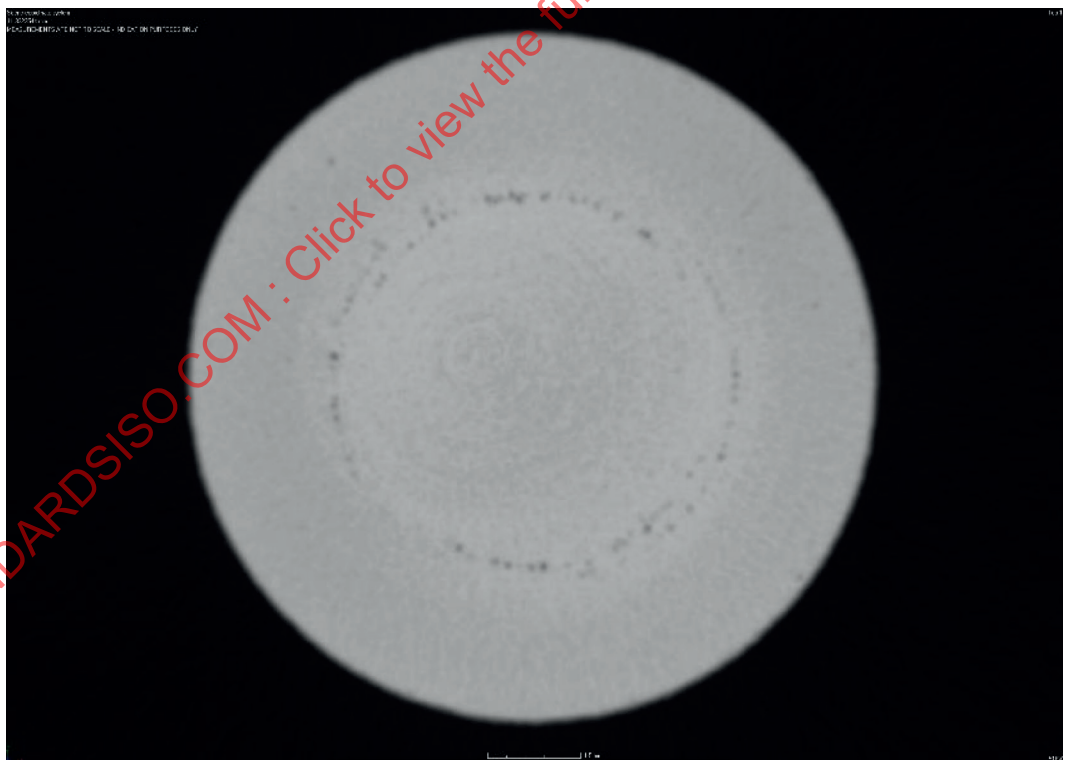
Poor surface finish	The surface roughness on the part does not meet the specification. For example, the surface roughness is higher than acceptable limit[24].

Table 2 *(continued)*

Flaw type	Description
	P = 50 W, V = 200 m/s 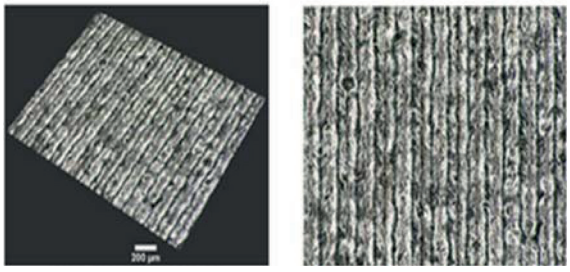 P = 195 W, v= 1 200 m/s 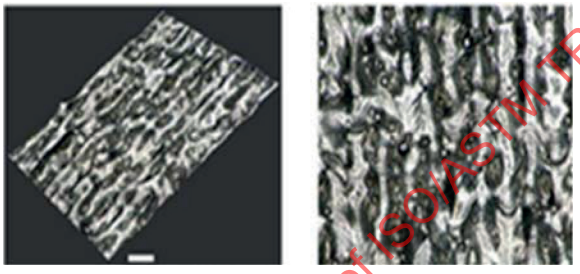
Layer shift/ lack of geometrical accuracy/ steps in the part	Variation of the part dimension from the CAD model will not be currently part of the review. Nevertheless, steps and gross variation which can be detected by visual examination are included.
Reduced mechanical properties	A certain region of the part has different mechanical properties to the rest of the part.
Inclusions	Inclusions can come from the contaminants in the powder. The image below is an XCT image of an inclusion taken from project AMAZE 2. 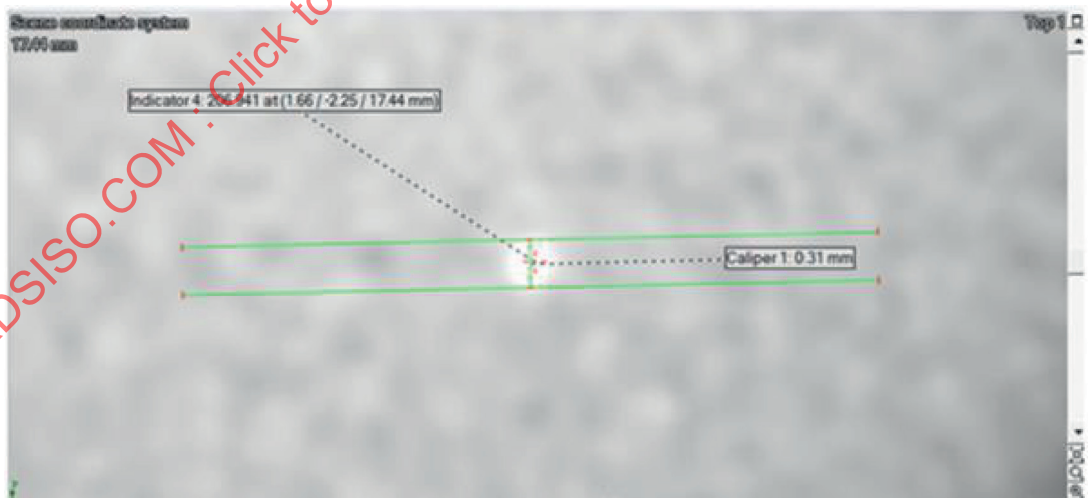
Void	Flaws created during the build process that are empty pockets or filled with partially or wholly un-sintered powder, or partially or wholly un-fused wire. These pockets can exist in a variety of shapes and sizes. The image below is a horizontal slice of an X-ray computed tomography scan.

Table 2 *(continued)*

Flaw type	Description
	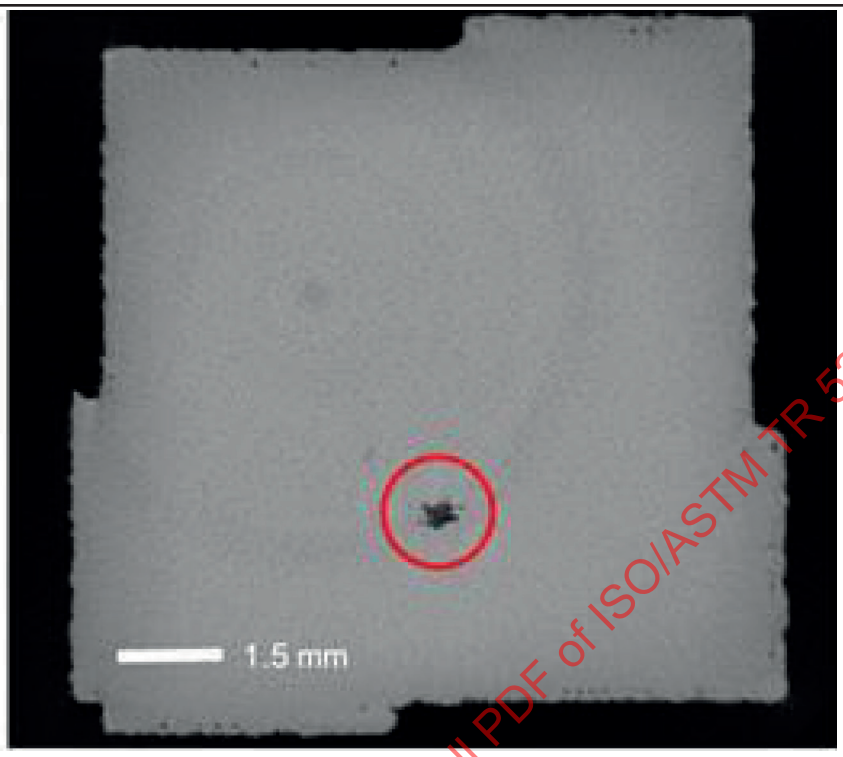

6.3 Defect classification strategies for AM

As pointed out in ISO 11484 and Reference [25], there are longstanding NDE standard defect classes for conventionally manufactured cast, wrought, forged, and welded production parts. The defects produced by these conventional processes will generally not be similar to those produced by AM processes. In addition, the NDE signal attenuation characteristics in AM parts may differ from those in conventional parts. Therefore, legacy physical reference standards and NDE procedures can be used with caution when inspecting AM parts[25]. This implies that until an accepted AM defect classification and associated NDE detection limits for technologically relevant AM defects are established, the NDE methods and acceptance criteria used for AM parts will remain part specific to design point. Variation of AM process parameters and disruptions during build may induce a variety of defects (anomalies) in AM parts that can be detected, sized, and located by NDE, see ISO/ASTM 52900.

In addition to defect classification strategies based on NDE detection limits for technologically relevant defects, or acceptance criteria for the minimum allowable defect sizes, a classification strategy based on the physical attributes possessed by defects is also possible and, perhaps, is more intuitive. For example, defect morphology, orientation, size, and location have been found to be useful attributes for classifying defects. Together, physical defect attributes such as morphology, orientation, size, and location provide a powerful framework for classifying defects and can be used to complement defect classification strategies delimited by NDE capability (minimum detectable flaw size) or acceptance criteria (critical initial flaw size). Ultimately, the goal is to determine which of the physical defect attribute(s) play a prominent role in influencing properties and performance.

Further refinement of NDE is possible by looking at still other physical defect attributes related to morphology, orientation, size and location. For example, in Reference [30], tensile tests on 17-4 PH stainless steel AM dogbones were carried out to show effect of defects on its mechanical properties. The results revealed that the number of defects exhibited the strongest correlation to yield strength compared to the other attributes. In addition to the defect attributes of morphology, orientation, size, and location discussed above, the selection of an appropriate NDE method is governed by a range of practical and material considerations[21][22]. Practical considerations include

a) special equipment and/or facilities requirements,

b) cost of examination,

c) personnel and facilities qualification,

d) geometrical complexity of the part,

e) part size and accessibility of the inspection surface or volume relative to NDE used (for example the ability to detect embedded flaws), and

f) process history and post-processing (see ASTM E3166).

While application of conventional NDE techniques is possible for AM parts with simple geometries, topology optimized AM parts with more complex geometries require specialized NDE techniques. The ability of each technique to detect different types of defects, as well as to locate them in the interior or exterior surface of a part is listed. Finally, the NDE techniques are further characterized by the ability to globally screen or detect and locate a defect.

7 NDT standards review

7.1 Post-process NDT standards

In DED, material is fused together by melting as it is being deposited. DED processes are primarily used to add features to an existing structure or to repair damaged or worn parts. DED has many variants of processes. The material deposited can be either powder or wire based. The heat source can be a laser, electron beam, electric arc among others. DED processes have similarities to welding processes, and consequently the flaws generated in DED are expected to be similar to the flaws generated in welding. For this reason, the NDT standards for welding have been used in the review.

In PBF, powder is deposited onto a build platform bed and selectively fused using a localized energy source (typically electron or laser beam) to form a section through the component. The build platform is then lowered and the process is repeated until the part is produced. Unlike DED, PBF processes do not have similarities to welding. However, there are flaws generated in PBF such as voids and porosity that have some similarities to welding flaws. Therefore, the review of NDT standards for welding is still relevant to PBF. In addition to welding, some common casting flaws, gas porosity, cracking and inclusion, are similar to DED and PBF flaws. For this reason, NDT standards for castings have also been reviewed and their applicability to AM flaws is assessed.

7.1.1 ISO review

7.1.1.1 Welding standards

The NDT standards for welding comprise of a number of standards that cover different aspects of inspection in welding. This is described by the tree diagrams in ISO 17635:2016, Figure B.1. The welding quality standards are specified in ISO 5817 and ISO 10042. These standards feed into ISO 17635 which is an interface between the quality levels and the acceptance levels for indications. This standard also describes the NDT method selection process, which splits into six method-specific standards. These are radiographic, eddy current, magnetic particle, penetrant, ultrasonic and visual examination. At this stage, an NDT method has been decided, and a corresponding standard describes the test procedure and the characterisation acceptance levels. Each method has its own limitations and it is possible that, for a given component or a target flaw, a combination of different methods is required.

The method standards are only available for conventional NDT. For radiography and ultrasonic, there are more sub-method standards as shown in ISO 17635:2016, Figures B.2 and B.3. NDT standards for more advanced NDT methods are not available; for example, ultrasonic phased array, X-ray computed tomography, and thermography. It is possible that these methods are not widely accepted and used by NDT operators within the welding industry. However for AM, there are opportunities for new standards to be developed for the advanced methods.

7.1.1.2 Casting standards

The NDT standards for casting have a simpler structure to those for welding. ISO 4990 categorises casting flaws into surface discontinuities and internal discontinuities. There are standards for five main conventional NDT methods. Each method is either for surface or internal discontinuities. The five NDT methods are:

1) Visual examination ISO 11971 (surface)

2) Magnetic Particle Inspection ISO 4986 (surface)

3) Liquid Particle Inspection ISO 4987 (surface)

4) Ultrasonic examination ISO 4992 (internal) — Part 1 (general purposes) and Part 2 (highly stressed components)

5) Radiographic testing ISO 4993 (internal)

Similar to welding, there is no standard available for advanced NDT methods for castings such as X-ray computed tomography, phased array ultrasonic and thermography. These methods are not regarded as standard methods in castings, although they could have been used following company specific internal standards or procedures. Castings typically have simpler geometry compared to AM and welding. Some NDT methods might not be suitable e.g. ultrasonic. Additionally, surface roughness for castings is typically better than as-built AM components.

7.1.1.3 Welding and casting standards applicable to AM flaws

The summary of the review of current standards for welding and casting (see Table B.1) is shown in Table 3. Flaws that would be covered by other types of inspection e.g. dimensional measurement or material characterisation are categorised as 'non-NDT'. All flaws listed in the table for DED are generally covered by current NDT standards, except for the non-NDT ones. For PBF, seven flaws are not covered by current NDT standards. Three of these are non-NDT, and four are flaws unique to AM (unconsolidated powder, layer, cross layer, and trapped powder). The unique flaws require new NDT recommendations which will be addressed in this document. It will also refer to newly developed standards in other sectors such as aerospace.

As shown in Table 3, the following are the identified flaws unique to AM (PBF only) which require new standards:

— Layer;

— Cross layer;

— Trapped powder;

— Unconsolidated powder;

Table 3 — Classification of directed energy deposition and powder bed fusion flaws (Flaws unique to additive manufacturing are in bold)

	Flaw type	Non-NDT	Common in DED & PBF	Covered by current standards	Unique to AM
DED	Poor surface finish		■		
	Porosity		■	■	
	Incomplete fusion			■	
	Lack of geometrical accuracy/steps in part		■		
	Undercuts			■	
	Non-uniform weld bead and fusion characteristic			■	
	Hole or void		■	■	
	Non-metallic inclusions		■	■	
	Cracking		■	■	
PBF	**Unconsolidated powder**				■
	Lack of geometrical accuracy/steps in part		■		
	Reduced mechanical properties				
	Inclusions			■	
	Void		■	■	
	Layer				■
	Cross layer				■
	Porosity		■	■	
	Poor surface finish		■		
	Trapped powder				■

7.2 In-process NDT review

Conventional NDE methods such as X-ray, UT, EC, have been used for post build inspection of Additive manufacturing (AM) components. Due to the limited number of studies available and the technical constraints, the capability of these NDE techniques is limited, indicating a technical gap[21][27]. It is foreseen that in-process monitoring can be used to improve control of the process to minimise quality issues. In addition, in-process inspection has the added ability to inspect the part as it is built, which for some very complex AM parts may be the only NDE capable solution.

AM processes offer freedom over other manufacturing methods, such as the integration of multiple parts, which generally increase their geometry complexity. In order for an AM process to be successful, the product quality can first be ensured. Typically, quality inspections are performed after the build of

the full part, which becomes difficult for complex geometries. Taking advantage of the unique layer-by-layer build method, an ideal place to verify the part quality is after a layer or number of layers, with the potential advantage to reduce or eliminate the need to inspect after the full build.

Current AM in-process monitoring relies mainly on surface measurements, potentially missing subsurface defects. LPBF and DED AM processes work at elevated temperatures; therefore, non-contact methods are required.

In powder bed fusion processes, problems with layer-wise coatings and untimely laser melting can lead to porosity, stress and further variations in the built part, or of material properties. Therefore, it is important to not only perform measurements to inspect the finished build, but also to monitor in-process and ultimately implement an efficient feedback system that could compensate time dependent setup deficits, for example decreasing of laser input due to aging/soot pollution or similar effects.

A study that was carried out to map the NDE technologies available for inspection in-situ is reported and discussed in detail by References [22][28]. Also, References [29][30] addressed the matters inside the NDE inspection methodologies compatible with AM process. The topics addressed during this review were:

— optical control methods;

— coating control system;

— in-process control methods;

Only the in-process control methods were covered which involved NDT techniques. The methods reviewed were XCT, Thermography, Laser ultrasonic, Eddy currents, Neutron characterisation, Acoustic emission and X-ray Backscattered. It was concluded that these less conventional inspection methods offer many possibilities for in-situ inspection of AM processes. Cracks have been successfully detected using Ultrasonic, Laser ultrasonic, thermography and X-ray backscatter methods. In particular, X-ray backscatter inspection is not limited by surface finish and, therefore, would be particularly suitable. Residual stress/strain has been identified using neutron beam diffraction.

Infrared thermography not only monitors the melt pool emissions but also enables the user to detect temperature distributions in the powder bed or of the built parts during the build process. Heat distribution variations indicative of process anomalies can be included in error evaluation and, in addition, the measurement of temperatures allows to correlate the measured data to metallurgic properties and therefore to intrinsic material characteristics.

Laser scanning or laser profiling allows closed loop control of Wire DED build height but could also be used in the scanning of powder beds for defects. Laser ultrasound (LU) is another technique which may be used to inspect AM parts. Laser ultrasonic testing is a non-contact inspection technique with potential for in-process defect monitoring of AM processes. It uses lasers to both generate and detect ultrasonic waves which can be used for defect detection, materials characterisation and thickness determination. A pulsed laser is used to generate an ultrasonic wave and a continuous-wave laser interferometer detects the small surface displacement when the waves arrive at the detection point.

LU is capable of working at elevated temperatures of at around 1000 °C, and some systems are capable to work on rough surface samples which are expected to be in AM built parts. LU generates both surface and bulk waves at the same time; therefore, allowing inspection of surface, close to surface and bulk of material. Additionally, surface wave penetration depth can be optimized remotely depending on the process.

LU has shown good capability to detect laser machined notches with dimensions as small as 50 µm × 75 µm × 50 µm (L × D × W) on DED samples as built, that is without any post build surface finishing. The method can be used on curved or difficult to access areas and is capable to work at elevated temperatures, therefore is suitable for Laser-PBF and DED AM processes (Figure 2 and Figure 3)[31].

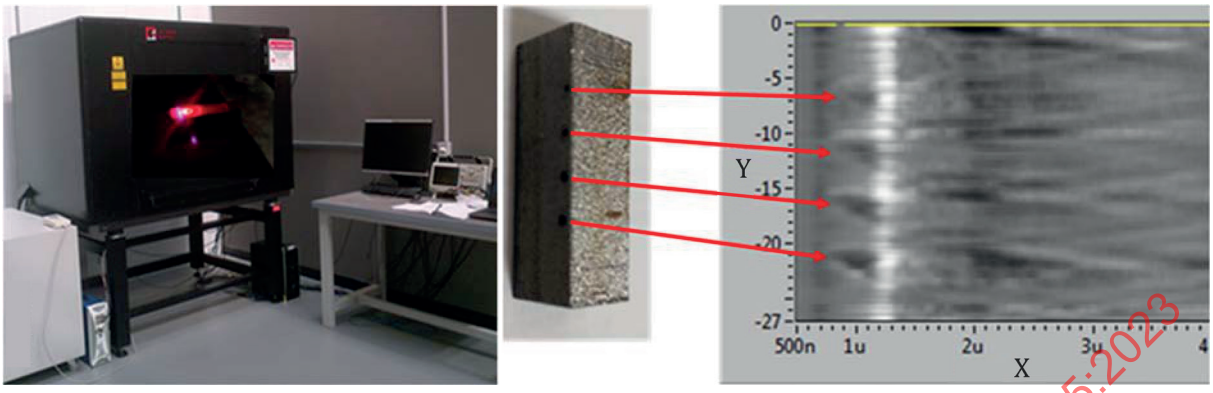

Figure 2 — LU system (left); and L-PBF sample calibration sample with B-Scan results identifying detected features (right)

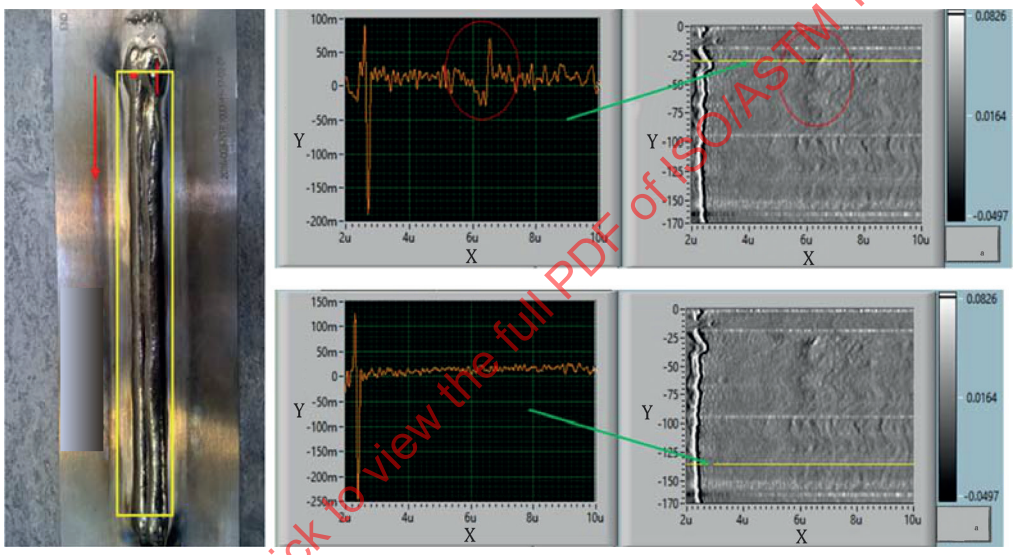

Figure 3 — Photograph of DED sample with scan details (left); A-Scans (centre); and B-Scans showing an area with LOF (right)

Figure 4 summarises the review carried out for NDE technologies applicable for in-situ monitoring and inspection for AM parts. This diagram shows that optical methods are the easiest and capable ones for the in-process monitoring and inspection methods attempted to scope. Nevertheless, other methods such as LU and X-ray based potentially would have better results but integration and development are more complex. A more comprehensive review can be found in ASTM WK73289.

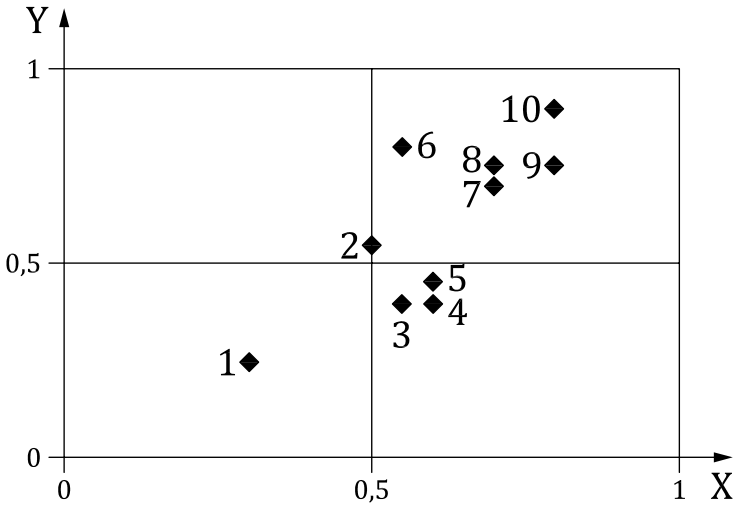

Key

X capability
Y difficulty
1 power meter/laser profiler
2 contact ultrasound (PA)
3 surface scanner
4 optical vision
5 IR/thermography
6 X-ray diffraction
7 laser ultrasound
8 X-ray
9 X-ray backscatter
10 X-ray CT

Figure 4 — Quadrant diagram of in-situ monitoring and inspection technologies relative capability vs difficulty to integrate/use

8 Standard selection structure for AM

Based on the review of the current standards, a new structure for NDT standards for AM is proposed as shown in Figure 5. This structure is built on the current welding standards structure shown by the light boxes. The required development of new standards is shown by the dark boxes.

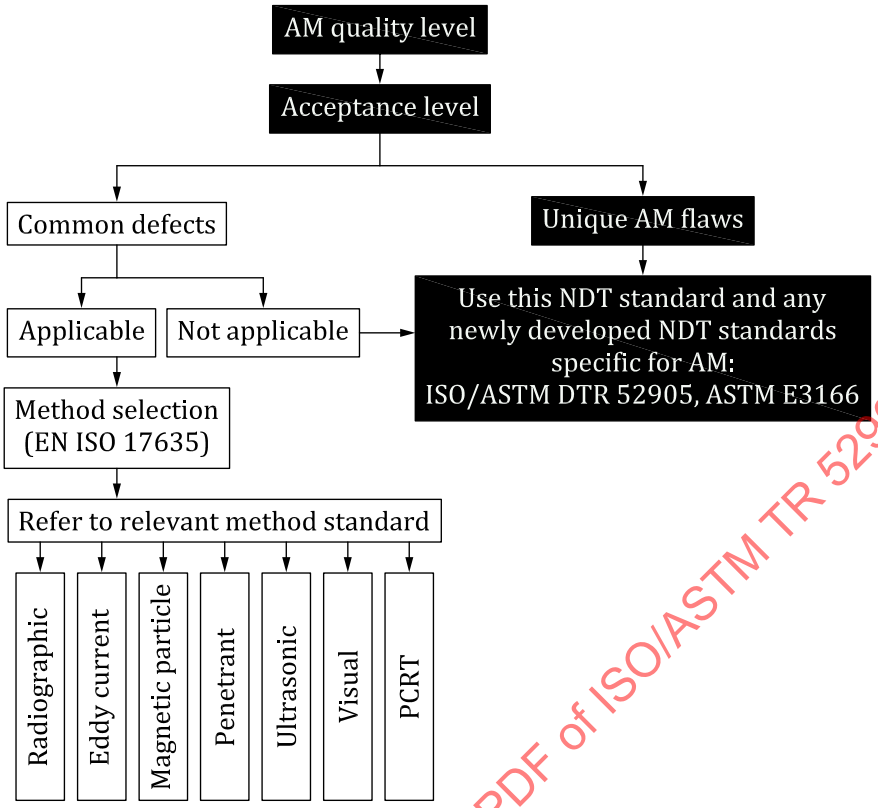

Figure 5 — Proposed NDT standards structure for additive manufacturing. The black boxes indicate development of new NDT standards for AM

9 NDT techniques potential for AM only defects

As discussed in Clause 6, variation of AM process parameters and disruptions during build may induce a variety of defects (anomalies) in AM parts that can be detected, sized, and located by NDE[32]. NDT is an essential aspect of a fitness-for-service assessment. The NDT technique(s) used for flaw evaluation can be chosen to provide the type of information required to an acceptable degree of accuracy. Such information can include some or all of the following items:

— NDT method;

— geometrical complexity;

— surface finish;

— flaw type.

A study to establish the potential detection capability of the NDE method for post-build and In-process for AM was developed in References [22] and [33]. A selector tool has been created in order to demonstrate the capability of each NDT method for inspecting AM parts. This tool considers the micro and macro complexity of the part, and the potential defects of interest as listed in Clause 6. The tool considers a range of component structures and surface finishes, ranging from simple machined blocks/cylinders to inspection of as built EBM (rougher) lattice components. Figure 6 shows an example of the different part categories considered in the matrix of capabilities. From bottom to top the geometric complexity of the part increases, and from left to right the surface complexity increases.

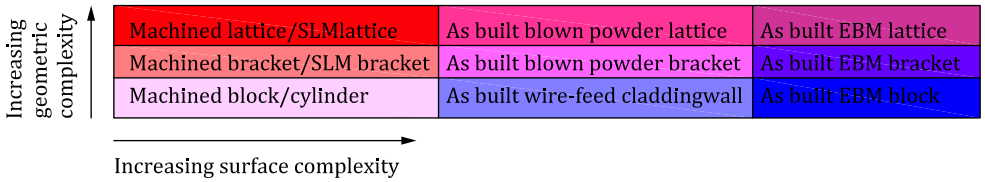

Figure 6 — Examples of different AM parts considered for the capability matrix (parts range from less complexity in the bottom left corner to more complex in the top right)

A matrix of capabilities was created which captures the abilities of each NDT technique for inspecting the various different component conditions. Each NDT method is given one of the following ratings:

— high capability;

— medium capability;

— low capability;

— no capability.

For each type of defect, the inspection method is given a score based on its capability for detecting that type of defect in each of the different build categories. Each build category is colour coded to facilitate simple identification.

The matrix of capabilities is used to populate the selector tool matrices and can be used for reference only. It is worth noting that there are very few NDT techniques that are capable of detecting microstructure variations and residual stresses. These defect types are not often encountered in the majority of NDT inspections, and this is reflected in the reduced range of applicable inspection methods for these defects.

The selector tool may be used as an initial indication to identify the most capable NDT method for inspection of each category of component. To use the selector tool the component under test can first be defined in terms of its geometric and surface complexity, based on the descriptions given in Figure 6. Each category is represented by a number which is used as the input to the selector tool. For each different category the number and type of capable NDT methods vary and each method is given a representation of its inspection capability as is shown in Figure 7.

High capability	H
Medium capability	M
Low capability	L
No capability	

Figure 7 — Capability indicator for the NDT technique shown in Table 4 and Table 5

To demonstrate the functionality of the selector tool, two examples are given. The first concerns a simple machined block, a component with a simple geometry and surface finish. In this case the selector tool scenario input into the tool would be a 1, resulting in the selector tool output shown in Table 4. The output of the selector tool indicates that the most appropriate NDT method for the majority of defects is ultrasonic contact or immersion, or inspection using Electromagnetic Acoustic Transducer ultrasound. However, the output also indicates that these methods would not be suitable for detection of defects such as near surface residual stress, which the tool indicates would only be detectable using X-ray diffraction.

The second example is at the other end of the spectrum, with a complex geometry and surface condition, such as an as built EBM lattice component, high level of roughness surface. In this case the entry into the selector tool scenario would be a 9, resulting in the output shown in Table 5. With this complex type of component it is immediately apparent from Table 5 that inspection is a more challenging proposition compared to the simple machined block presented in Table 4. Here the most appropriate inspection

method is X-ray computed tomography for the majority of defects, however it does not have good capability for certain defects, such as surface breaking cracks or lack of fusion.

An additional tool has been developed for determining the most appropriate NDT methods for post-build inspection of metal cladding (DED) components. This selector tool operates in the same fashion as the AM tool, with the user entering a number corresponding to the scenario which best describes the component required to be inspected.

Table 4 — Review of NDT technique potential for AM parts. Post built NDE method potential for lowest surface roughness and least complexity geometry, e.g. machined block/cylinder (capability levels are H – High, M – Medium, L – Low and Empty – None)

Class	Type	Sub-type	Including...	Surface breaking cracks / lack-of-fusion	Surface breaking voids	Internal cracks / lack-of-fusion / layer defects	Isolated / clustered porosity	Internal voids, incl. cross-layer defects	Inclusions	Trapped powder (Powder Bed Fusion only)	Near surface microstructure variation	Sub-surface microstructure variation	Near surface residual stress	Sub-surface residual stress
Mechanical	Ultrasonic	Contact or near-contact (air-coupled)	Single / twin / array probe, Time of Flight Diffraction	H	H	H	H	H	H	H				
		Immersion		H	H	H	H	H	H	H				
	Vibration analysis	Resonance testing	Acoustic pattern recognition	M	M	L	L	M		M				
Optical / visible light	Simple		Aids such as lighting / borescope etc.	M	H					H				
	Dye-penetrant		Fluorescent / visible	H	H									
Radiographic	X-ray	Conventional, 2D	Film / Computed / Real-time / Digital	M	H	M	H	H	H	H				
		Computed Tomography	2D (fan beam) / 3D (cone beam) CT / Laminography	M	H	M	H	H	H	H				
		Diffraction									M		H	L
Thermal	Optically excited	Flash			L			L		M				
		Laser		H	M	L		L		M				
	Electrically excited		Induction-heated	H	H	L		L		M				
	Vibrationally excited		Thermosonics	H	L	H		M						
Electromagnetic	Eddy current		Single / array probe	H	M						H			
	Magnetic field	Magnetic particle		H	H									
		Barkhausen									M	M		
		Alternating Current Field Measurement		H	H									

Table 4 *(continued)*

Class	Type	Sub-type	Including…	Surface breaking cracks / lack-of-fusion	Surface breaking voids	Internal cracks / lack-of-fusion / layer defects	Isolated / clustered porosity	Internal voids, incl. cross-layer defects	Inclusions	Trapped powder (Powder Bed Fusion only)	Near surface microstructure variation	Sub-surface microstructure variation	Near surface residual stress	Sub-surface residual stress
Mixed	Eletromagnetic-Mechanical	Electromagnetic Acoustic Transducer Ultrasound		H	H	H	H	H	H	H				
	Optical-Mechanical	Laser Ultrasound		H	H	M	L	M	L	L			H	M
		Spatially Resolved Acoustic Spectroscopy		H	H						H			
		Shearography	Electronic speckle pattern interferometry	H	H	M	L	M		M				
		Laser Speckle Photometry		L	L	L		L		L	M			
		Grazing Incidence Ultrasound Microscopy		M	M						H			

Table 5 — Review of NDT technique potential for AM parts. Post built NDE method potential for a complex lattice structure with as built surface finish (capability levels are H – High, M – Medium, L – Low and Empty – None)

Class	Type	Sub-type	Including…	Surface breaking cracks / lack-of-fusion	Surface breaking voids	Internal cracks / lack-of-fusion / layer defects	Isolated / clustered porosity	Internal voids, incl. cross-layer defects	Inclusions	Trapped powder (Powder Bed Fusion only)	Near surface micro-structure variation	Sub-surface micro-structure variation	Near surface residual stress	Sub-surface residual stress
Mechanical	Ultrasonic	Contact or near-contact (air-coupled)	Single / twin / array probe, Time of Flight Diffraction											
		Immersion												
	Vibration analysis	Resonance testing	Acoustic pattern recognition	M	M	L	L	M		M				
Optical / visible light	Simple		Aids such as lighting / borescope etc.		M					M				
	Dye-penetrant		Fluorescent / visible											
Radiographic	X-ray	Conventional, 2D	Film / Computed / Real-time / Digital		M		M	M	M	M				
		Computed Tomography	2D (fan beam) / 3D (cone beam) CT / Laminography	L	H	L	H	H	H	H				
		Diffraction												
Thermal	Optically excited	Flash						L		L				
		Laser		L	L	L		L		L				
	Electrically excited		Induction-heated											
	Vibrationally excited		Thermosonics	M	L	M		L						
Electromagnetic	Eddy current		Single / array probe											
	Magnetic field	Magnetic particle												
		Barkhausen									L			
		Alternating Current Field Measurement												

Table 5 *(continued)*

Class	Type	Sub-type	Including…	Surface breaking cracks / lack-of-fusion	Surface breaking voids	Internal cracks / lack-of-fusion / layer defects	Isolated / clustered porosity	Internal voids, incl. cross-layer defects	Inclusions	Trapped powder (Powder Bed Fusion only)	Near surface microstructure variation	Sub-surface microstructure variation	Near surface residual stress	Sub-surface residual stress
Mixed	Eletromagnetic-Mechanical	Electromagnetic Acoustic Transducer Ultrasound												
	Optical-Mechanical	Laser Ultrasound		M	M			L	L				M	M
		Spatially Resolved Acoustic Spectroscopy		L	L									
		Shearography	Electronic speckle pattern interferometry	M	M	L		L		L				
		Laser Speckle Photometry		L	L	L		L		L				
		Grazing Incidence Ultrasound Microscopy												

While application of conventional NDE techniques is possible for AM parts with simple geometries, topology optimized AM parts with more complex geometries require specialized NDE techniques. Following References [22][25][27][33][34], the effect of design complexity on NDE method selection is summarized in Table 6.

Table 6 — AM design complexity groupings[27]

Group	Design	Description
1	Simple parts	These parts are simple with well-established designs that do not capitalize on the advantages of AM. Such parts may already have consensus NDE inspection procedures.
2	Optimized standard parts	These parts are based on conventional designs, but some of the advantages of AM, such as lighter weight or fewer parts, are incorporated into the design.
3	Parts with embedded features	The added features add complexity to a part, thereby decreasing NDE inspectability. Access is limited to internal inspection surfaces.
4	Design-to-constraint parts	These parts appear to be free-formed without straight lines or parallel surfaces and have no analogue made by conventional subtractive techniques. The presence of detailed external and internal features greatly reduces NDE inspectability because the amount of inspection surface has increased and the vast majority of the structure is detailed and embedded.
5	Lattice structures	These parts consist of a free-form metallic lattices that have a high strength-to-weight ratios, increased surface areas, and tailored stiffness and damage tolerance. The structures pose the greatest challenge for existing NDE technologies, requiring the use of new or creative NDE techniques.

Table 7 lists industrial NDE procedures that are used to inspect AM parts. The ability of each technique to detect different types of defects, as well as to locate them in the interior or exterior surface of a part is listed. Finally, the NDE techniques are further characterized by the ability to globally screen or detect and locate a defect.

Table 7 — General inspection capabilities for selected conventional post-build NDE techniques for AM (adapted from ASTM E3166)

Method	Material and defect types detected	Surface or interior defect sensitivity	Global screening or detect location
CT, macro	In any solid material, any condition and/or defect affecting X-ray absorption, with the exception of reduced mechanical properties	Surface and subsurface, >200 µm resolution	Detects and images defect location; field of view dictated by detector size and distance between test article and imaging plane and x-ray source.
CT, microfocus	In any solid material, any condition and/or defect affecting X-ray absorption, with the exception of reduced mechanical properties	Surface and subsurface, typically 10 µm to 200 µm resolution for parts 10 mm to 200 mm thick	Detects and images defect location; field of view minimized, focal spot may be optimized for resolution at the expense of scan speed
CT, SX	In any solid material, any condition and/or defect affecting hard and soft X-ray absorption, with the exception of reduced mechanical properties	Surface, subsurface and bulk, usually 5 µm resolution for a field-view of 10 mm in 42 mm thick.	Detects and images defect location; field of view minimized, focal spot may be optimized for resolution at the expense of scan speed
Abbreviations used: CT = Computed Tomography, ET = Eddy Current Testing, VI = Visual Inspection, PCRT = Process Compensated Resonance Testing, PT = Penetrant Testing, RT = Radiographic Testing, TT = Thermographic Testing, UT = Ultrasonic Testing, NI=Neutron Imaging, SX = Synchrotron X-Ray.			

Table 7 *(continued)*

Method	Material and defect types detected	Surface or interior defect sensitivity	Global screening or detect location
CT, NI	In any solid material, any condition and/or defect affecting Neutron, with the exception of reduced mechanical properties	Surface, subsurface and bulk, usually 10 µm resolution in 42 mm thick. In general it's the size of the field of view divided by 2000, all other elements being optimal.	Detects and images defect location; resolution affects the scanning time. Neutrons have higher penetration to most metals (*e.g.,* Aluminium, Titanium, Nickel) and are isotope sensitive (light elements).
ET	In electrically conducting and/or magnetic materials for local defects (for example, cracks) and distributed flaws (for example, porosity)	Surface and near subsurface	Detects and images location
VI	In any solid material, any condition and/or defect affecting visible, structured and laser light reflection	Surface	Detects and images location
PCRT	Any solid material. Any defect or condition	Surface and subsurface	Global screening
PT	Any solid material. Discontinuities — cracks, pores, nicks, others	Surface breaking	Detects and identifies location
RT	In any solid material, any condition and/or defect affecting X-ray absorption, with the exception of reduced mechanical properties	Surface and subsurface	Detects and images location but no depth information
TT	In any solid material, any condition and/or defect affecting heat conduction	Surface and subsurface	Detects and images location but limited penetration in metals
UT	In any solid material, any condition and/or defect affecting sound attenuation, propagation, acoustic velocity and/or sensor-part connexion	Surface and subsurface	Detects and identifies location
Abbreviations used: CT = Computed Tomography, ET = Eddy Current Testing, VI = Visual Inspection, PCRT = Process Compensated Resonance Testing, PT = Penetrant Testing, RT = Radiographic Testing, TT = Thermographic Testing, UT = Ultrasonic Testing, NI=Neutron Imaging, SX = Synchrotron X-Ray.			

Based on the analysis performed in the NDE methods, the potential approaches to be used in post-process inspection and in-process of AM components would be those presented in Table 8.

Table 8 — NDT methods with the most potential for post-processing and in-process inspection for AM

Inspection type	NDT methods				
Post-process	X-ray	X-ray CT, Neutron CT	Thermography	UTPA & TFM	PCRT, RAM and NLA
In-process	Laser scan line	Optical imaging	Thermography	X-ray backscattered Digital X-ray	LUT

10 AM artefacts

The objective of the specimen is to cover the AM types of defects not covered by current NDT standards, and unique for the additive process such as layer, cross-layer and unconsolidated powder/trapped powder. Some of these defects (layer and cross-layer) are also being covered in ASTM E3166. A two-level approach is proposed. Firstly to use an extruded star geometry to provide initial image quality indicator (IQI) of AM seeded defects detectability using a specific NDT method, and may be used for relatively simple geometries. The second is an à la carte design with a particularly more representative geometry to the production part, where defects are seeded at geometrically or structurally critical places, required defect sizes and defect types.

10.1 Design

10.1.1 Star artefact

This specimen will be used to assess the detectability of identified AM typical layer defects, cross-layer defects, unconsolidated powder/trapped powder and inclusions. The seeding technique is one of the proposed methods in ISO/ASTM TR 52906, CAD seeding technique. The specimen has a cross-section of a 5 point star as shown in Figure 8. The dimensions shown in the design are general guidance only. The dimensions of the artefact are dependent on several factors including the material, accelerating voltage (kV), and type of filter. The exact dimensions will be determined using XCT Standard: EN 16016-2. For example, using 450 kV, 500 µm Gadolinium oxysulphide scintillation screen and 3 mm Pb filter, XCT can achieve 10 % transmission on 80 mm of aluminium. This level of transmission can give an optimal signal-to-noise ratio in the CT image. In this case, the total material thickness of the artefact can not exceed 80 mm if the scan is rotated on the star axis. The red arrows in Figure 8 indicated the thickness. Details of the preliminary star artefacts design and final design specifying seeded defects location and their distribution are presented in detail in Annex C, Figure C.1 (Preliminary star-shape) and Figure C.2 (Final star-shape).

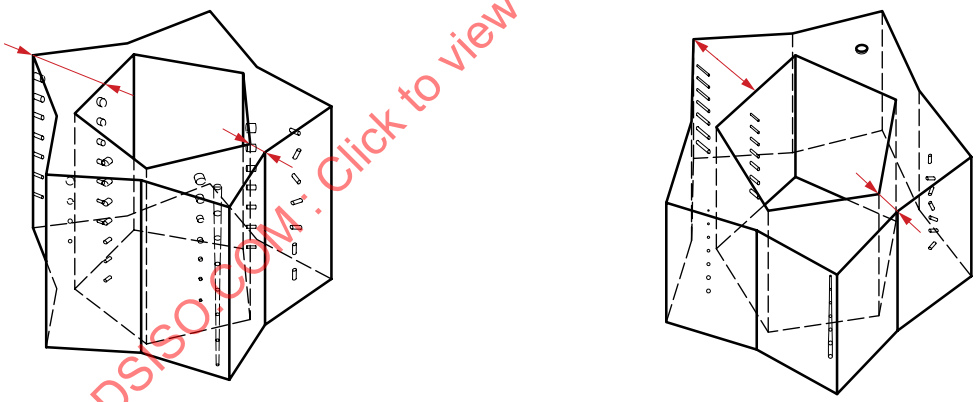

a) Initial design b) Final design

Figure 8 — Proposed specimen designs to assess the detectability of layer defects, cross-layer defects, unconsolidated powder and trapped powder (the red arrows indicated the maximum and minimum material thickness of the specimen)

For the preliminary star-shape artefact design labelled as SP, those stars have been seeded with artificial defects unique to AM process represented by cylinders and spheres. The sizes of the defects vary between 0,02 mm to 1,5 mm in diameter and 0,5 mm to 6,4 mm in length. Six titanium artefacts and four Inconel®[1)] artefacts have been built. For titanium stars, four of them were built using the L-PBF process, and two of them were built using the EBM process. Two of the L-PBF built artefacts did not have artificial defects and were intended for reference.

1) Inconel is an example of a suitable product available commercially. This information is given for the convenience of users of this document and does not constitute an endorsement by ISO of this product.

For the new star artefacts design proposed by MTC, the defect sizes vary between 0,1 mm to 0,7 mm in diameter and 2,0 mm to 5,0 mm in length. Three versions of star artefacts have been created based on the initial design showing in numeral 9.1 (size of seeded defects changed). The three design are:

— Reference S0 — No nominal defects.

— Version S1: Defects are positioned close to the tip and on the surface of the internal pentagon, as first design but with the very small defects removed.

— Version S2: Same defects as S1 but positioned at the corner, away from the tip. This position has minimum material on.

The type of seeded defects and their dimensions assessed during the trials are summarised in Table 9, for the preliminary design, while Table 11 presents the values for the final design. Detailed information of the process, manufacturers and builds is specified in Annex D, Table D.1.

Table 9 — Defects dimension and location for star artefact preliminary design 1 and design 2

Design	Description [a]	Diameter [a] ϕ_1 mm	Length l_1 mm	Total seeded defects Q_{ty} number
SP[b]	**Region 1.** Vertical cylinders interconnected and open at both top and bottom.	0,02, 0,05, 0,1, 0,2, 0,5, 1,0 and 1,5	6,4	7
	Region 2. Cylinders in various orientations (Unconsolidated/trapped powder). Orientation offsets of 45° and 90° relative to the first instance	0,3	2,0	7
	Region 3. Reference section.	ND[c]	ND[c]	ND[c]
	Region 4. Horizontal cylinders open at the outside edge (Layer defects).	0,02, 0,05, 0,1, 0,2, 0,5, 1,0 and 1,5	2,0	7
	Region 5. Spheres (Voids/porosity, unconsolidated/trapped powder).	0,02, 0,05, 0,1, 0,2, 0,5, 1,0 and 1,5	2,0	7
	Region 6. Horizontal cylinders, open at the inside face (Layer defects).	0,02, 0,05, 0,1, 0,2, 0,5, 1,0 and 1,5	1,5	7
	Region 7. Horizontal cylinders open at the inside face (Layer defects).	0,02, 0,05, 0,1, 0,2, 0,5, 1,0 and 1,5	2,0	7
	Region 8. Reference section.	ND[c]	ND[c]	ND[c]
	Region 9. Horizontal cylinders, open at the inside face (Layer defects).	0,02, 0,05, 0,1, 0,2, 0,5, 1,0 and 1,5	0,5	7
	Region 10. Horizontal cylinders, open at the inside face (Layer defects).	00,02, 0,05, 0,1, 0,2, 0,5, 1,0 and 1,5	2,0	7

[a] The defects order from TOP to BOTTOM are as follows: smaller defects is number 1 (20 µm) increasing to number 7 (1 500 µm). It is with the star face up where the reference holes are set.

[b] SP abbreviation to indicate the star artefact correspond to the preliminary design

[c] Abbreviation used: ND = Not defect

To achieve the 10 % transmission of X-ray energy, the dimensions are modified based on material density. The overall star geometry is driven by two diameters that control the positions of the vertices on the outer star profile. The sketch views in Figure 9 and Figure 10 give a clearer indication of the diameters and pentagon dimension needed to achieve the desired wall thickness. The height of the star is kept constant. Table 10 shows the dimensions of the star artefact build for the different materials tested here. The STL build files are available at the following ISO link: https://standards.iso.org/iso/tr/52905/ed-1/en/.

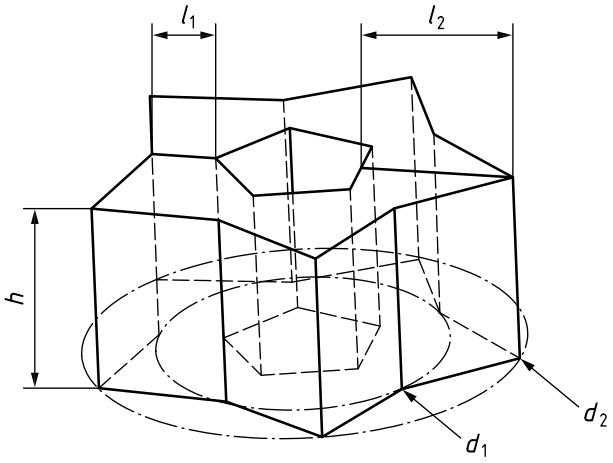

Key

d_1	inner star diameter
d_2	outer star diameter
h	height
l_1	thin wall section
l_2	thick wall section

Figure 9 — General sketch showing the main dimension of the start artefact to be achieved for 10 % transmission of X-ray accomplish based on material density

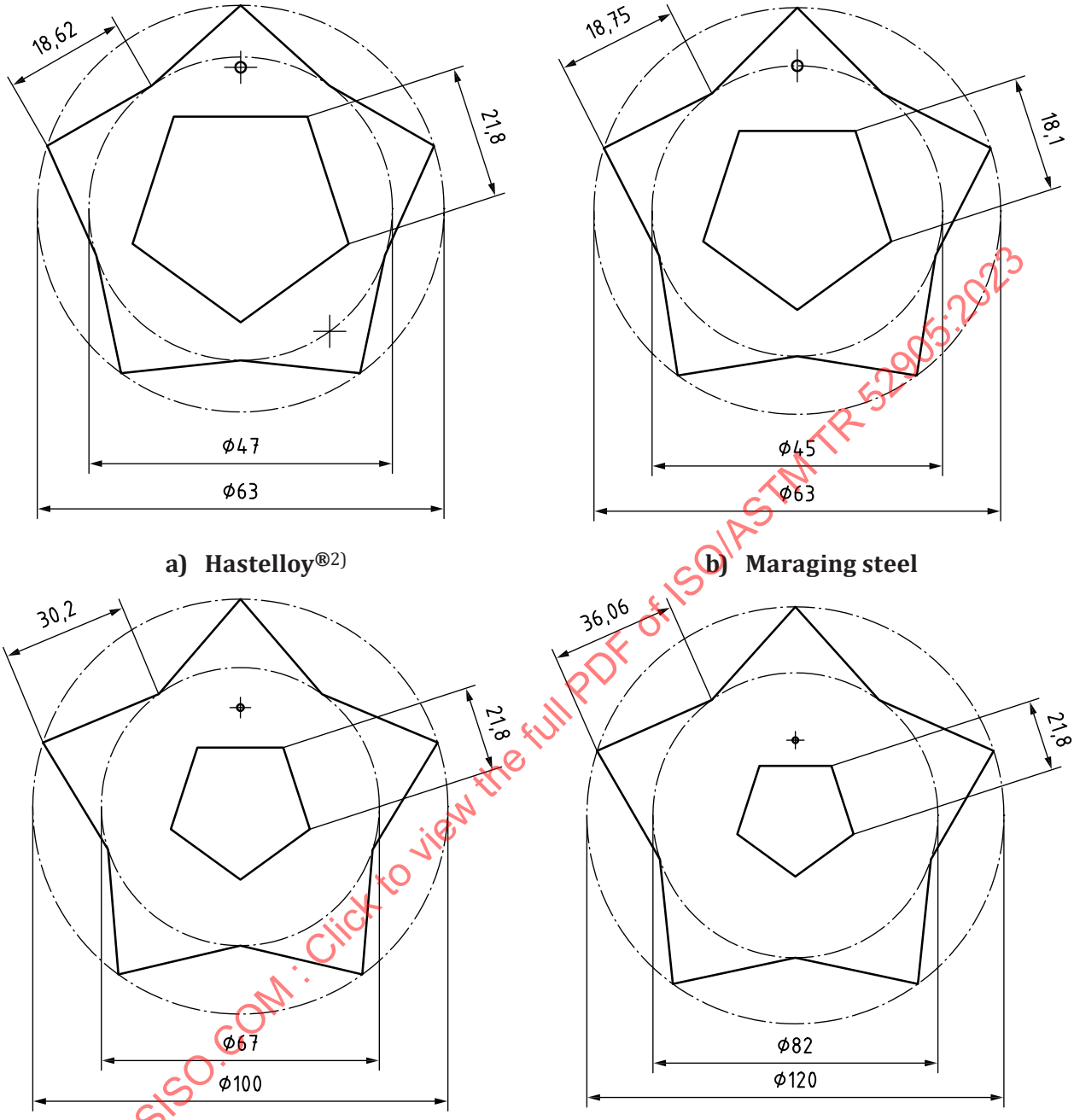

a) Hastelloy®[2)]

b) Maraging steel

c) Titanium

d) Aluminium

Figure 10 — Artefact material design comparison for the new star design

2) Hastelloy is an example of a suitable product available commercially. This information is given for the convenience of users of this document and does not constitute an endorsement by ISO of this product.

Table 10 — Star artefact dimensions based on material density

Material	Density[a] ρ g/cm^3	Height[b] h_1 mm	Material group	Ideal scale factor	Actual scale factor	Ideal cumulative wall thickness mm	Cumulative wall thickness mm	Thin wall section l_1 mm	Thick wall section l_2 mm
Hastelloy®[1)]	8,89	45	Nickel	–	1	21,46	21,46	4,96	16,5
Inconel®[2)]	8,5	45	Nickel	0,96	1	20,52	21,46	4,96	16,5
Cobalt-Chromium	8,50	45	Nickel	1	1	21,46	21,46	4,96	16,5
Maraging steel	7,87	45	Iron	1,08	1,09	23,18	26,14	7,1	19,04
Stainless steel 17-4	7,8	45	Iron	1,09	1,09	23,39	26,14	7,1	19,04
Titanium CP	4,51	45	Titanium	1,88	1,92	40,45	39,96	4,96	35
Ti6Al4V	4,43	45	Titanium	1,92	1,92	41,18	39,96	4,96	35
Aluminium	2,80	45	Aluminium	3,04	3,04	65,15	67,46	45	22,46

[a] Density source (https://www.matweb.com/search/MaterialGroupSearch.aspx).

b The height of the star artefacts for full size is constant.

1) Hastelloy is an example of a suitable product available commercially. This information is given for the convenience of users of this document and does not constitute an endorsement by ISO of this product.

2) Inconel is an example of a suitable product available commercially. This information is given for the convenience of users of this document and does not constitute an endorsement by ISO of this product.

Figure 11 shows the defects on the tip sections of the star, which covers the region (1) to (5), while Figure 12 shows the defects on the inner pentagon, which covers the region (1) to (5) too. However, noted the position of the seeded defects varied with design 1 shown in Figure 11. Table 11 show the dimensions of the defects seeded on the star artefacts.

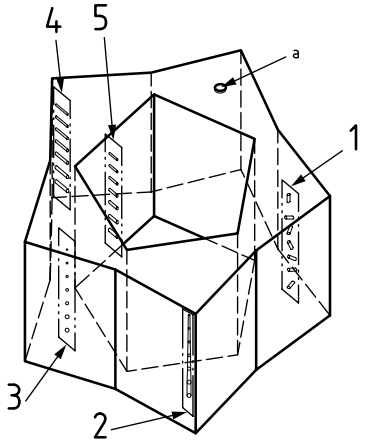

NOTE Details of the defects on the tip sections are shown in region (1) to (5).

Figure 11 — Proposed specimen design 1 (S1) to assess the detectability of layer defects, cross-layer defects, unconsolidated powder and trapped powder

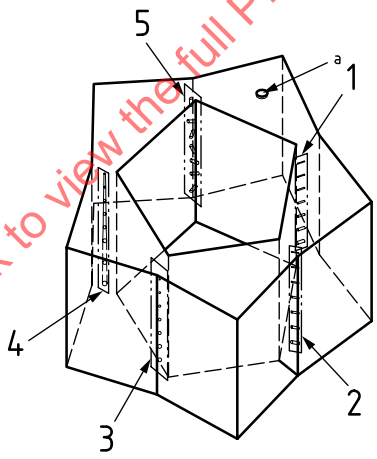

NOTE Details of the defects in the inner pentagon are shown in region (1) to (5).

Figure 12 — Proposed specimen design 2(S2) to assess the detectability of layer defects, cross-layer defects, unconsolidated powder and trapped powder

Table 11 — Defects dimension and location for star artefact final design S1 and design S2

Design	Description [a]	Diameter [a] ϕ_1 mm	Length l_1 mm	Total seeded defects Q_{ty} number
S0	Reference star without defects	ND[b]	ND[b]	ND[b]

[a] The defects order from TOP to BOTTOM are as follows: smaller defects is number 1 (0,1 mm) increasing to number 7 (0,7 mm). It is with the star face up where the reference holes are set.

[b] Abbreviation used: ND = Not defect

Table 11 *(continued)*

Design	Description [a]	Diameter [a] ϕ_1 mm	Length l_1 mm	Total seeded defects Q_{ty} number
S1	**Region 1.** Cylinders in various orientations (Unconsolidated/trapped powder). Orientation offsets of 45° and 90° relative to the first instance.	0,3	2,0	7
	Region 2. Vertical cylinders interconnected and open at both top and bottom.	0,1, 0,2, 0,3, 0,4, 0,5, 0,6 and 0,7	5,0	7
	Region 3. Spheres (Voids/porosity, unconsolidated/trapped powder).	0,1, 0,2, 0,3, 0,4, 0,5, 0,6 and 0,70	–	7
	Region 4. Horizontal cylinders open at the outside edge (Layer defects).	0,1, 0,2, 0,3, 0,4, 0,5, 0,6 and 0,7	2,5	7
	Region 5. Horizontal cylinders, open at the inside face of the pentagon (Layer defects).	0,1, 0,2, 0,3, 0,4, 0,5, 0,6 and 0,7	2,0	7
S2	**Region 1.** Horizontal cylinders, open at the inside face of the pentagon (Layer defects).	0,1, 0,2, 0,3, 0,4, 0,5, 0,6 and 0,7	2,0	7
	Region 2. Horizontal cylinders open at the outside edge (Layer defects).	0,1, 0,2, 0,3, 0,4, 0,5, 0,6 and 0,7	2,5	7
	Region 3. Spheres (Voids/porosity, unconsolidated/trapped powder).	0,1, 0,2, 0,3, 0,4, 0,5, 0,6 and 0,70	–	7
	Region 4. Vertical cylinders interconnected and open at both top and bottom.	0,1, 0,2, 0,3, 0,4, 0,5, 0,6 and 0,7	5,0	7
	Region 5. Cylinders in various orientations (Unconsolidated/trapped powder). Orientation offsets of 45° and 90° relative to the first instance.	0,3	2,0	7

[a] The defects order from TOP to BOTTOM are as follows: smaller defects is number 1 (0,1 mm) increasing to number 7 (0,7 mm). It is with the star face up where the reference holes are set.

[b] Abbreviation used: ND = Not defect

10.1.2 À la carte artefact

For cases where geometry is considerably more complex than the design in the previous section and further validate an NDT method, it is recommended to use an à la carte approach. In this case, the actual part geometry design is recommended to be built, inserting typical or expected defects at strategic locations such as critical places (geometrical/structural), deep sections, hard to reach sections, close to surface, surface regions and any other region required. Using the part geometry, the recommended steps to follow in the à la carte framework are:

— Identify structurally critical defect locations and sizes to be required for detection, ideally through modelling or mechanical test;

— Seed those defects to the part in the identified critical areas;

— Build the part which is now the NDE test/calibration artefact;

— Test the built calibration artefact with NDE methods (UT, XCT, resonance, any other novel NDE method that may have become available) to qualify it is capable for the part quality requirements.

Figure 13 shows an example based on à la carte generic airfoil geometry. CAD seeded cylinders with openings at the surfaces are located on various locations on the airfoil (shown by red circles), as examples of potentially critical regions and hard to detect by XCT. The primary focus of this is to determine the sensitivity of the XCT detection of the same defects (sizes and shapes) at various locations

on the airfoil. The STL build file for this geometry is also available at the following ISO link: https://standards.iso.org/iso/tr/52905/ed-1/en/.

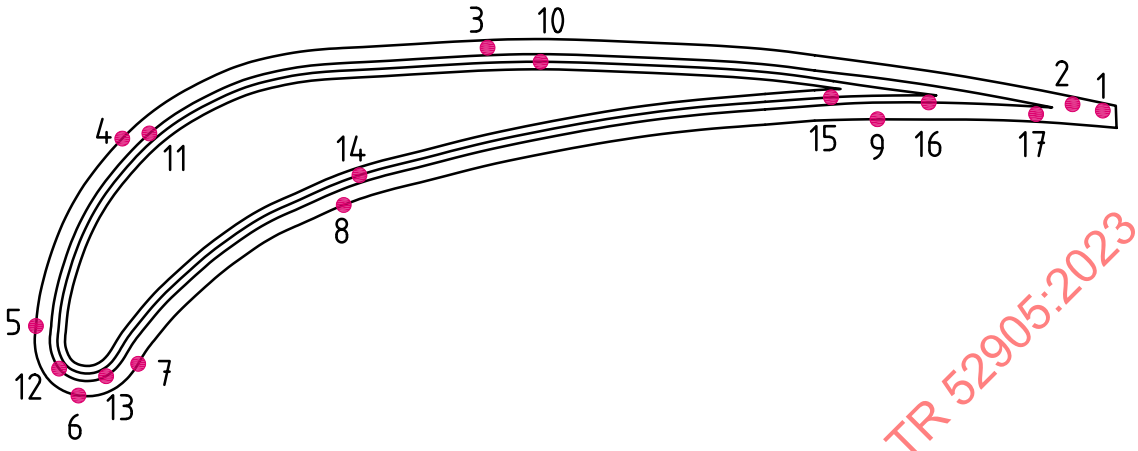

Key

1	holes set 1 to 5	located at the external concave side
2	holes set 10 and 11	located at the internal concave side
3	holes set 7 to 9	located at the external convex side
4	holes set 14 to 17	located at the internal convex side
5	hole set 6	located at the external curve side
6	holes set 12 and 13	located at the internal curve side

NOTE Holes location are indicated by red diamonds.

Figure 13 — Generic airfoil geometry with critical defects locations inside and outside of the concave and convex side

The airfoil contains 17 sets of holes at various locations with each set containing three (3) clusters of holes. Each cluster has four holes with diameter of 0,1 mm, 0,3 mm, 0,5 mm and 0,7 mm as is shown in Figure 14. The depth of each holes is the same as the diameter, however, the material thickness varies depending on the location on the airfoil. The holes were designed in this way in order to have sensitivity relative to location, such that defects of the same size will give contrast at different locations. This is summarised on Table 12 based on Figure 13 layout.

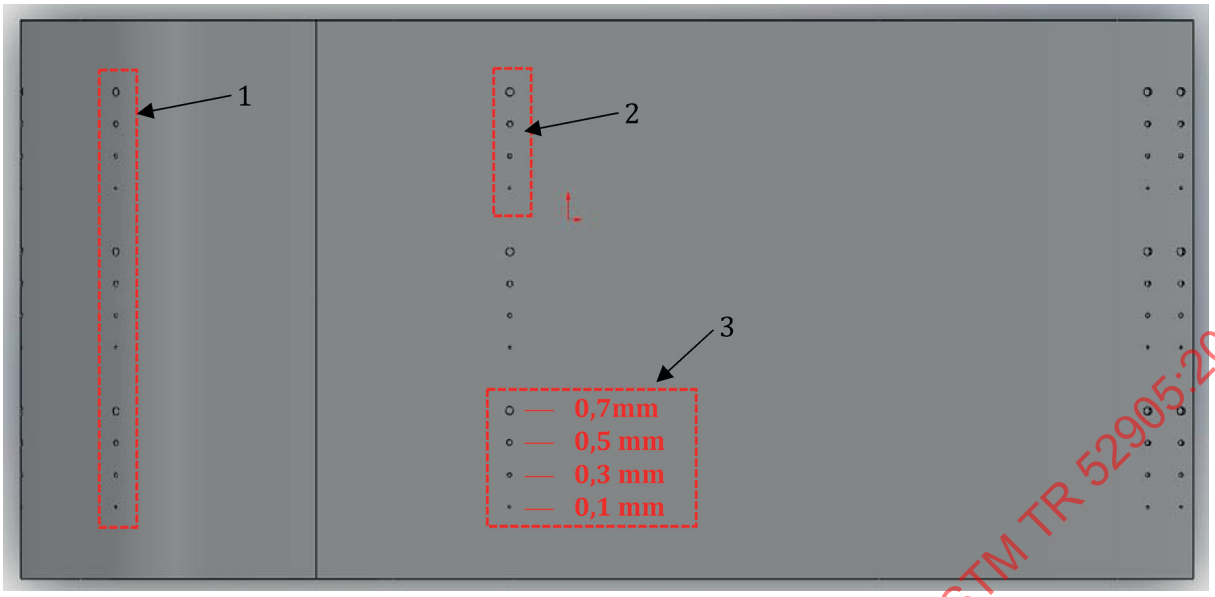

Key

1 sets of holes containing 3 cluster
2 number of holes per cluster
3 holes dimensions per cluster

Figure 14 — Top view of the CAD model showing an example of the rows, sets and dimensions of the holes in the airfoil

Table 12 — Dimensions of the seeded defects in the à la carte design of the generic airfoils

Region	Side	Number of sets[a]	Holes[b] d_1 mm
1	Concave outside	5	0,1, 0,3, 0,5 and 0,7
2	Concave inside	2	0,1, 0,3, 0,5 and 0,7
3	Convex outside	3	0,1, 0,3, 0,5 and 0,7
4	Convex inside	4	0,1, 0,3, 0,5 and 0,7
5	Curve outside	1	0,1, 0,3, 0,5 and 0,7
6	Curve inside	2	0,1, 0,3, 0,5 and 0,7

[a] Total number of sets 17.
[b] Total number of holes 204.

10.2 Manufacturing

10.2.1 Star artefact

The goal of the star artefacts is to represent the defects/flaws unique to additive manufacturing represented by seeded geometries to replicate them as follows:

— Cross-layer defects: Vertical cylinders of different diameter but the same length. Those are connected by a small link to release powder at the largest diameter.

— Layer defects: Horizontal cylinders of different diameters but the same length. Open end to release powder.

— Unconsolidated/trapped powder: Internal spheres of different diameter and cylinders in various orientation with the same length and diameter.

The defects are located in critical areas or locations at a different depth to ensure they are representative of flaws that can be generated during the AM process. Figure 15 shows examples of the star artefact builds for Hastelloy®[3] and Titanium.

a) Hastelloy® **b) Titanium**

NOTE Sample star design S1 showing size difference due to diameter variation to achieve 10 % transmission X-ray energy.

Figure 15 — Hastelloy® and titanium star artefact build using EOS system

The star artefacts built during this study are summarised as followed:

10.2.2 À la carte artefact

In this section, a build example is shown in Figure 16 for an à la carte specimen made from Inconel®[4] by GE power. The selected geometry was a generic air foil seeded with defects which were selected in regions of interest as presented in 10.1.2.

3) Hastelloy is an example of a suitable product available commercially. This information is given for the convenience of users of this document and does not constitute an endorsement by ISO of this product.

4) Inconel is an example of a suitable product available commercially. This information is given for the convenience of users of this document and does not constitute an endorsement by ISO of this product.

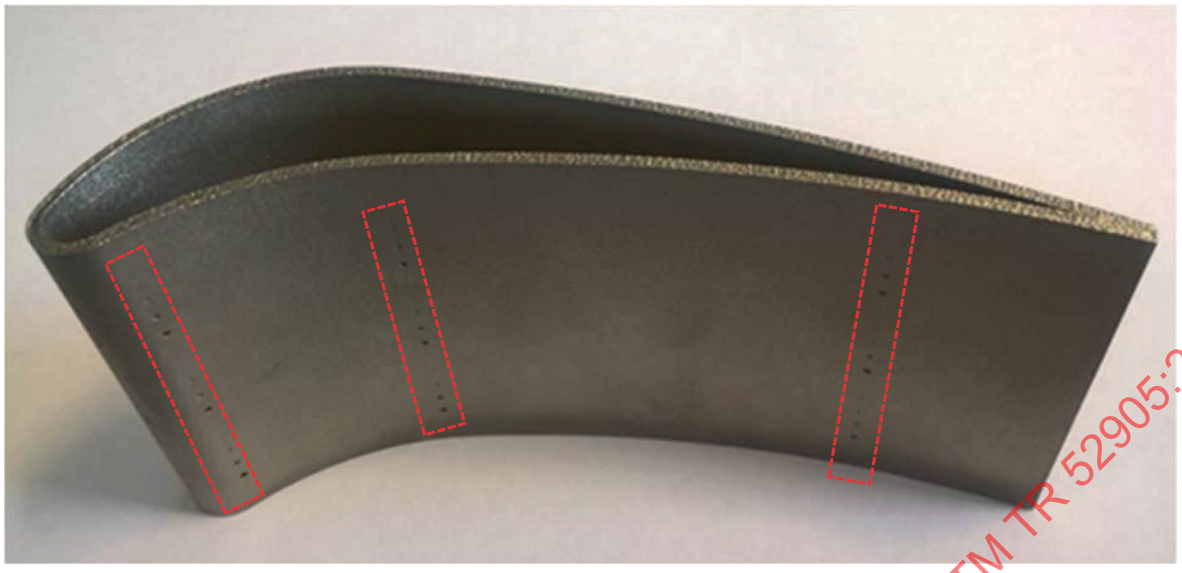

Figure 16 — Generic airfoils build as à la carte design provided by GE power (red rectangles show simulated defects manufactured by PBF)

11 NDT method trials and validation using star artefact

Following the review from Clause 9 for NDT approaches, the methods with the most potential for AM were selected. Trials of these methods will be presented in this clause, which can include material extracted from collaborators' reports including background, experimental, results and analysis.

11.1 Experimental trials

The experimental trials in this section compile the main information of the test as well as main outcomes from the analysis performed in the star artefacts built (S0, S1 and S2 design) using different alloys such as Inconel®, Hastelloy®, Maraging steel, stainless steel, titanium, cobalt-chrome and Aluminium alloys. Details of the star artefact manufactured, NDT technologies and collaborators are presented in Table D.1 and Table D.2. Some of the findings reported are based on trials performed on the preliminary star designs while others were on new star versions.

The scope of the trials is to assess the capability of detection of the NDT technique involved. These trials are giving information on the presence of the defect rather than sizing them. If dimensions of the seeded defects are measured, it is considered as an additional information or capability of the technique used. Seven NDT techniques were involved in the trials carried out as follows:

— x-ray computed tomography (XCT);

— neutron imaging (NI);

— synchrotron radiography;

— synchrotron CT;

— neutron CT;

— thermography;

— process compensated resonance testing (PCRT);

— non-linear resonance testing (NLR);

— conventional ultrasonic testing (CUT);

— pulse-echo ultrasonic testing (PE);

— phase array ultrasonic (PAUT);

— phase array ultrasonic and full matrix capture/total focus method (FMC/TFM);

— neutron diffraction (ND).

11.1.1 X-ray Computed Tomography – XCT (MTC & GE & EWI)

X-ray computed tomography (XCT) is one of the most common Nondestructive evaluation (NDE) techniques for additive manufacturing parts. XCT technique can produce 2D (fan beam) and 3D (Cone beam) cross-sectional images of an object from flat X-ray images. X-ray computed tomography consists of probing a test part with X-ray at different angular positions of the part, recording the interactions of these waves with the test part for each angle independently, and post-processing these data with a reconstruction algorithm to give a volumetric image.

All trails have used the 3D XCT method. Characteristic of the internal structure of an object imaging is visualised through a process known as reconstruction. Object dimensions and shape, internal defects and density are the typical information obtained by XCT.

11.1.1.1 Summary of procedure

The general procedure for the XCT inspection includes the following steps:

— Position of the star artefact on the table oriented on the X-axis and sample faced up with the reference point.

— Scan of the star artefact.

— Reconstruct the star artefact rotational image.

— Analyse XCT data to determine seeded defects detected.

— Obtain XCT images of the area of interest to link it with the nominal CAD.

— Report.

For the XCT scan trials, three systems have been used, belonging to EWI, GE and MTC. The material used by EWI was Stainless Steel, Cobalt-Chrome, while GE and MTC used Inconel®[5], Hastelloy®[6], Maraging steel, and Ti6Al4V. A summary of the samples built is presented in Table 13.

11.1.1.2 Apparatus/settings

The XCT systems used for GE, MTC and EWI were 450 kV systems. The systems used an X-ray generator as a radiation source. The parameters used for each system for the inspection are shown in Table E.1 and Table E.2, while the set up used by MTC and GE is shown in Figure E.1 and Figure E.2.

5) Inconel is an example of a suitable product available commercially. This information is given for the convenience of users of this document and does not constitute an endorsement by ISO of this product.

6) Hastelloy is an example of a suitable product available commercially. This information is given for the convenience of users of this document and does not constitute an endorsement by ISO of this product.

Table 13 — Summary of the star artefacts version used during the XCT trials

Material	Version S0	Version S1	Version S2
Hastelloy® (HX)[b,c]	HX-S0-001 to HX-S0-005	HX-S1-001 to HX-S1-005	HX-S2-001 to HX-S2-005
Maraging steel (MS)[b,c]	MS-S0-001 to MS-S0-005	MS-S1-001 to MS-S1-005	MS-S2-001 to MS-S2-006
Stainless Steel (SS)	NT[d]	SS-S1-001	SS-S2-001
Cobalt-Chrome (CoCr)	NT[d]	NT[d]	CoCr755-S2-001
Inconel®[a] (IN)	NT[d]	IN-S1-300A	IN-S2-300A
Ti6Al4V[a]	NT[d]	S_{LB}-001[f]	S_{EB}-001[e]

[a] The star artefact correspond to the preliminary design.

[b] Nikon XT H 450 kV system reflection target. System located in the UK.

[c] Nikon XT H 450 kV system reflection target. System located in Germany.

[d] NT = Not tested.

[e] S_{EB}: Star artefact manufactured by EB-PBF process.

[f] S_{LB}: Star artefact manufactured by L-PBF process.

11.1.1.3 Significance of data/interpretation of results

The results of the XCT trials performed by GE and MTC for the preliminary star artefacts version are summarised in Table 14. Examples of the XCT image scan are also shown in Annex E.

The XCT results showed that the EBM artefact was successful in creating all the artificial defects. The smallest unconsolidated powder or trapped powder detected was between 0,3 mm to 0,5 mm in diameter. The smallest layer defect detected was between 0,2 mm to 0,5 mm in diameter. The smallest cross-layer defect detected was 0,05 mm in diameter.

The XCT results for the preliminary star artefacts designed by MTC (SP) did not show any indication of unconsolidated powder or trapped powder (see Figure C.1). It is not clear whether this is due to the XCT detection limit or the limit of L-PBF built. Therefore, validation is required through cut-ups and observation under the microscope. The SP artefacts were successful in creating layer and cross-layer defects. The XCT results showed the smallest defects detected was between 0,3 mm to 0,5 mm in diameter. In addition, the data also revealed some indications of defects that were not designed in the artefact.

Table 14 — Summary of the smallest defects detected in the star artefact built in Inconel®[7] and Ti6Al4V alloys by XCT scan

Defects dimensions in millimetres

Design[a]	Defect region	MTC		GE	
		Inconel 300A	Ti6Al4V	Inconel 300A	Ti6Al4V
SP	1	0,5	0,02	0,2	TBU[c]
	2	ND[b]	All detected	ND[b]	TBU[c]
	3	Reference	Reference	Reference	TBU[c]
	4	0,5	0,5	0,2	TBU[c]
	5	ND[b]	0,5	ND[b]	TBU[c]
	6	0,5	0,5	0,2	TBU[c]
	7	0,5	0,5	0,2	TBU[c]
	8	Reference	Reference	Reference	TBU[c]
	9	0,5	0,5	0,2	TBU[c]
	10	0,5	0,2	0,2	TBU[c]

[a] The CAD file of the star artefact corresponds to the preliminary version design by MTC.

[b] ND = Not detected.

[c] TBU = To be updated.

For the inspection with the new version of the stars (S0, S1 and S2) a summary of the findings is presented in Table 15 and Table 16. The smallest defect per region is given, however, details of individual outcomes are included in Table E.1 to Table E.9 and Figure E.3 to Figure E.11, E.3, numeral 2.

Table 15 — Summary of the smallest defects detected in the final star artefact design by XCT scan in Stainless Steel and CoCr

Defect dimensions in millimetres

Design[a]	Defect region	EWI[b]	GE[b]
		Stainless steel[b]	CoCr755
S0	All	NT[d]	NT[d]
S1	1	All detected	NT[d]
	2	0,1	NT[d]
	3	0,4	NT[d]
	4	0,2	NT[d]
	5	0,3	NT[d]
S2	1	0,2	0,3
	2	0,2	0,3
	3	0,3	0,5
	4	0,1	0,3
	5	All detected	All detected except horizontal (tangential)

[a] The CAD file of the star artefact correspond to the new design version S0, S1 and S2 supplied by MTC.

[b] The analysis was performed in one sample per each design.

[c] ND = Not detected.

[d] NT = Not tested.

7) Inconel is an example of a suitable product available commercially. This information is given for the convenience of users of this document and does not constitute an endorsement by ISO of this product.

Table 16 — Summary of the smallest defects detected in the final star artefact design by XCT scan in Hastelloy®8) and Maraging materials

Defect dimensions in millimetres

Design[a]	Defect region	GE-UK[b]			MTC[c]	
		Hastelloy®[d]	Hastelloy®[b]	Maraging steel[b]	Hastelloy®[c]	Maraging steel[c]
S0	All		ND[e]	ND[e]	ND[e]	ND[e]
S1	1	NT[f]	All detected	All detected	All detected in 4 stars and 6 in two stars	All detected in 5 stars and 6 in one star
	2	NT[f]	0,1	0,1	0,1	0,2
	3	NT[f]	0,4	0,3	0,4	0,5
	4	NT[f]	0,3	0,3	0,1	0,2
	5	NT[f]	0,3	0,2	0,1	0,2
S2	1	0,3	0,3	0,2	0,1	0,1
	2	0,3	0,3	0,2	0,3	0,1
	3	0,3	0,3	0,3	0,1	0,3
	4	0,1	0,3	0,3	0,1	0,1
	5	All detected	All detected	All detected	All detected in 2 stars and 6 in three stars	All detected in 1 star and 6 in four stars

[a] The CAD file of the star artefact correspond to the new design version S0, S1 and S2 supplied by MTC.

[b] The analysis was performed in one sample per each design.

[c] The analysis was performed in 6 Hastelloy® stars (design S1) and 5 stars (design S2). The nominal features diameter size reported correspond to the average of the diameter detected using the set sample per each design.

[d] Test carry out using the DYN|41 detector -100 in one sample.

[e] ND = Not detected.

[f] NT = Not tested.

11.1.1.4 Comments/observations

The XCT analysis performed on the Hastelloy®9) X, Maraging steel and stainless steel star artefacts design S1 and design S2 clearly showed that the observable defects on the three materials are very similar. Although EWI attempted to use similar parameters used from previous imaging experiments carried out at the MTC, since the Nikon 450 kV systems were the same, the results achieved are slightly different in contrast, resolution and accuracy.

EWI found that challenges with scattering resulted in the detectability being rather limited for the spheres with trapped powder (0,3 mm to 0,4 mm). Also, after several attempts at imaging the star face-up, tilted, and face-on, it was determined that imaging the star face on resulted in the least amount of scattering and beam hardening, thus producing the best results. Therefore, it would be recommended that pursuing CT imaging of these stars would also perform the imaging face-on.

The XCT scan carried out by GE using the Dynamic 41 100 um detector was not used to increase nominal resolution by a factor of two, but to enable sharper imaging at a lower magnification and only a more marginal increase in nominal resolution. Detectability is not dependent only on nominal resolution but a combination of factors. It was found that the quality of the image is enhancing substantially and increasing resolution capability.

8) Hastelloy is an example of a suitable product available commercially. This information is given for the convenience of users of this document and does not constitute an endorsement by ISO of this product.

9) Hastelloy is an example of a suitable product available commercially. This information is given for the convenience of users of this document and does not constitute an endorsement by ISO of this product.

11.1.2 Neutron Imaging — NI and Synchrotron radiation — SX (HZB & ESRF)

The ability of neutrons to penetrate easily through materials such as steel and titanium, revealing interior details of engineering components such as coolants channels or verifying the absence of defects such as cracks or pores made NI a unique and valuable tool. At the same time, the advent of synchrotrons enabling focalised high-energy x-rays has revolutionized tomographic methods, pushing boundaries of spatial and temporal resolution to the nanometre and microsecond.

Neutron imaging is complementary to X-ray imaging. Whereas x-rays are scattered and absorbed by the electron of an atom, neutrons interact with the atom nuclei. Therefore, some features easily visible with neutron imaging can be very challenging or impossible to be detected with X-ray imaging. Neutrons have more sensitivity than X-ray to light elements and their degree of attenuation depends on the neutron energy. For metals, a strong energy dependency of the attenuation is observed due to Bragg scattering from the crystal lattice. Even though, it is mentioned that X-ray resolution is better the than neutron method it is highly dependent on the system used and on the material, for example, new neutron imaging instruments combined with high flux sources, the resolution achieved is at the same scale (50 µm). However, a particular advantage of neutron imaging is the high penetration depth, allowing to inspect large samples with a medium resolution, which X-ray cannot do[35][36].

As with radiography, visualisation of the sample in three-dimensions is available by neutron imaging. For the tomography technique, the resultant digital projectional radiographs taken at defined rotational steps of the sample are reconstructed using algorithms similar to those used for classical X-ray computed tomography, taking into account specific beam geometry characteristics. The concept of Neutron Imaging (NI) is shown in Figure 17, but the basic set-up is very similar to that used by X-ray synchrotron radiation (SX) source. Neutron transmission through the sample leaves a neutron imprint on the scintillator screen which transforms it into photons. A mirror downstream of the scintillator reflects these photons towards a camera (CDD or sCMOS for example) placed at 90° which transforms the photons into an ensemble of digital grey scale signals (the camera is protected from the primary beam to ensure its lifetime). The whole or only the optical part is placed in a black box (enclosure sealed to light).

The resultant digital projectional radiographs taken at defined rotational steps of the sample are then reconstructed using algorithms similar to those used for classical x-ray computed tomography, taken into account specific beam geometry characteristics.

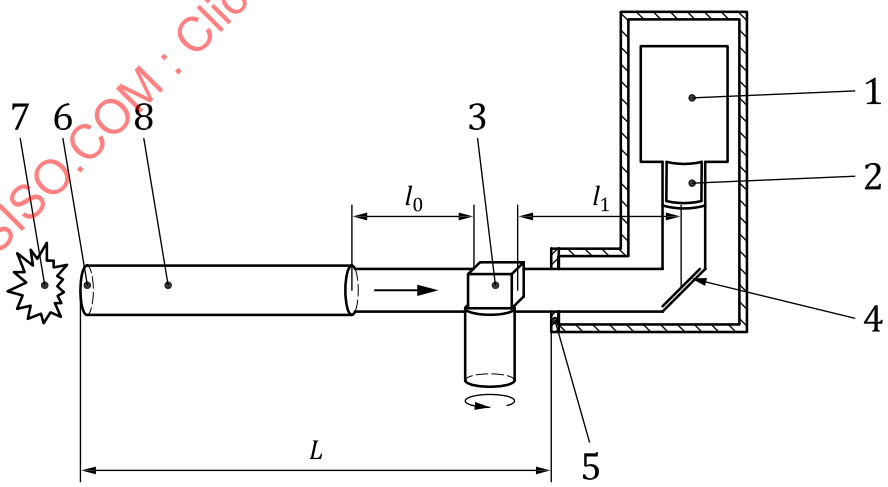

Key

1	camera CCD/CMOS	7	radiation source
2	lens	8	collimator
3	sample of thickness X	l_o	distance collimator to sample
4	mirror	l	distance sample to detector
5	scintillator	L	distance aperture source to the detector

6 aperture of diameter D

Figure 17 — Sketch showing the basics of neutron imaging (adapted from Reference [35])

Figure 17 also gives the general transmission law for photons and neutrons through the material, known as the Beer-Lambert Law. X-ray interacts with an atom's electron clouds and the probability of interaction, given by the attenuation coefficient (or the mass attenuation coefficient) is directly proportional to the element's mass number. Of course, high energy x-rays (250 keV) such as those used on ID19 have a far higher penetration than XCT laboratory machines. For neutrons, the interactions are also energy-dependent (a rule of thumb being that their absorption cross-section is inversely proportional to their speed) and can take several forms but in general absorption and scattering by the atom's nucleus are predominant. Unlike x-rays, there is no direct dependence on mass number. Therefore, the interaction of x-rays and neutrons with the material is different and complementary. For example, in transmission (radiography), light elements like H, Li, B and C absorb neutrons more readily than x-rays, and the reverse is true for heavy elements (for example metals like Fe, Al, Cu and W — with the notable exception of Gd). In addition, the neutron absorption cross-section isotopically varies for some elements, for example, 1H/2H or 3He/4He, which is not the case with x-rays.

11.1.2.1 Summary of procedure

One Cobalt-Chrome star version S2 (LNE & NIST) and two Ti6Al4V samples labelled as $S1_{EBM}$ and $S1_{SLM}$ were tested (MTC). Details of the samples can be found in Annex D, Table D.1, while a sample and drawing are shown in Figure F.1 and Figure F.2, Annex F. Samples were positioned face up and the beamline was aligned with the X-axis of the sample. Titanium star S_{EB} and S_{LB} were scanned using cold neutrons and Synchrotron radiation, while CoCr star was inspected only using monochromatic SX. A CCD camera recorded the XCT projections and those were acquired for 3D reconstruction using a mathematical algorithm. Details of the parameters used for the NI and SX test can be found in Table F.1, while the set up for NI test are shown in Figure F.3. and Figure F.4, Annex F. $S1_{SLM}$ sample was manufactured by L-PBF while $S1_{EBM}$ was build built using L-EBM as is shown in Figure F.5 and Figure F.6, Annex F.

11.1.2.2 Apparatus

For these tests, the neutron scans were led by ILL and carried out at the Helmholtz Zentrum Berlin (HZB) by beam time exchange policy (https://www.helmholtz-berlin.de/forschung/oe/ce/materialforschung/methoden/n-tomo_en.html), while the synchrotron test was performed at the European Synchrotron Research Facility (ESRF), http://www.esrf.eu/. The HZB institute has a cold neutron energy spectrum, whereas the ESFR owned the state-of-the-art micro-tomography instrument ID19.

11.1.2.3 Significance of data/interpretation of results

The results of the neutron and synchrotron test are discussed in this subclause. For the reconstructed 3D images of the titanium stars, the analysis covered first the quality of the imaging results, followed by the capability to detect the seeded defects in the region of interest (ROIs), followed by other defects noted – cracks and porosities-, and finally geometrical comparison with the 3D CAD drawing. For the CoCr star-shape, the analysis covered only the seeded geometries for the star artefact design S2 on the ROI. Comprehensive results of the analysis carried out on the titanium samples are presented from Figure 18 to Figure 22, while Figure 23 to Figure 24 show the findings for the CoCr star artefacts.

The relative quality of images is due to various parameters such as beam-hardening caused by sample geometry and thickness, along with those inherent in the use of these imaging techniques (e.g. light diffusion from neutron or X-ray/photo conversion scintillators), both sets of data underwent correction/optimisation processing to minimize artefacts. This procedure is normal and is applied to most data sets to enhance image clarity. It is clear from the images that those obtained from ID19 are superior in quality — both in resolution and in signal quality. This is due to three main imaging parameters already mentioned: the number of projections through 360° (for best spatial voxel resolution in a tomography

the number of projections needed is outlined by the Nyquist-Shannon theorem, and is given for a 360° scan). It is defined by Formula (1) as follows:

$$N_{\text{projections}} = \pi \cdot \text{Object's dimension}_{\text{pixel}} \quad (1)$$

where

π It is the mathematical constant defined as the ratio of a circle's circumference to its diameter. It is approximately equal to 3,141 592 6;

N is the number of projections recorded through a 360° scan of the object;

And the Signal-Noise Ratio described by the Poisson distribution standard deviation is defined as follows:

$$SNR = \sqrt{N} \quad (2)$$

where N is the number of equivalent incident neutrons or photons per pixel in the detector

For ID19, the SNR is maximized because each projection is an accumulation of 23 images, whereas only one image is taken for CONRAD 2. Also, these parameters are a direct consequence of the difference in photon and neutron beam intensities. Another fundamental parameter is the propagation phase-contrast which enhances the data quality. The number of projection and accumulation level is important, but without the phase contrast, increasing the dynamic of the pictures would never have brought the detection level reached. If the test would have worked in absorption only, the results obtained would have been really poor in quality. The final voxel resolution of ID19 lends itself to the detection of micro-artefacts such as pores for objects of large volumes such as these stars. Neutron imaging is also capable of detecting such surface details but for 'zooms' on smaller regions of interest.

Titanium star artefact - The results for the Titanium star reference as $S1_{(SLM)}$ inspected by NI on the seeded ROI's indicated that defects seeded on the inner faces with geometries from 0,19 mm to 1,08 mm were detected (Figure 18) and visualised by SX (Figure 19). The sample labelled as $S2_{(EBM)}$ the minimum size of the seeded defects resolved was from 0,240 mm to 1,34 mm as shown in Figure 20 and imaging by SX in Figure 21.

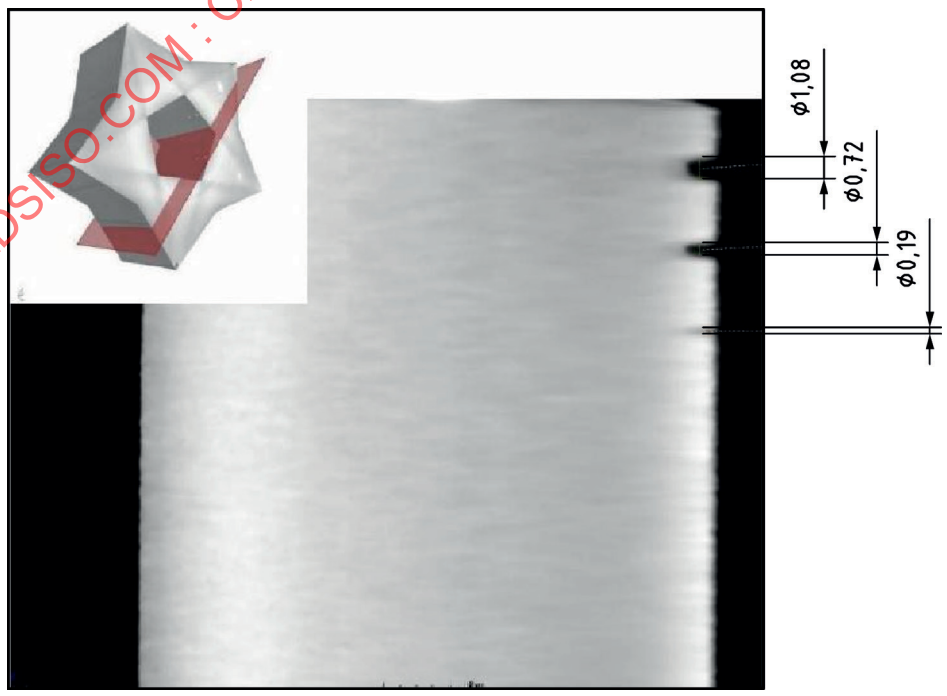

Figure 18 — Image of the sample $S1_{(PBF)}$ obtained by NI (CONRAD 2)

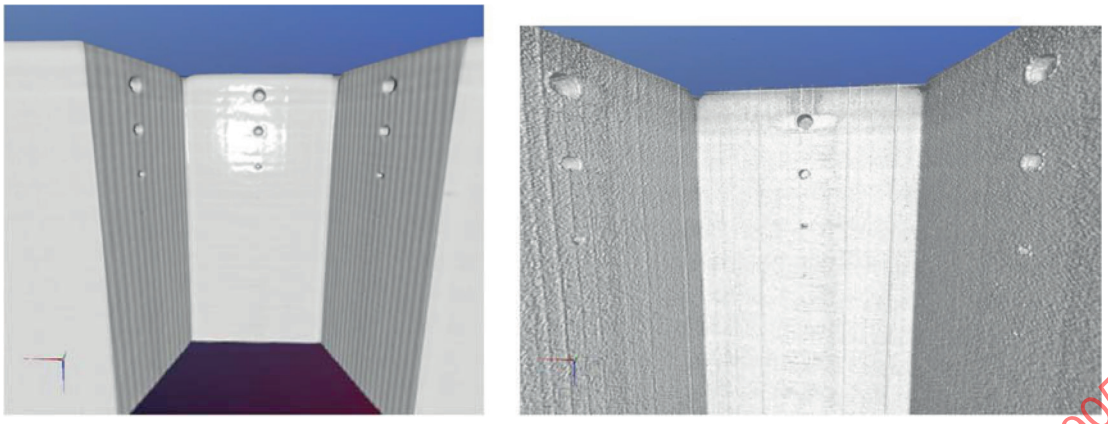

Figure 19 — Image of region 1 on sample $S1_{(PBF)}$ obtained by SX (ID19)

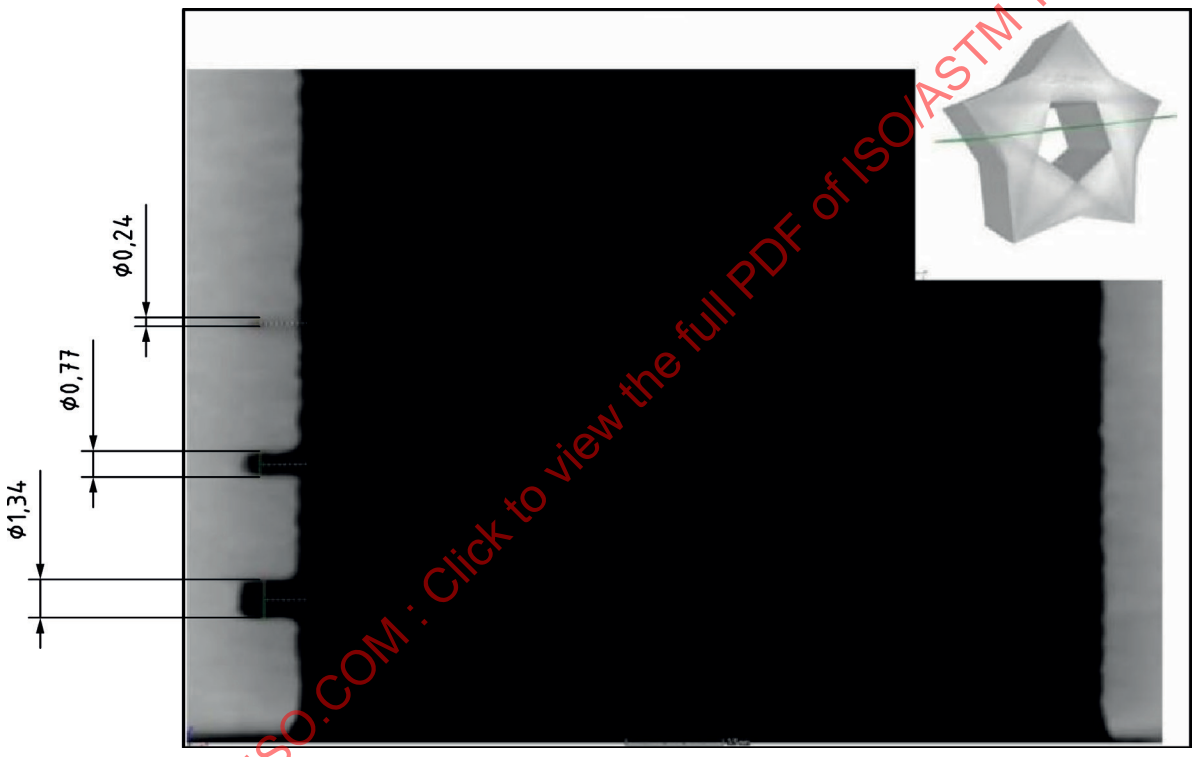

Figure 20 — NI image of the sample $S1_{(EBM)}$ obtained by NI (CONRAD 2)

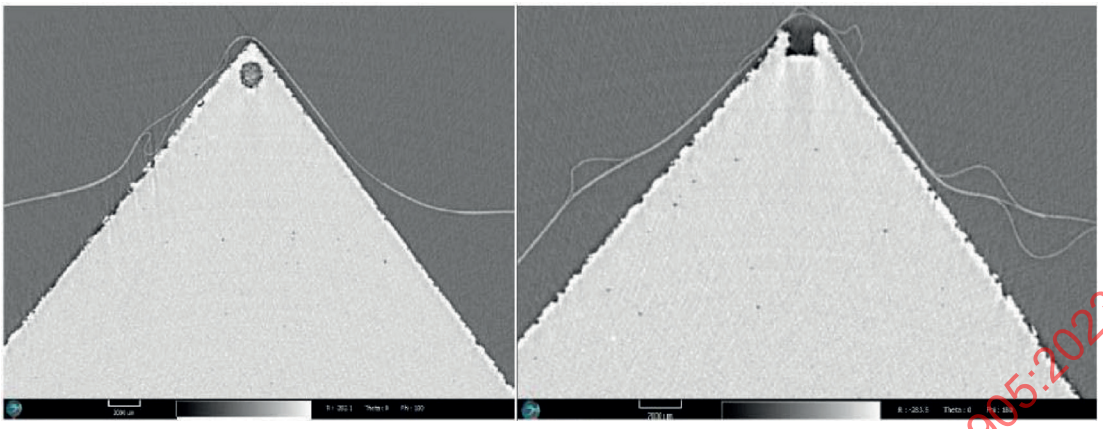

Figure 21 — Image of the sample $S1_{(EBM)}$ obtained by SX (ID19)

In addition, star $S1_{PBF}$ contain several fissures, both throughout the sample volume and particularly a large circumferential crack on one of the top surfaces. Indeed the material was relatively brittle and prone to damage at the sharp star polygon vertices edges. Reconstructed images, both from CONRAD 2 and ID19, give examples of these cracks where the height of one of them being measured at 0,690 mm. An example is shown in Figure 22. Star artefact $S1_{EBM}$ had a relatively rough surface with very large pores and surface cracks. Calculations for the sample's Fraction of Porosity accounted for 0,018 9 %.

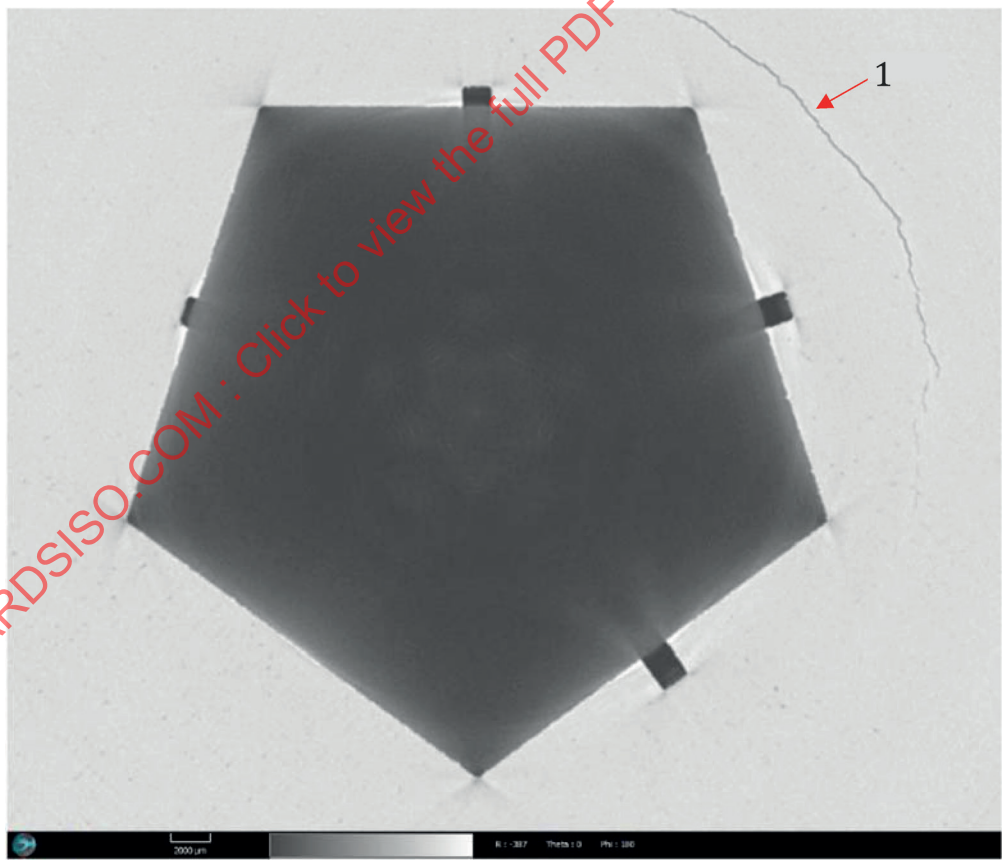

Key

1 crack

Figure 22 — SX image of the sample $S1_{(PBF)}$ manufactured via LPBF — (ID19)

Regarding the CAD drawing, some defects corresponding to other (Region 4 and 5) of created defects on the CAD drawing were not found in the XCT images, presumably because their dimensions were below the fabrication tolerances for the AM method used. Indeed, this was also the case for the defects on the inner surfaces with seven (7) of them present on the drawing, but only three apparent visualise by the naked eye on the star, and also found in the tomographical studies with both X-rays and neutrons.

Dimensional conformity of the manufactured titanium star artefact samples was carried out by NOVITOM on star $S1_{(EBM)}$. Comparing the reconstructed 3D geometry obtained on ID19 with the provided CAD drawing, the result has shown variations on dimension between a scale + 1,0 mm to — 1,5 mm. Also, the SX test was focused to emphasize surface roughness capabilities. Similar results could have been obtained with the neutron tomography data from CONRAD 2.

CoCr Star artefact - The microtomography analysis performed with the high-energy synchrotron radiation on the Co-Cr star artefacts evidenced the technique was capable to detect defects with a size over 100 µm. Figure 23 and Figure 24 show an example of the XCT images obtained from Co-Cr star version 2 in region 3 (spheres) and region 4 (vertical cylinders) respectively. In addition, the images corroborated that the AM process using the PBF EOS M290 system was capable of building all the artificial defects seeded on the CAD drawing both full-size CoCr start artefact.

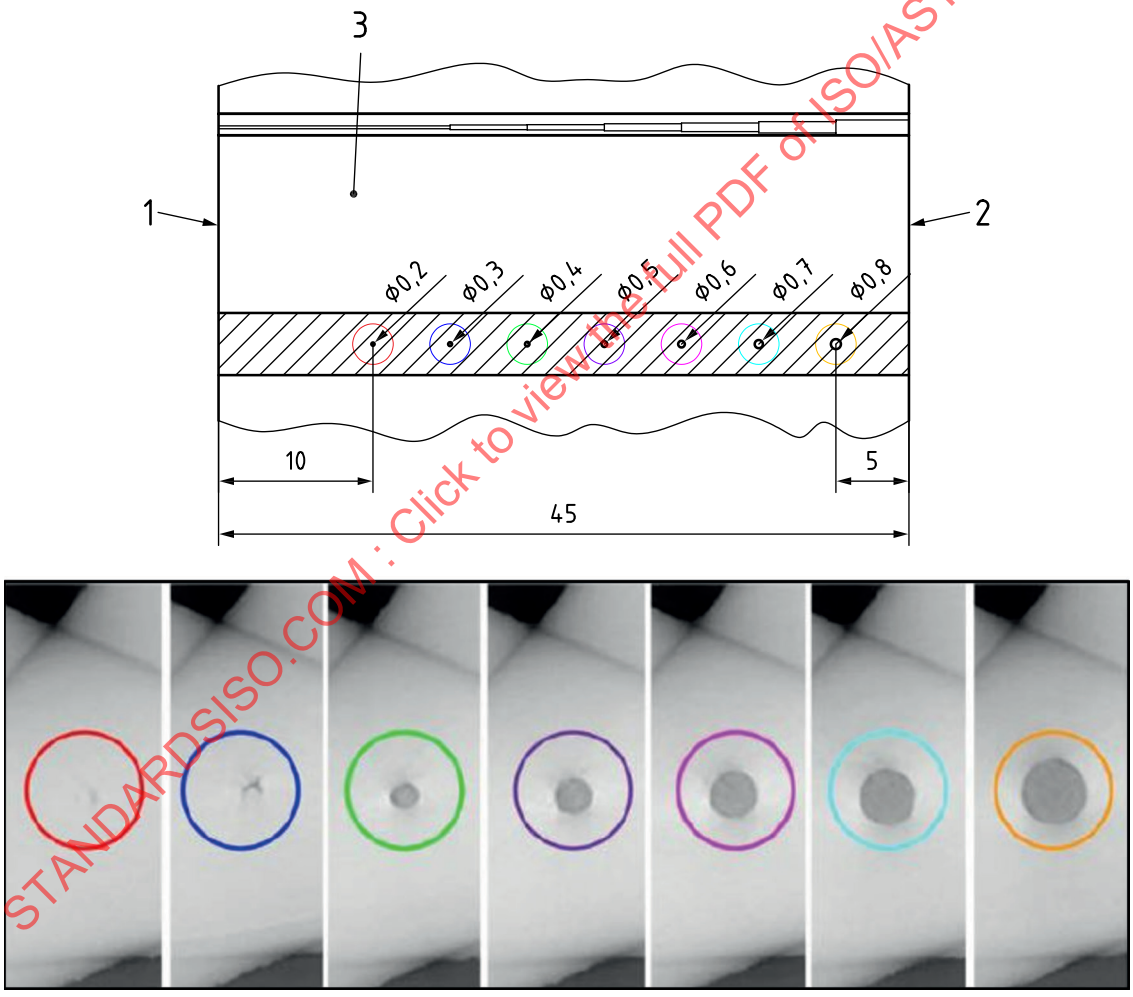

Key

1 top surface
2 bottom surface
3 region - spheres

Figure 23 — XCT results from CoCr star region 3 (S2) showing the 7 spherical cavities built in the bulk of the star, with diameter varying from 0,2 mm to 0,8 mm

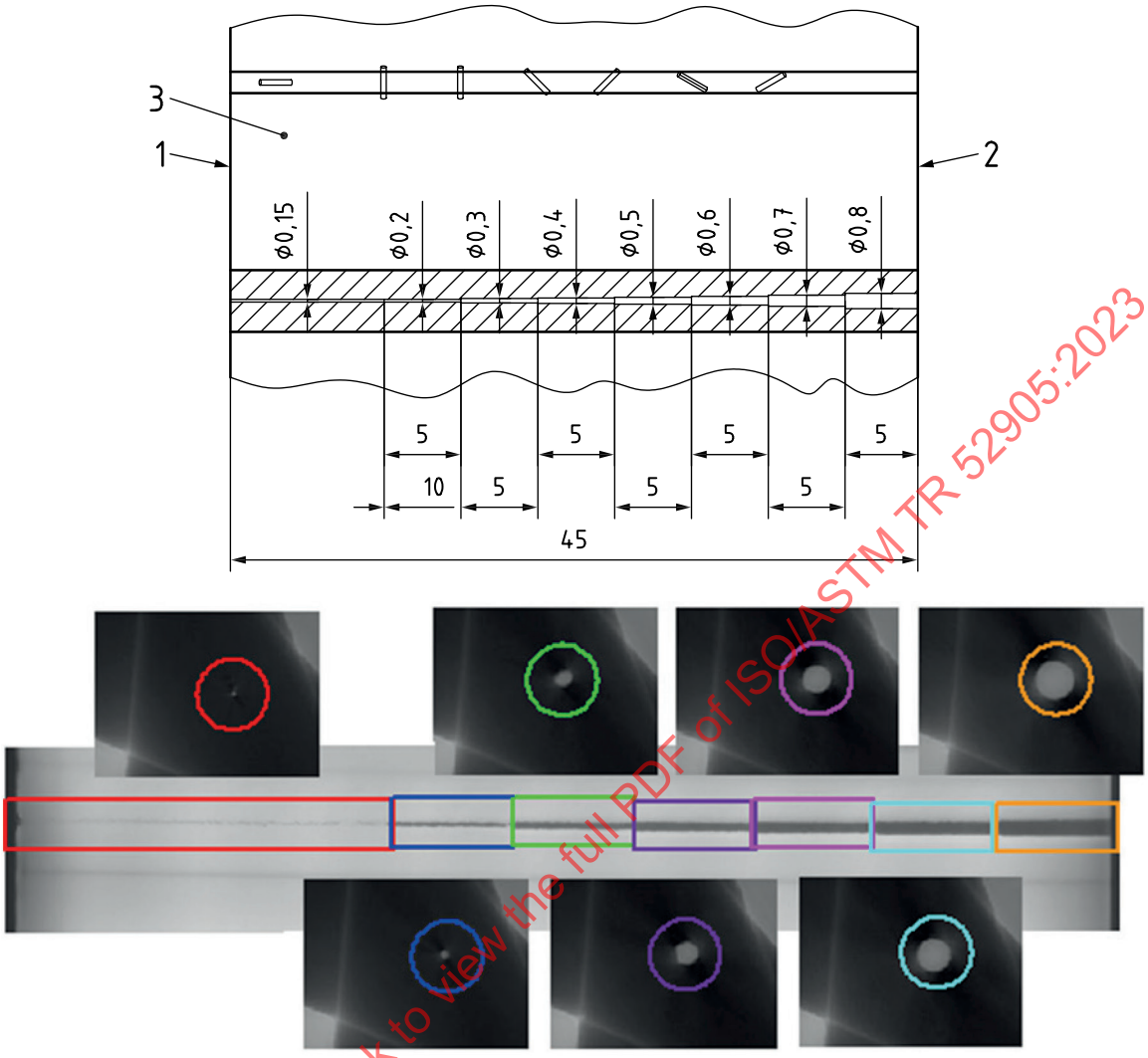

Key

1 top surface
2 bottom surface
3 region – vertical cylinders

Figure 24 — XCT results from Co-Cr star region 4 (S2) showing 8 connected vertical cylinders, open to outside on both sides of the star, 5 mm height, ⌀ vary from 0,15 mm to 0,8 mm

Table 17 gives a summary of each star artefact trailed both Titanium and Cobalt-Chrome materials and which sample was involved, whether the result was from CONRAD 2 or ID19.

Table 17 — Summary of the features detected in the star artefact by Neutron and Synchrotron in Ti6Al4V and Cobalt-Chrome alloys

Defect dimensions in millimetres

Design [a]	Defect region	Neutron CONRAD2[b]	Synchrotron ID19[c]	
		Ti6Al4V	Ti6Al4V	CoCr
SP_{SLM}	1	0,2	0,1	NT[g]
	2	0,2	0,1	NT[g]
	3	0,2	0,1	NT[g]
	4	ND[f]	ND[f]	NT[g]
	5	ND[f]	ND[f]	NT[g]
	Other [d]	Crack & pores	Crack & pores	NT[g]
SP_{EB}	1	0,2	0,2	NT[g]
	2	0,2	0,2	NT[g]
	3	0,2	0,2	NT[g]
	4	ND[f]	ND[f]	NT[g]
	5	ND[f]	ND[f]	NT[g]
	Other [d]	Crack & pores	Crack & pores	NT[g]
S2	1	NT[g]	NT[g]	0,2
	2	NT[g]	NT[g]	0,2
	3	NT[g]	NT[g]	0,2
	4	NT[g]	NT[g]	~0,15[e]
	5	NT[g]	NT[g]	All detected

[a] The CAD file to build the star artefact was supplied by MTC.

[b] Test performed at the Helmholtz Zentrum Berlin (HZB) in Germany.

[c] Test performed at the European Synchrotron Research Facility (ESRF) in France.

[d] Other defects included cracks and porosities.

[e] Size detected but cannot be sorted 0,2 mm diameter from 0,15 mm diameter.

[f] ND = Not detected.

[g] NT = Not tested.

11.1.2.4 Comments/observations

Neutron and synchrotron X-ray tomography methods, with their inherent capacity for high penetration of metals such as Titanium and Cobalt-Chrome, have been applied to inspect two Ti6Al4V artefacts and one Co-Cr star artefact fabricated using different AM techniques. The spatial resolution of both methods, being the range of 0,04 mm to 0,06 mm for these specific samples, made it possible to detect all designed-in defects at and above these dimensions as well as other defaults resultant from the respective manufacturing processes such as cracks and porosity. For optimised sample geometries, it is possible to obtain resolutions of several microns for n-imaging and in the range of 100 nm and better for synchrotron X-rays.

The results from the Ti6Al4V and Co-Cr star artefacts demonstrate without any possible ambiguity the applicability of neutron and synchrotron X-ray tomography in the non-destructive testing of modern metallic AM components for industry.

11.1.3 Thermography Testing — TT (University of Bath)

Infrared thermography (IRT) is a technique that detects radiation in the infrared range of the electromagnetic spectrum and produces images of that radiation, called thermograms. These thermal images display the amount of infrared energy emitted, transmitted and reflect for an object. The ability of objects to emit radiant energy is called emissivity while absorbed radiation is called absorptivity.

There are two basic types of thermography: passive and active. In passive thermography, the object of interest is naturally at a higher or lower temperature than the background. In active thermography, a source of energy is required to produce thermal contrasts between the object and the background. For NDT inspection, passive and active thermography has been used depending on the application being active thermography more suitable for AM process.

Active thermography approaches cover optical, mechanical and electromagnetic excitation. The main techniques used for each of these are:

— Optical (External excitation) — Pulse thermography, Lock-in or modulated thermography.

— Mechanical (Internal excitation) — Step heating thermography, Lock-in vibrothermography, burst vibrothermography and frictional heating.

— Electromagnetic (Internal excitation) — Pulsed eddy current and Induction lock-in thermography.

Here, the Pulse thermography (PT) and step heating thermography (SHT) is described in detail as these two techniques were used to inspect the star artefacts at the University of Bath.

Pulsed Thermography (PT) — PT is a rapid NDE process that uses a high-intensity pulse of light to heat the surface of a test piece via the photothermal effect. Very short duration flashes (ranging between 0,1 ms and 50 ms) are typically employed, depending on the sample thermal properties and defect depths. To quantify the material damage an IR camera with a computer is used to monitor the temperature gradients of the sample surface. Sub-surface defects reduce the conduction of heat away from the surface, decreasing the surface cooling rate compared to that of a non-defective region. The transient temperature field $T(z, t)$ in PT is obtained as a solution of an inhomogeneous one-dimensional (1D) heat equation. It is shown in Figure G.1.

Step Heating Thermography (SHT) — In SHT low-intensity step-pulse (heat source) is applied for a long period (typically from milliseconds to few seconds), thus enabling a longer heating time to locate deeper defects. Output data are measured during the application of the step-pulse and the cooling phase. The temperature response $T(0,t)$ measured at the surface of a homogeneous and semi-infinite medium is obtained as a solution of the homogeneous 1D heat diffusion equation by applying a step-pulse heating source Q_0. It is shown in Figure G.2.

11.1.3.1 Summary of procedure

Defect identification was carried out using two different thermography techniques: pulse and step-heating thermography methods. PT was carried out using a flashlight and thermal images were recorded before and after the thermal excitation. The camera was placed perpendicular to the analysed sample's surface to acquire optimal thermal images. The acquisition system was set up to acquire a certain amount of frames before the heatwave generation. Using these initial frames, background subtraction was then performed to increase the general quality of the output data. Artefacts were placed at 20 cm from the camera Oculus where the focal point was adjusted to converge on the interested surface.

This adjustment operation was performed for every analysed surface on all different samples. Reference marks were fixed on the object support to have a consistent object exposition and prospective. SHT was performed using an advanced air heating device to generate a uniform heatwave on the artefact. Different positions of heat source were used during the test to create the optimal heat distribution during heating and cooling phases in function of the analysed surface. Thermal images were recorded during both these phases. Several attempts were made to find the optimum heating position. A preliminary scan of the artefact surfaces is performed using the pulsed thermography while a more accurate analysis of the single surfaces was carried out using the step-heating thermography. For the thermography trials, the star artefacts provided by MTC were built using Hastelloy®[10] and Maraging steel. A summary of the samples built is presented in Table 18.

10) Hastelloy is an example of a suitable product available commercially. This information is given for the convenience of users of this document and does not constitute an endorsement by ISO of this product.

Table 18 — Star artefacts used during the thermography trials

Alloy	Version S0	Version S1	Version 2.
Hastelloy®	HX-S0-001	HX-S1-003	HX-S2-003
	HX-S0-004	HX-S1-004	HX-S2-004
Maraging steel	MS-S0-003	MS-S1-002	MS-S2-002
	MS-S0-005	MS-S1-003	MS-S2-005

11.1.3.2 Apparatus/settings

Table G.1 summarises the main parameters and device used during the test. Both PT and SHT used an infrared camera and a heating source. An acquisition system was used with a software package for data post-processing and image processing. To obtain noise-reduced thermal images, background subtraction was performed for each pixel.

11.1.3.3 Significance of data/interpretation of results

The analysis and results obtained from the PT and SHT test performed are reported in Table 19. The output data showed consistency among the star artefacts for the same configurations inspected. The scan performed using flash thermography of the star artefacts for all the configurations (S0, S1 and S2) covered all the regions of interest alongside the surface of the star (top, side, edges and bottom). The thermal data obtained indicated that only the regions with open surfaces defects were possible to detect as follows:

— Version S0 — No defect or damage was detected on the star built-in Hastelloy® and Maraging steel.

— Version S1 — Open surfaces defects were detected in region 4 and region 5 for star artefacts built in Hastelloy® and Maraging steel.

— Version S2 –Defects were detected in region 1 and region 2 that is an open surface for the star built-in Hastelloy® and Maraging steel.

Table 19 — Summary of the smallest defects detected in the stars artefact built in Hastelloy® and Maraging alloys by thermography

Defects dimensions in millimetres

Design[a]	Defect region	PT[b]		SHT[b]	
		Hastelloy®	Maraging steel	Hastelloy®	Maraging steel
S0	All	ND[c]	ND[c]	ND[c]	ND[c]
S1	1	ND[c]	ND[c]	ND[c]	ND[c]
	2	ND[c]	ND[c]	ND[c]	ND[c]
	3	ND[c]	ND[c]	ND[c]	ND[c]
	4	0,4	0,4	0,3	0,3
	5	0,4	0,4	0,3	0,3
S2	1	0,4	0,4	0,2	0,2
	2	0,4	0,4	0,2	0,2
	3	ND[c]	ND[c]	ND[c]	ND[c]
	4	ND[c]	ND[c]	ND[c]	ND[c]
	5	ND[c]	ND[c]	ND[c]	ND[c]

[a] The CAD file to build the star artefact was supplied by MTC.

[b] The analysis was performed on one sample per each design.

[c] ND = Not detected.

Representative thermal images using flash thermography are shown in Figure 25 and Figure 26 for Maraging steel and Hastelloy®[11] respectively. Other examples of the flash thermography images are presented in Figure G.3 and Figure G.4.

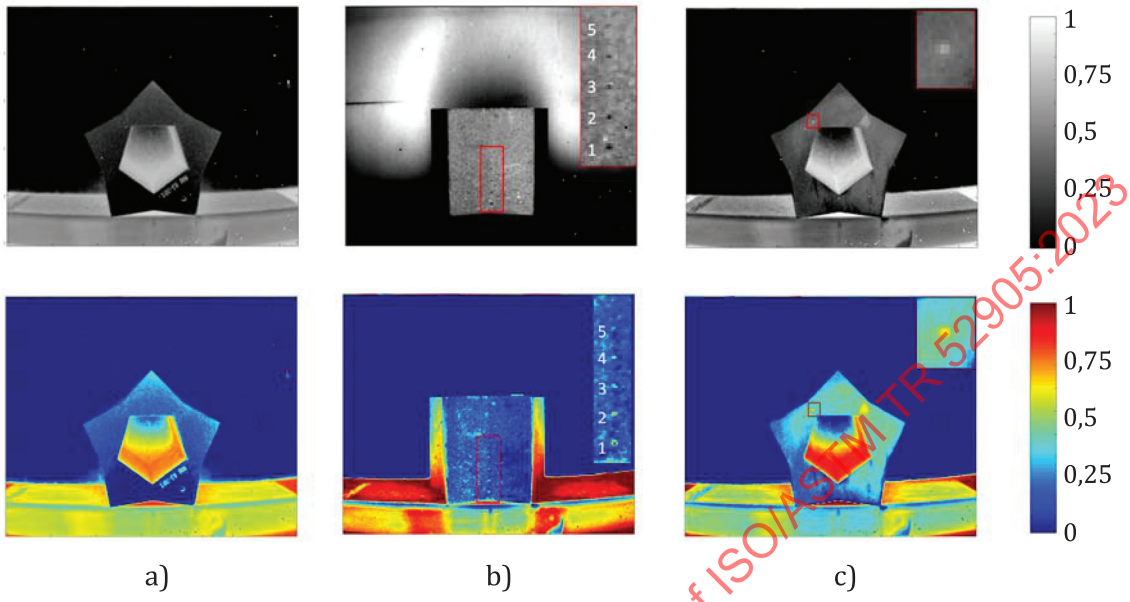

Figure 25 — Flash thermography inspection on star artefact MS-S2-002

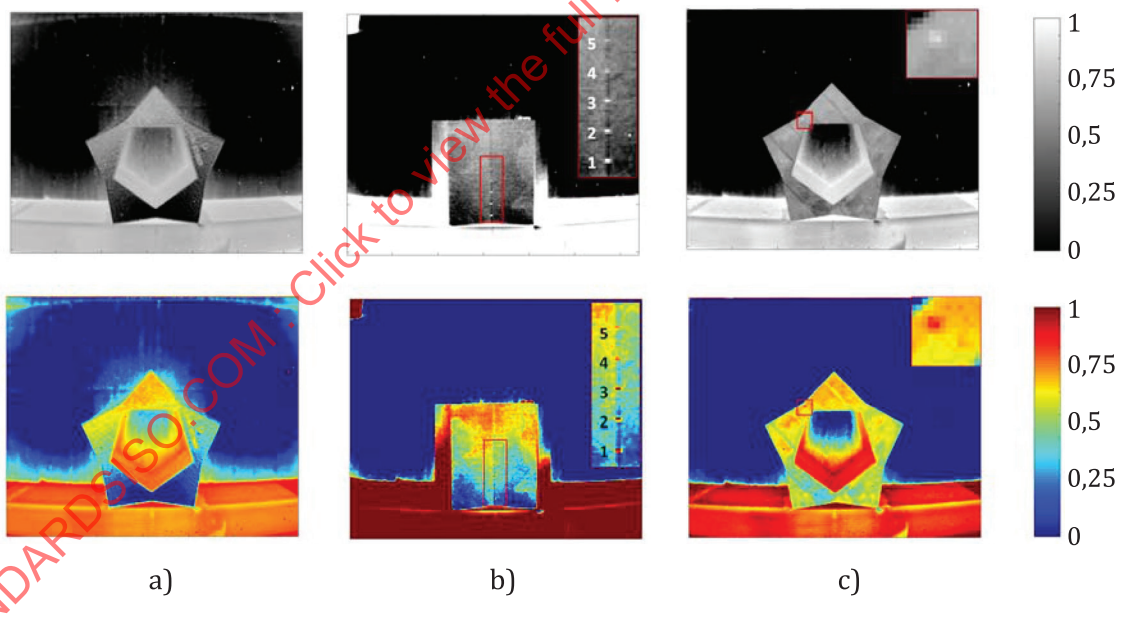

Figure 26 — Flash thermography inspection on star artefact Hx-S2-003

To establish if the defects detected with flash thermography correspond with the seeded defects indicated, Step-Heating thermography analysis was carried out. The results obtained from both the thermal images and cooling phase allowed to identify some peaks that indicated defects presence both star artefact design S1 and S2. These images correspond to the temperature-distance plots along the edge line of the star and its inner area. An example of the thermal images and the thermograms obtained for the Maraging steel (MS) for the star artefact labelled as MS-S1-003 is shown in Figure 27 and Figure 28 respectively.

11) Hastelloy is an example of a suitable product available commercially. This information is given for the convenience of users of this document and does not constitute an endorsement by ISO of this product.

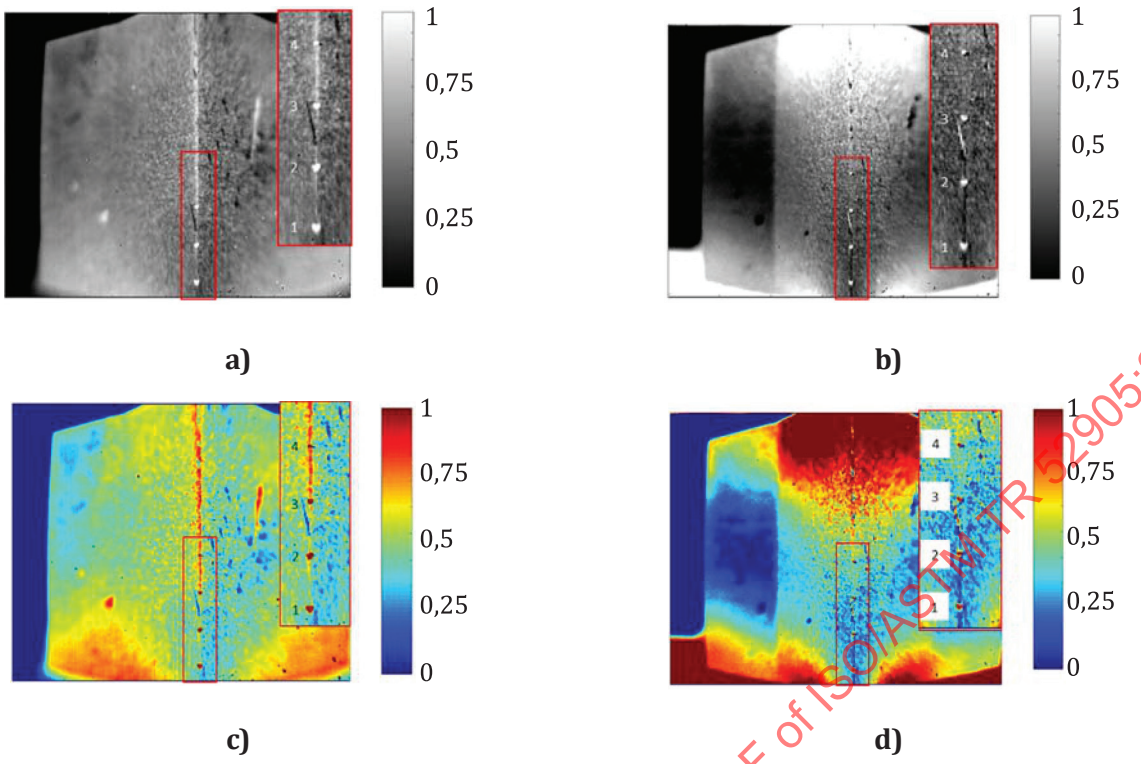

NOTE a), c) thermal images during the heating phase, b), d) thermal images during the cooling phase.

Figure 27 — Detailed analysis of artefact configuration MS-S1-003

From the thermal images, it is possible to identify the first 4 defects at greater diameter. The 5th defect is masked by superficial scratches or imperfection, and the background of the signal noise. The last two smallest defects (size 0,1 mm and 0,2 mm) are undetected due to the surface condition (rough roughness) of the artefact edge due to the manufacturing process or further damage due to handling of the part. Defects on the inner surface of the star artefact (region 5) were also detected (Figure 29) but the plot is not presented here, as it seems similar.

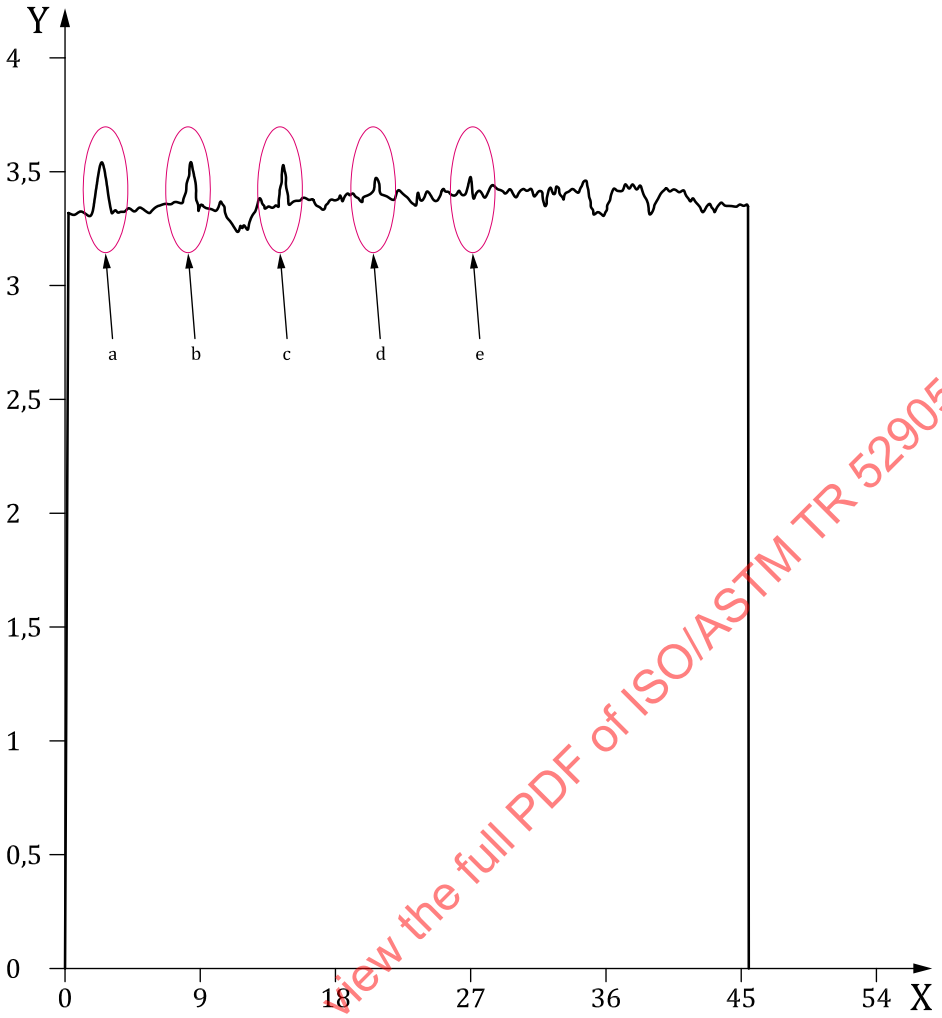

Key

X distance, mm

Y temperature, digital levels

[a] Defect 1 = 0,7 mm.

[b] Defect 2 = 0,6 mm.

[c] Defect 3 = 0,5 mm.

[d] Defect 4 = 0,4 mm.

[e] Defect 5 = 0,3 mm.

NOTE Distance - temperature plot during cooling phase at region 4 (edge line of the artefact) where the peak highlighted in circle red correspond to five open surface defects detected.

Figure 28 — Star artefact MS-S1-003

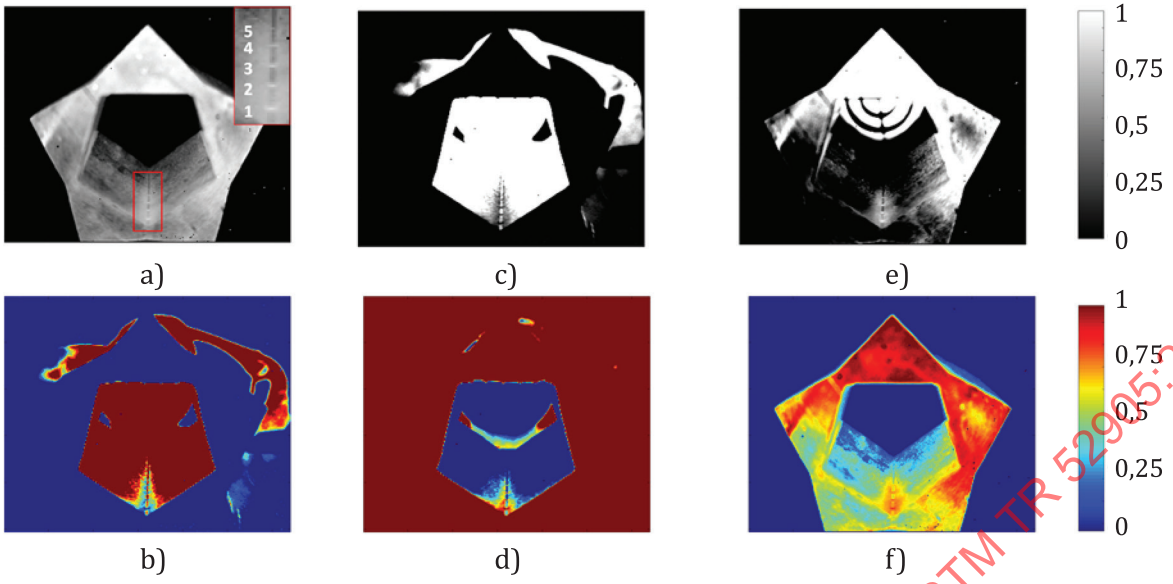

NOTE Thermal images of the inner defects of Region 4 (a, b, c, e, f).

Figure 29 — Star artefact MS-S1-003

Figure 30 show a detailed analysis of artefact HX-S2-004. From the images, the presence of defects aligned along the curvature of the part is visible. Using the thermal images, it is possible to detect five defects on the relative surface with possible detection of the two remaining ones.

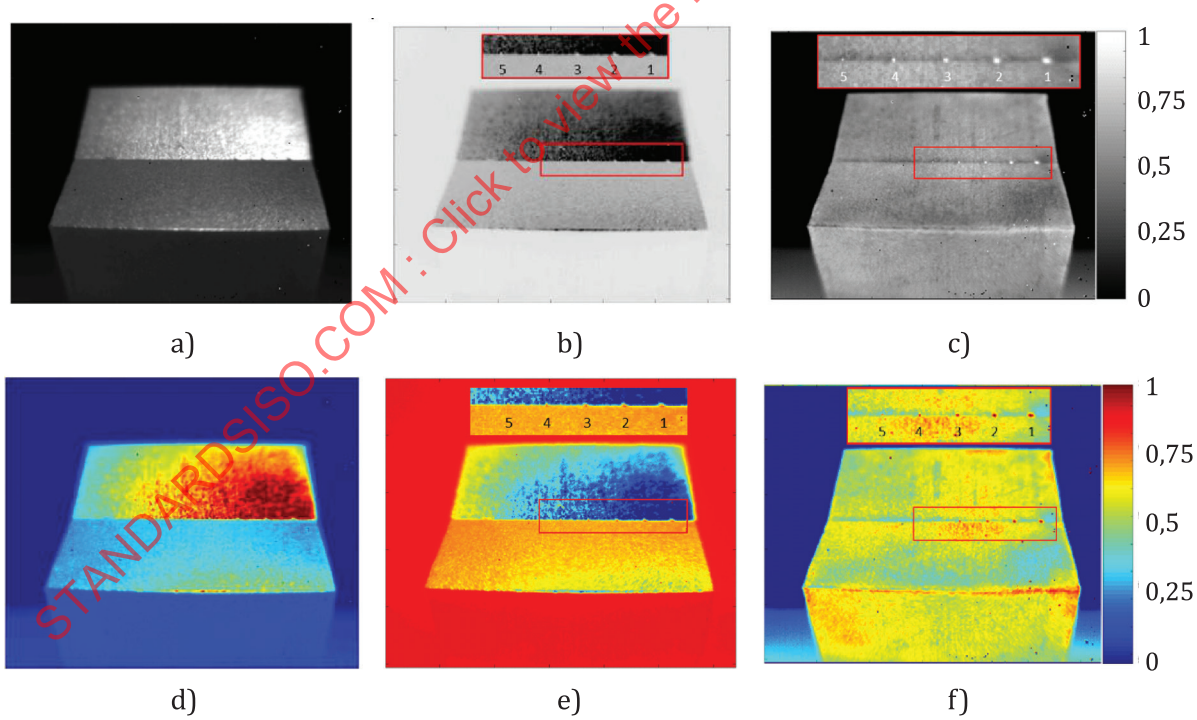

NOTE Thermography images showing the five defects detected by the SHT approach. a, c) thermal images during the heating phase, b, d) thermal images during cooling phase (early), and c, f) thermal images during cooling phase (late).

Figure 30 — Star artefact HX-S2-004

From the x-distance-temperature plot, each peak indicates a different defect. Five peaks are identified and an average inter-distance of 6 mm is evaluated (see Figure 31). For the two smallest defects, their peaks are partially masked with the background noise but still visible. To reduce the background noise masking effect, the area was zoomed and a detailed view of the last smallest 4 defects is shown in Figure 32. From the plot, it is possible to identify the defect with 0,2 mm diameter, however, the smallest one (0,1 mm) is not distinguishable from the noise background.

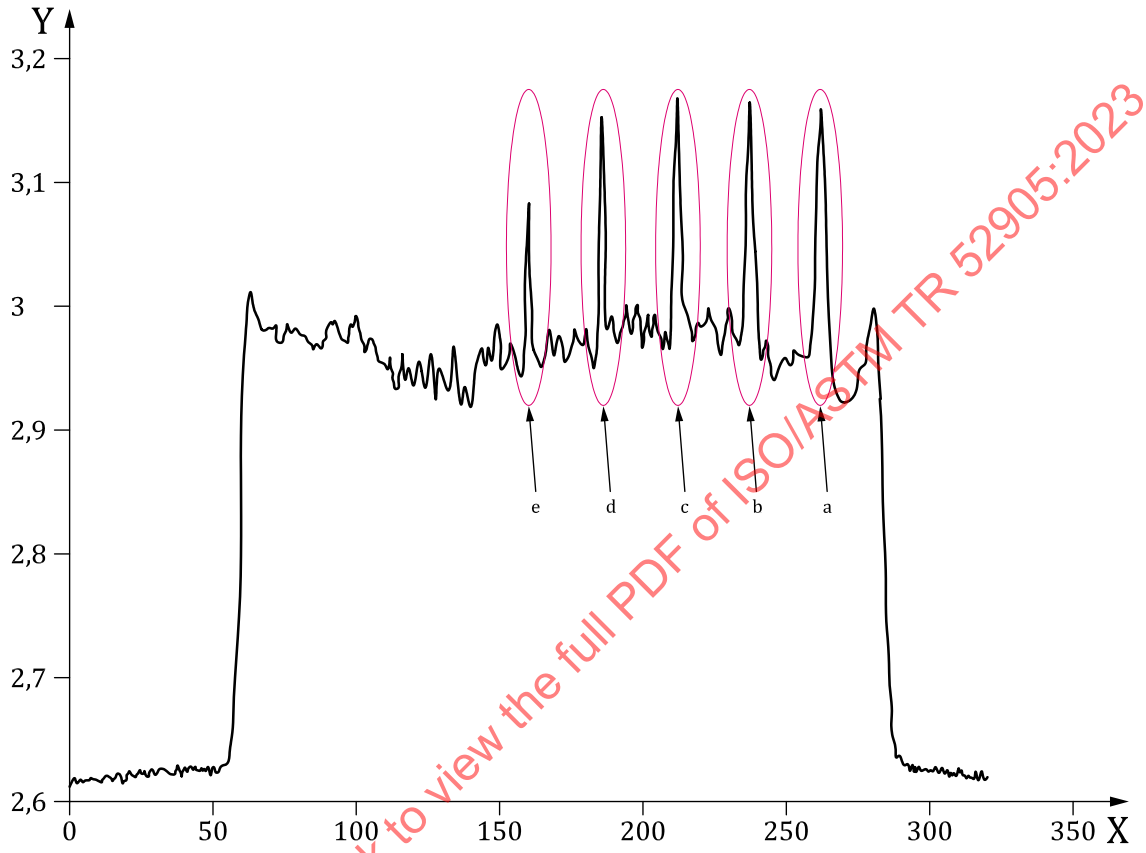

Key

X distance, pixels

Y temperature, digital levels

[a] Defect 1 = 0,7 mm.

[b] Defect 2 = 0,6 mm.

[c] Defect 3 = 0,5 mm.

[d] Defect 4 = 0,4 mm.

[e] Defect 5 = 0,3 mm.

NOTE Distance - temperature plot during cooling phase at region 2 (edge line of the artefact) where the peak highlighted in circle red correspond to five open surface defects detected.

Figure 31 — Star artefact HX-S2- 004

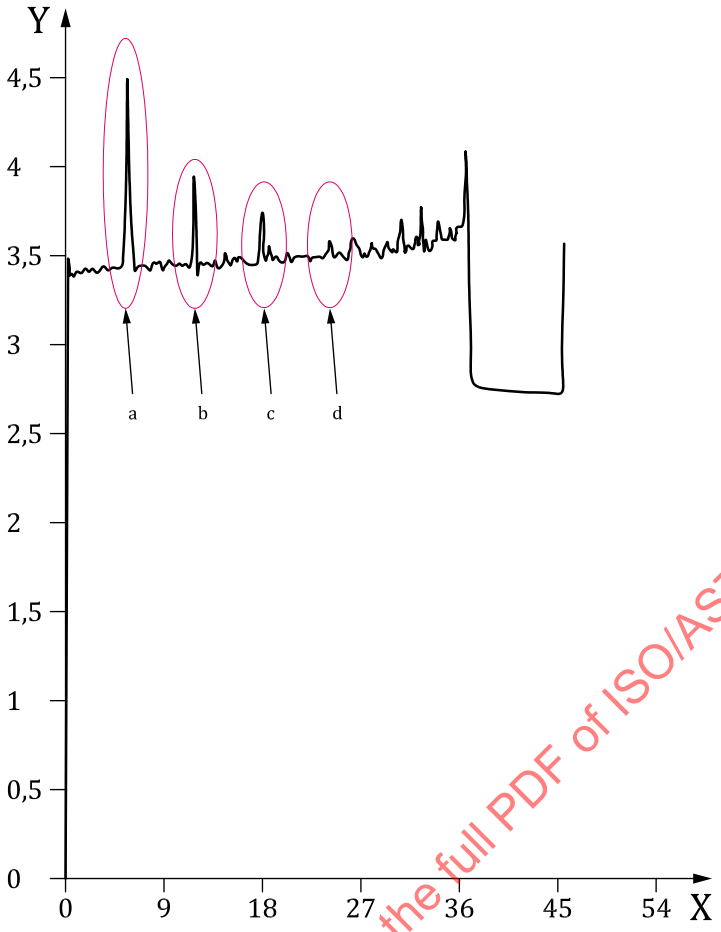

Key

X distance, mm

Y temperature, digital levels

a Defect 1 = 0,7 mm.

b Defect 2 = 0,6 mm.

c Defect 3 = 0,5 mm.

d Defect 4 = 0,4 mm.

NOTE A close-up view for the distance - temperature plot during the cooling phase at region 2 shown the smallest defects detected by the SHT method.

Figure 32 — Star artefact HX-S2- 001

11.1.3.4 Comments/observations

The results of defect imaging using thermal wave techniques in three different configurations of two different star artefacts (HX and MS) made via additive manufacturing were presented. Defect identification was carried out using two different thermography techniques: pulse and step-heating. From the analysis, it is concluded that open surface defect can be detected using the thermography approach, but limited for internal defects. It was observed that defects with a diameter greater than 0,4 mm are detected using flash thermography. The step-heating method shows that it is capable to detect open surfaces defects not less than 0,2 mm in diameter. Some limitations of the method are due to the high diffusivity and thermal conductivity of metallic materials.

11.1.4 Resonant Ultrasound Spectroscopy methods — RUS

PCRT and RAM both belong to the normalised resonant ultrasound spectroscopy (RUS) methods[37]. There are whole-body or bulk techniques. These are pass/fail assessments, which do not provide location or morphological detail. These inspection approaches compare the frequency spectrum of the mechanical resonances of a set of reference parts, known as “good parts”, with the frequency spectrum of the mechanical resonances of the test parts. These are based on a fundamental physical property of solid object meaning any rigid component will resonate at specific frequencies that are a function of its mass, shape, and material properties. Material alterations or flaws, process deviations, raw material inputs and service fatigue can change the normal resonant pattern of components.”

11.1.4.1 Process compensated resonance testing — PCRT (MTC and vibrant NDT and LNE/NIST)

PCRT is based on a fundamental physical property of solid objects meaning any rigid component will resonate at specific frequencies that are a function of its mass, shape, and material properties. Material alterations or flaws, process deviations, raw material inputs and service fatigue can change the normal resonant pattern of components. PCRT systems combine proprietary software algorithms that detect structural changes in components and compensate for normal manufacturing parameter variations that may obscure out-of-specification conditions.

PCRT can be applied in many different ways depending on the customer’s need. Applications may make use of targeted defect detection, outlier screening and/or part-to-itself comparisons. All of these applications use PCRT’s proprietary software to develop sorting modules that evaluate the frequency responses of tested components. With the sorting modules developed, the software provides rapid, accurate, and operator-independent pass/fail assessments. This can increase production yield, optimize part life, and significantly reduce field failures of components.

11.1.4.1.1 Summary of procedure

The PCRT System has to be configured for a given component prior to testing. The following task needs to be performed for each test including:

— hardware development;

— temperature compensation characterization;

— development of broadband;

— creation of design database;

— creation of sorting module.

A typical configuration of a PCRT system is shown schematically in Figure 33.

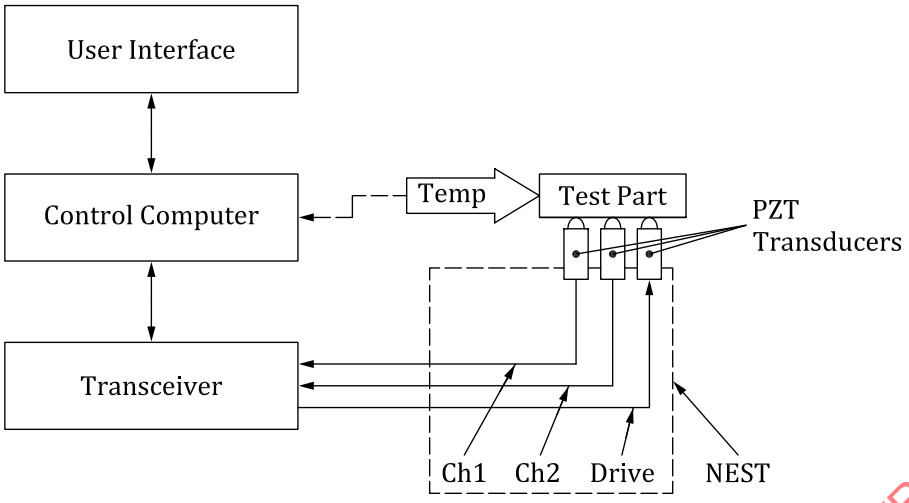

Figure 33 — Typical PCRT system schematic

11.1.4.1.2 Apparatus/settings used

PCRT excites the part and records the resonance response with three piezoelectric transducers. The transducers contact the part directly with no couplant or other interfacing material required. One transducer acts as the transmitter, exciting the part with a swept sine input. The other two transducers are the receivers. Figure 34 presents the PCRT testing fixture used to obtain resonant spectra of the parts.

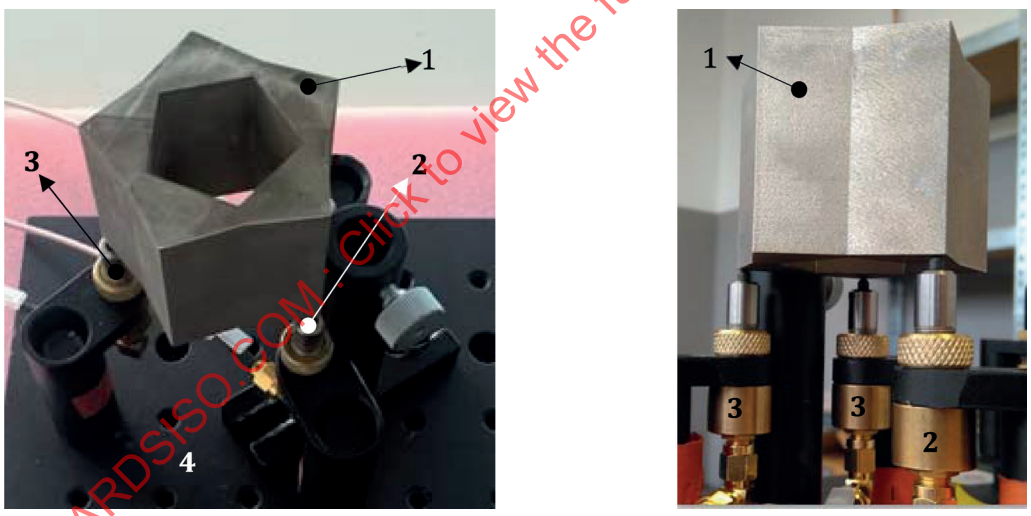

Key

1 star artefact
2 transmitter
3 receiver
4 support table

Figure 34 — PCRT Fixture showing piezoelectric transducer configuration and star position during the test

To build the fixture different locations for the three transducers and different positioning of the part were examined to determine the design that provides the best resonant data. One PCRT resonance data

was collected at Vibrant GmbH (Hastelloy®[12]) X and Maraging steel) while the other data was gathered at Vibrant USA (Stainless Steel). MTC supplied to Vibrant (Germany) 31 full-size star artefacts AM samples in three different designs and made of two different materials. Table 20 below summarizes the population and materials under study.

Table 20 — Summary of total star artefacts and materials used for the PCRT test at the MTC

Centre	Material	Number of parts			Total parts
		Good parts	Seeded parts		
		S0	S1	S2	
MTC	Hastelloy®	5	5	5	15
	Maraging steel	5	5	6	16

Seventy-four half stars (the height and width of the S0, S1 and S2 designs are divided by 2 but not the defects) with different numbers of defects were manufactured in stainless steel 17-4 (SS) originated from two very similar builds (i.e., the same location on the AM build platform, with two or three marginally different parts added on the platform between the first and second build). The number of stars manufactured regarding their design and the build is summarized in Table 21.

Table 21 — Summary of total star artefacts and materials used for the PCRT test at NIST & LNE

Material	Reference star	Specificities	Number of parts	
			Build 1	Build 2
Stainless steel 17-4	S0	Half	18	20
	S1		0	4
	S2		0	4
	S2	Half without defect in Region 1	4	3
	S2	Half without defect in Regions 1 and 2	4	3
	S2	Half without defect in Regions 1, 2 and 3	4	3
	S2	Half without defect in Regions 1, 2, 3 and 4	4	3

11.1.4.1.3 Data collection

— MTC

For the study of the Hastelloy®[13] X samples a usable resonance range of 8 kHz to 250 kHz was established in which a total of 49 usable resonance frequencies were identified. For the Maraging steel a functional resonance range of 12 kHz to 202 kHz was established, in which a total of 85 usable resonance frequencies were identified. These frequencies provide the basis for the later population analysis. To reject any potential influence of the fixture on the data acquisition and to assure the repeatability of the measurements one of the good parts was selected for the HVT (Hardware Verification Test). In eight measurements with the HVT part, the repeatability of each of the 49 resonance frequencies for the Hastelloy® and 85 for the Maraging steel used in the analysis was tested. The deviations ranged was 0,003 % to 0,051 % in Hastelloy® and 0,001 % to 0,035 % in Maraging steel, therefore, ensuring the accuracy and consistency of the study.

Figure 35 below shows a section of the resonant fingerprint of the Hastelloy® X samples where resonance frequencies 5 to 10 are recognized (each horizontal line represents an individual part) are

12) Hastelloy is an example of a suitable product available commercially. This information is given for the convenience of users of this document and does not constitute an endorsement by ISO of this product.

13) Hastelloy is an example of a suitable product available commercially. This information is given for the convenience of users of this document and does not constitute an endorsement by ISO of this product.

identified. It is observable that the frequencies move to the left in the S2 parts, whereas the S1 parts spectrum is slightly skewed to the left but looks more similar to the good parts. Figure 36 shows a section of the resonant fingerprint of the Maraging steel stars artefact, where resonance frequencies 58 to 61 are identified. It is interesting to notice that the frequencies of part MS-S0-003 (which is considered a good part) move all significantly to the left.

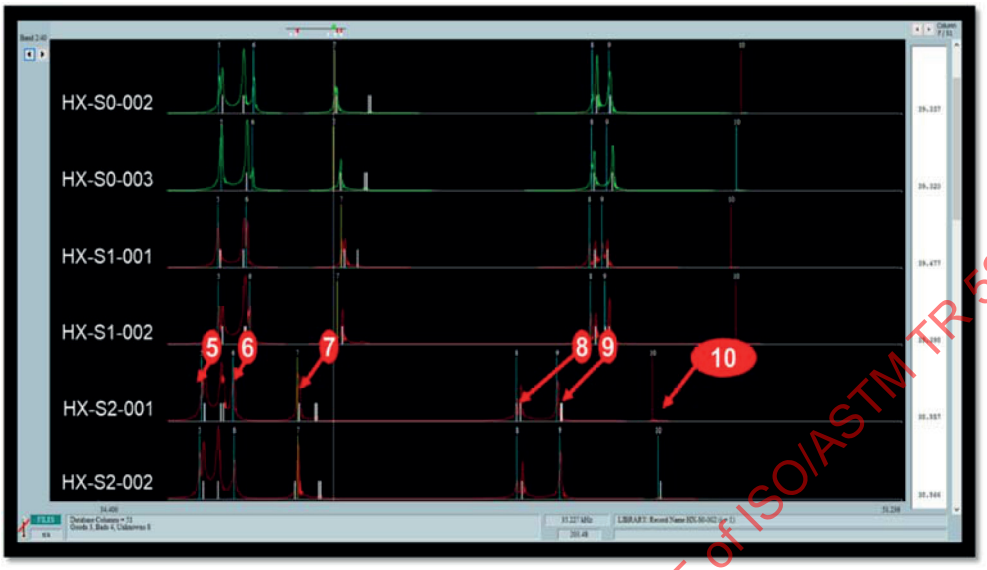

Figure 35 — PCRT spectra for Hastelloy®, 34 kHz to 51 kHz (resonance frequencies 5 to 10)

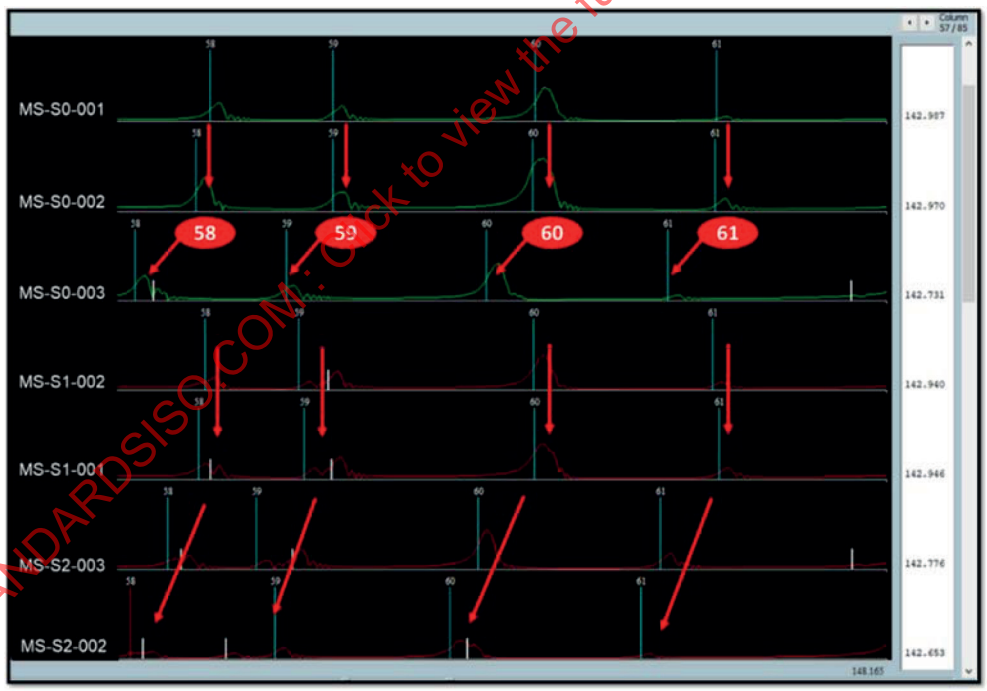

Figure 36 — PCRT spectra for Maraging steel, 144 kHz to 148 kHz (resonance frequencies 58 to 61)

— LNE & NIST

For each part, data were collected between 25 kHz and 225 kHz and then processed using Z-score and MTS analysis. The tests scanned six resonant peaks (60 kHz, 70 kHz, 110 kHz, 116 kHz, 132 kHz, 180 kHz) and the calculations are based on those six frequencies. The data collection settings and

scoring criteria were identical for both builds in the sample population. The shift in frequency between good and bad parts is not the same for every resonant peak. To deal with this, the proprietary pattern recognition VIPR (for Vibrational Pattern Recognition) algorithm is used to differentiate the parts with defects from the parts with no defects.

11.1.4.1.4 Significance of data/interpretation of results

— MTC

To characterise and compare populations, Vibrant used the Z-Score analysis and the VIPR analysis. A Z-score diagram shows the average Z value across all frequencies on the horizontal axis and the standard deviation in the vertical axis for each part. Using the Z-score approach on a population of parts allows to effectively screen for parts that mismatch the approved and confirmed resonant pattern, which is usually an indication for production or in-service anomalies associated with a higher risk of failure. VIPR (Vibrational Pattern Recognition) analysis is used to separate populations of parts when target defects are known. By looking at the frequency pattern relations, patterns are isolated that allow the best separation between the training set of OK and NOK parts.

Z-Score Analysis: The Z-score plot shows the distribution of the Hastelloy®[14] X samples population, where the red rectangular boundary represents a confidence interval of 99 %. Parts inside the confidence interval follow a similar frequency pattern to the average of the good population, whereas parts outside mismatch this pattern. An example of the Maraging steel analysis is shown in Figure 37.

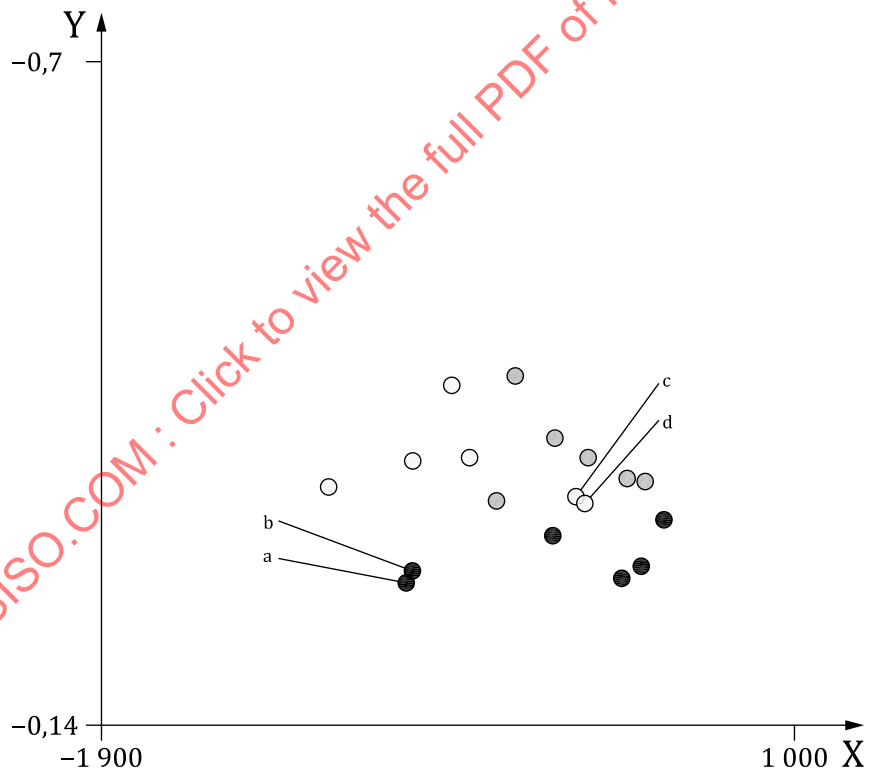

Key

X average Z-scores (across all peaks)
Y standard deviation average Z-scores
a star S0-003 (2nd).
b star S0-003 (1st).
c star S2-001 (1st).
d star S2-001 (2nd).

14) Hastelloy is an example of a suitable product available commercially. This information is given for the convenience of users of this document and does not constitute an endorsement by ISO of this product.

● S0
◎ S1
○ S2

Figure 37 — Example of the Maraging steel analysis

Even considering the small number of parts under study (in terms of statistical representability), the following conclusions can be deduced:

— The three different groups of parts for Hastelloy® and Maraging steel have been identified and are separated from each other.

— All S0 parts are inside the confidence interval limits and grouped around the centre of the rectangle, indicating that they are very similar one to another.

— S2 parts fall very far from the confidence interval, which shows that their resonant pattern differs distinctly from the pattern of the population of good parts (they "look" very different). It can also be noticed that S2 parts are lighter than S0/S1 parts and this fact also influences the results.

— Some S1 parts are inside the limits but they show a tendency to move to the upper left area. Their resonant pattern is different from that of the S0 parts but less pronounced than in the S2 parts.

VIPR analysis: VIPR (Vibrational Pattern Recognition) analysis is used to separate populations of parts when target defects are known. By looking at the frequency pattern relations, patterns are isolated that allow the best separation between the training set of OK and NOK parts. In this analysis, the reliability of the training set classification (OK/NOK) is of the utmost importance, as VIPR's results can be compromised if parts are misclassified. Figure 38 shows an example of the VIPR representation for the Hastelloy®[15] X samples population. Parts are classified based on the Mahalanobis-Taguchi System (MTS), which is a measure of similarity. The further from the MTS limit a part falls, the more "different" to the OK population is. The same analysis was performed for the Maraging steel artefacts.

15) Hastelloy is an example of a suitable product available commercially. This information is given for the convenience of users of this document and does not constitute an endorsement by ISO of this product.

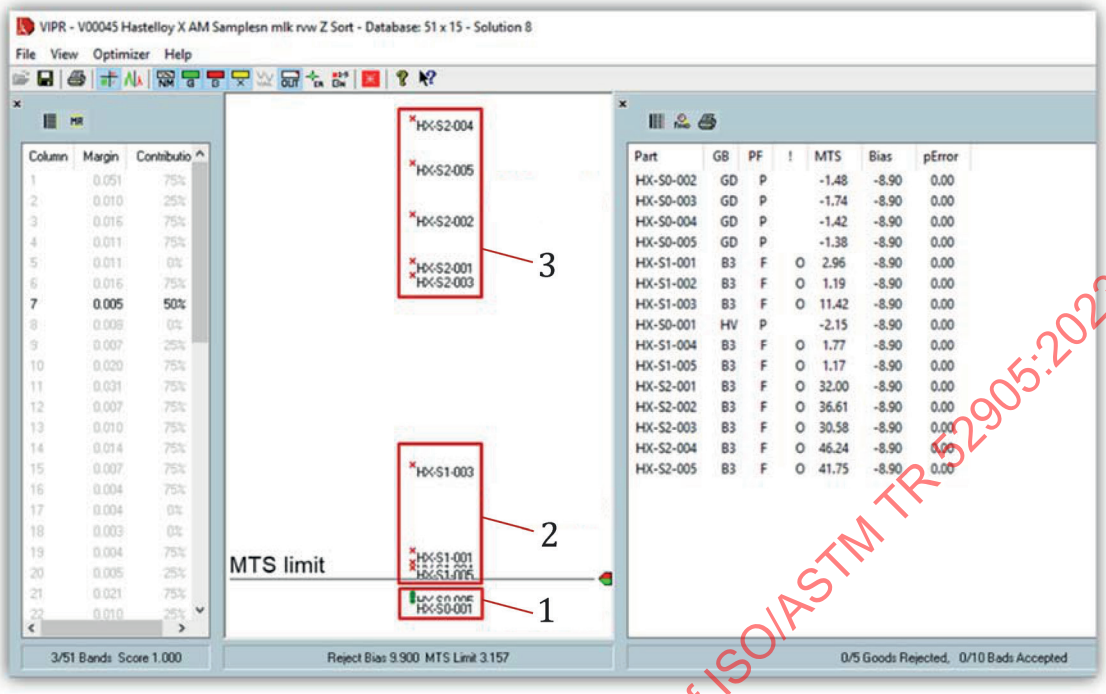

Key

1 samples pass

2,3 samples fail

Figure 38 — VIPR analysis Hastelloy® X samples

The results of the PCRT trials are summarised in Table 22.

Table 22 — Summary of the results of the PCRT test on Hastelloy® and Maraging steel full-size star artefacts

Material	Reference star	PCRT test	
		Pass	Fail
Hastelloy®	S0	4	1
	S1	0	5
	S2	0	5
Maraging steel	S0	4	1
	S1	0	6
	S2	0	5

LNE & NIST

The overall results of the test on the SS star artifacts are presented in Table 23.

Table 23 — Summary of the results of the PCRT test on stainless steel half-star artefacts

Reference star	Build 1		Build 2	
	Pass	Fail	Pass	Fail
Good parts (S0)	18	0	20	0
Bad parts with defects (S1 and S2 half star artefacts)	0	24	0	12

11.1.4.1.5 Comments/Observations

The following conclusions can be stated for the MTC analysis:

— VIPR can sort good and bad parts.

— The three different groups of parts (S0/S1/S2) are identifiable.

— S2 parts look “much more different” to the good parts than S1 parts.

— S0 parts are tightly grouped, which means that they are very similar between them.

— Deviation between parts is bigger within S1/S2 parts.

The main conclusions of the trials carried out at LNE and & NIST stated that PCRT enabled to sort the good parts from the ones with internal defects. However, the parts could not be sorted by the number of defects they contain. The main benefits of PCRT are:

— no restriction in size and shape,

— able to identify defective parts,

— fast and easy to use,

— part set-up required is minimum.

While the drawbacks of PCRT are stated as

— not possible to identify the type or location of defects in the part, and

— further investigations of PCRT are needed to address AM defects such as more accurate statistical tools to analyse the results.

11.1.4.2 Resonance acoustic method — RAM (LNE and NIST and TMS)

In the resonant acoustic method (RAM), the excitation of the test part is done by an impact hammer and the resulting acoustic frequency data is obtained with a microphone. There are no contact probes that need to interact with the test part. The output of the microphone is converted into a frequency spectrum using a high-speed analogy to a digital converter performing a fast Fourier transform to determine resonant peaks. Finally, a statistical analysis conducted with software reveals if the test parts fall within the defined criteria or not. If at least one of the measured resonant peak frequencies of the test part lays outside of the established frequency ranges of the good part, the test part is considered bad. For a part to pass RAM testing, it must pass every individual criteria point. For a part to fail RAM testing, it only needs to fail one criteria point.

11.1.4.2.1 Summary of procedure

— Mechanical impulse, with the hammer, of the test part to measure its natural resonant frequencies;

— Monitoring, by a microphone, of the response of the test part to acquire its frequency spectrum;

— Comparison of the spectrum of the test parts with the spectrum of the reference parts:

1) identification of the well-defined resonant peaks based on testing a reference set of good and bad parts;

2) selection of a subset of resonant peaks that are consistent for all reference parts and have distinct separation with the peaks of the test parts;

3) evaluation of the ranges in variations in each selected resonant peak frequency of the reference parts to define criteria;

4) sorting of the test parts with regard to the criteria to sort the pass/fail test parts.

Eighty-eight half-sized stars (the height and width of the S0, S1 and S2 designs are divided by 2 but not the defects) with different numbers of defects were manufactured in stainless steel 17-4 originated from two very similar builds (i.e., the same location on the AM build platform, with two or three marginally different parts added on the platform between the first and second build). The number of stars manufactured regarding their design and the build is summarized in Table 24.

Table 24 — Summary of the Stainless Steel half-sized star artefacts used during the RAM trials

Material	Reference star	Specificities	Number of parts	
			Build 1	Build 2
Stainless steel 17-4	S0	Half	20	20
	S1		4	4
	S2		4	4
	S2	Half without defect in Region 1	4	4
	S2	Half without defect in Regions 1 and 2	4	4
	S2	Half without defect in Regions 1, 2 and 3	4	4
	S2	Half without defect in Regions 1, 2, 3 and 4	4	4

11.1.4.2.2 Apparatus/settings used

The data were collected in the frequency range between 500 Hz and 50 kHz using the setup display in Figure 39.

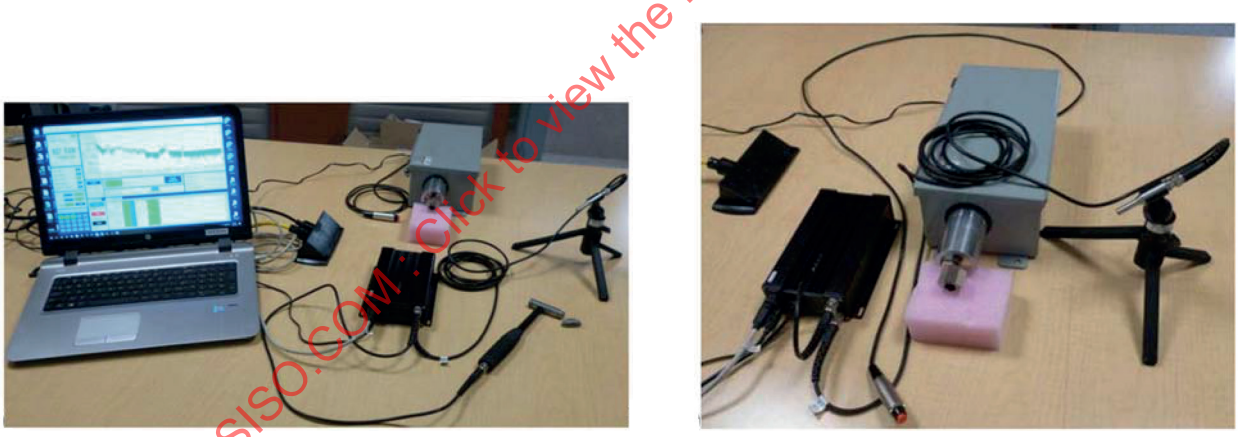

a) Global set up

b) Positioning of the star artefact in front of the automatic hammer

Figure 39 — Experimental set up for RAM tests

11.1.4.2.3 Significance of data/interpretation of results

Considering the defined criteria and analysing spectra such as the one display in Figure 40, the sorting of the Stainless Steel (SS) parts was performed (see Table 25).

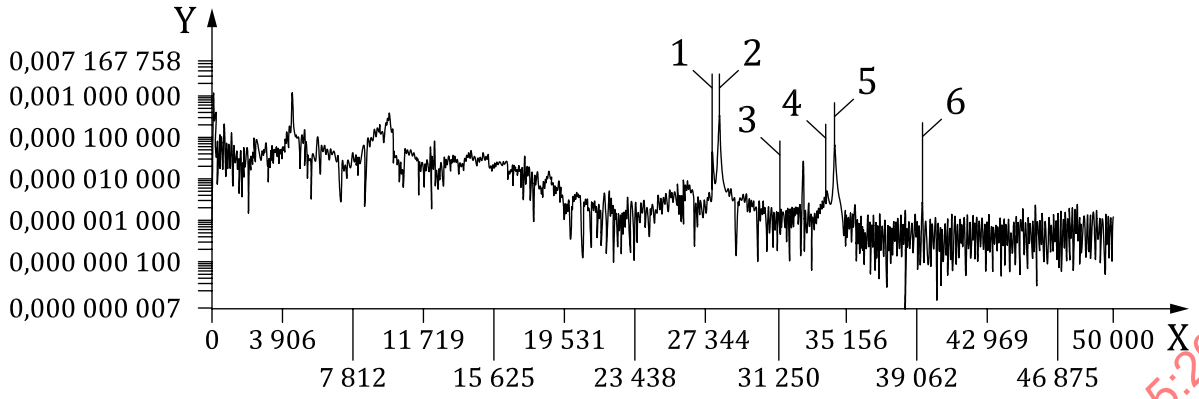

Key

X frequency (Hz)
Y amplitude (volts)
1 frequency 1
2 frequency 2
3 frequency 3
4 frequency 4
5 frequency 5
6 frequency 6

Figure 40 — Typical half-size Stainless Steel star artefact RAM spectrum showing the subset of the six resonant peaks used for comparison criteria

Table 25 — Summary of the results of the RAM tests on Stainless Steel half star artefacts

Material	Build 1		Build 2	
	Pass	Fail	Pass	Fail
Good parts (S0)	20	0	19	1
Bad parts with defects (S1 and S2 half star artefacts)	0	24	0	24

11.1.4.2.4 Comments/observations

The RAM enabled to define criteria that allowed differentiating the good parts from the ones with internal defects. The reference parts showed a significant difference in resonance compared to the ones with defects. However, one reference part out of twenty was rejected as its resonance peaks were too different from the other reference parts. This is probably due to an unintentional organic defect in that part resulting from small variations in the manufacturing process. In the range of frequencies analysed, the parts could not be sorted based on the number of defects they contain.

Benefits of RAM:

— easy to use and fast;

— no restriction in size and shape;

— no part set-up required;

— able to identify defective parts.

Drawbacks of RAM:

— not possible to identify the type or location of defects in the part;

— further investigations of RAM are needed to address AM defects such as more accurate statistical tools to analyze the results.

11.1.4.3 Non-linear acoustic testing — NLA (theta tech)

Non-linear acoustics is particularly pertinent to NDT due to its potential for early-stage detection of flaws and damage in structures. There is a variety of approaches available, grouped broadly into scanning techniques (such as pulse inversion or dual-frequency intermodulation) and whole-body or bulk techniques such as non-linear resonance testing (NLR).

Non-linear scanning: Normally conducted using ultrasound, offering the ability to localise crack-like flaws of the order of a few microns wide by hundreds of the order of a few micrometres wide by hundreds of micrometres long, and likely to be relevant to inter-layer AM flaws. Nonlinear imaging is an active area of research for both metals and composite structures but thus far no comprehensive studies have been carried out on AM components.

Non-linear resonance testing — NLR: NLR is a rapid (**'go/no-go'**) method, which does not provide location or morphological detail, involving exciting the component into resonance and analysing the strain-dependent behaviour. Flawed structures may exhibit non-linear strain response. These methods are particularly appropriate for metals and welded or joined materials, however, this method is only sensitive to close/touching cracks and lack of fusion, something that a radiography approach would struggle to detect. For additive manufacturing parts, the method is showing some potential applicability.

An example of NLR output is presented in Figure 41. The graphic shows the nonlinearity factors (NLF) for two Nacelle, demonstrating clear discrimination between intact and defective samples: It is possible to set a threshold (at, for example NLF = 100) above which the high-strain data for the defective sample is unequivocally located, and below which the high-strain data for the intact sample lies. In addition, the curve shows that ND2 exhibits a decreasing Nonlinearity factor compared with ND1. The envelope curves represent ±1 standard deviation calculated using 10 consecutive shots.

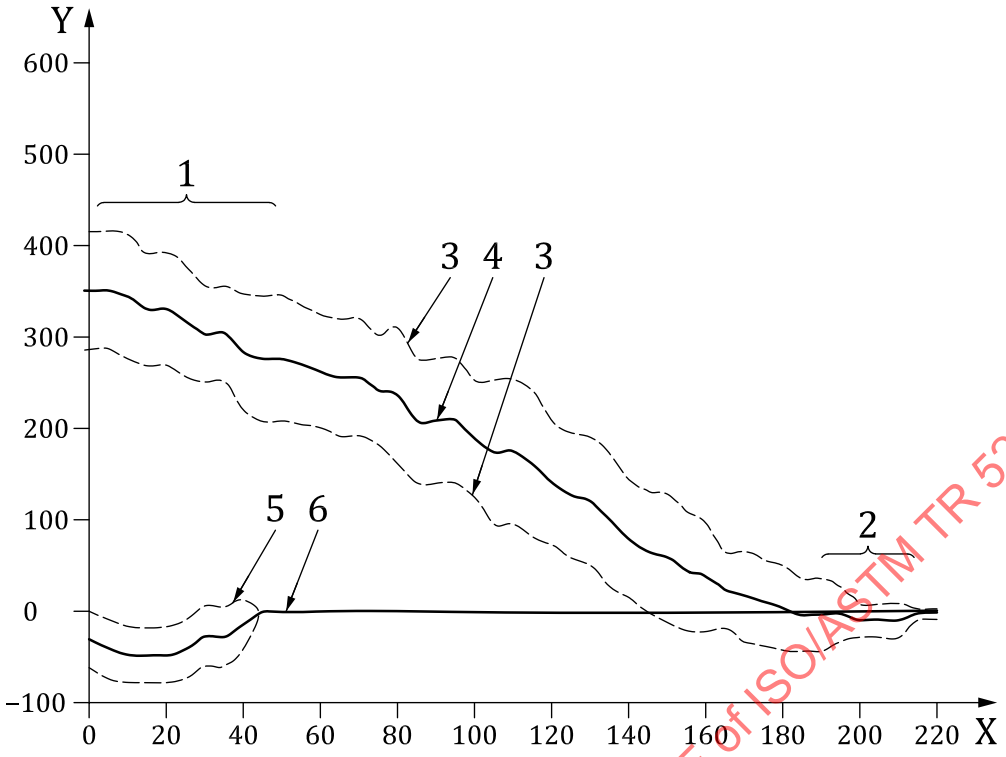

Key

X time, ms
Y nonlinearity factor
1 high strain, non-linear regime
2 lower strain, non-linear regime
3 envelope, ±1 standard deviation
4 sample with crack
5 envelope, ±1 standard deviation
6 sample planned without defect

Figure 41 — Non-linear resonance curves of two nacelles tested and labelled as ND1 and ND2

11.1.4.3.1 Summary of procedure

Sample mounting for NLR tests can generally either be fully clamped or fully freely supported, for example on a foam bed. Due to the nature of the star samples — high stiffness and complex external shape, the stars were placed on a foam bed. The general procedure for the NLR test is performed as follows:

— clamp or free support the part;

— set distance between sample-vibrometer;

— excite the samples either manually or automatically;

— collect data;

— analyse data;

11.1.4.3.2 Apparatus/setting

The experimental set-up used for the manual excitation is shown in Figure 42. The star and the laser vibrometer head were rested on separate pieces of foam. The distance between the vibrometer and the star was set to 295 mm, which is the visibility maximum of the vibrometer (Polytec NLV 2500).

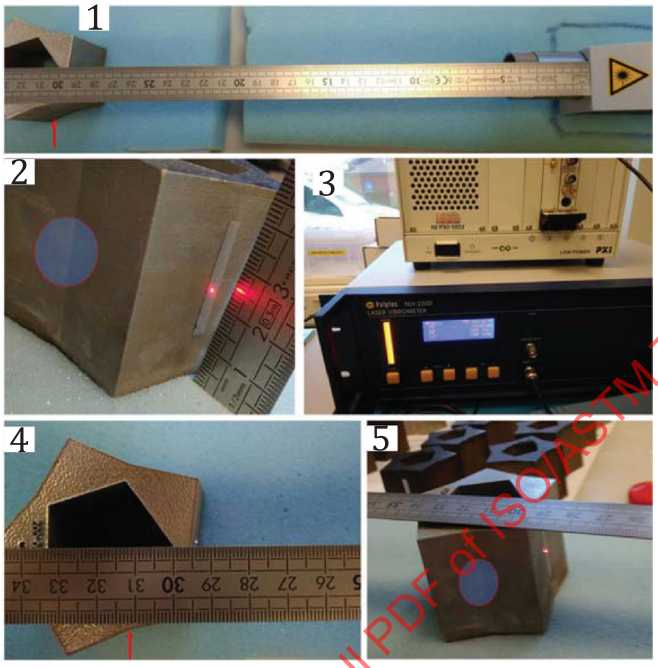

Key

1 star artefact-vibrometer set up
2 shimmed star
3 pxi oscilloscope
4 location of the strike zone and direction
5 both were rested on separate pieces of foam at 295 mm distance centre line star face with a laser. reflective tape is used to maximise signal received by laser vibrometer to measure velocity data from laser vibrometer

Figure 42 — Experimental set-up for NLR test using manual excitation

The stars were shimmed by placing paper under the foam until so the laser beam was at approximately the centre of the face of the star, and the serial number of the star was used as datum so all the samples were located in the same orientation. A reflective tape was used to maximise the amount of signal received by the laser vibrometer. The velocity data from the laser vibrometer was measured using a PXI oscilloscope with a 200 kHz sampling rate.

The settings of the vibrometer were set to velocity to voltage conversion of 20 mm/s/V to obtain the maximum signal to noise ratio during the strikes without clipping the data. The striker was made from an aluminium rod of length 120 mm × 5 mm diameter. Because the excitation was conducted using a manual strike, the data was subject to variation due to human factors. For this reason, multiple tests were conducted to produce mean and standard deviation graphs.

MTC supplied 31 AM star artefacts in three different designs built in Hastelloy®[16] and Maraging steel. Table 26 below summarizes the population and materials used for the NLR inspection.

16) Hastelloy is an example of a suitable product available commercially. This information is given for the convenience of users of this document and does not constitute an endorsement by ISO of this product.

Table 26 — Summary of total star artefacts and materials used for the NLR test

Centre	Material	Number of parts			Total parts
		Reference parts	Seeded parts		
		S0	S1	S2	
MTC	Hastelloy®	5	5	5	15
	Maraging steel	5	5	6	16

11.1.4.3.3 Significance of data/interpretation of results

Curves with mean values over many shots (approximately 15 per sample) were obtained and error bars adding ±1 standard deviations added to the data. The summary of all the averaged drift curves of all the samples is shown in Figure 43 and Figure 44 for the Hastelloy® and Maraging alloys, respectively.

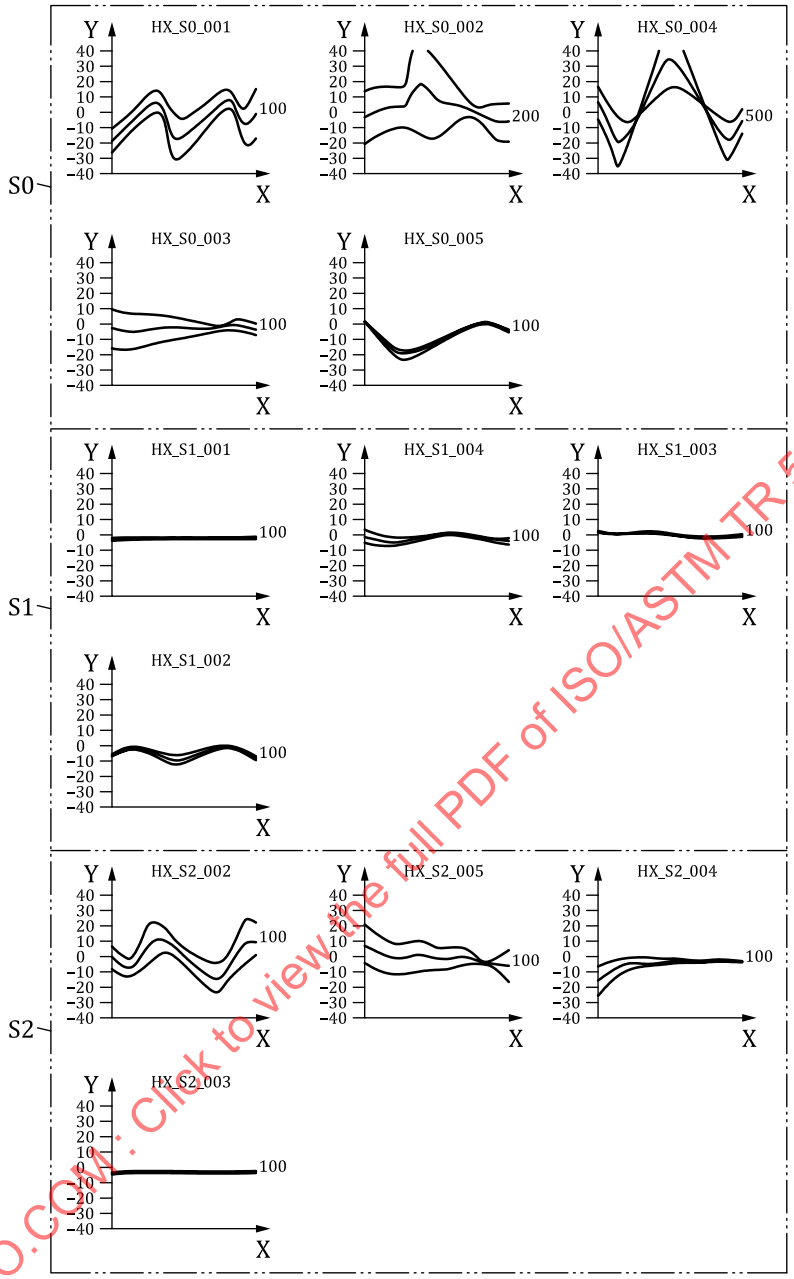

Key

X time, ms

Y Non-linearity factor

NOTE The non-linear factor is very small for all of them (±40 scale).

Figure 43 — All samples tested for the Hastelloy®[17] stars S0, S1 and S2 batches

17) Hastelloy is an example of a suitable product available commercially. This information is given for the convenience of users of this document and does not constitute an endorsement by ISO of this product.

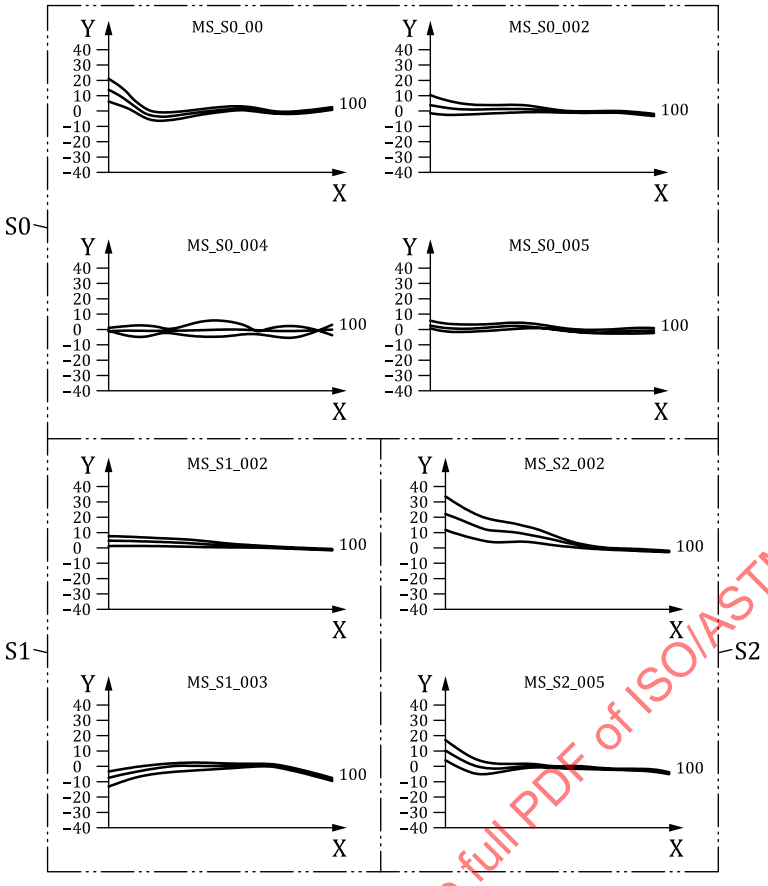

Key

X time, ms

Y nonlinearity factor

Figure 44 — Summary of the nonlinear factor curves for the Maraging steel (MS) samples tested from batches S0, S1 and S2

The results of the NLR trials are summarised in Table 27.

Table 27 — Summary of total star artefacts and materials used for the NLR test

Material	Reference star	NLR test	
		Pass	Fail
Hastelloy®	S0	Inconclusive	Inconclusive
	S1	Inconclusive	Inconclusive
	S2	Inconclusive	Inconclusive
Maraging steel	S0	Inconclusive	Inconclusive
	S1	Inconclusive	Inconclusive
	S2	Inconclusive	Inconclusive

11.1.4.3.4 Comments/observations

All the samples exhibited two peaks in the frequency very close to each other. The distance between the peaks is between 20 Hz and 40 Hz, representing a difference between 0,15 % and 0,5 %, which in turn indicated that the NLR algorithm needed to be adapted for these particular samples. In addition, the findings indicated the star was not excited into a nonlinear regime while resting on foam in a free-

supported state, with all the samples having a very low nonlinearity factor close to the systematic errors.

In overall, it is concluded that either the samples do not exhibit significant nonlinear resonance features, or higher excitation levels are required for them to do so. It could limit its applicability for inspection of AM parts unless some improvements to exciting the samples and NLR mathematical algorithm are done.

11.1.5 Ultrasonic testing — UT and Phase Array UT — PAUT (EWI and NIST and LNE)

Ultrasonic testing uses sound waves to interrogate a material. Discontinuities or other changes in material properties cause the sound waves to reflect or refract. When reflected sound returns to an ultrasonic transducer, the depth of the discontinuity can be determined by the time of flight. By scanning a material, more information such as size and length, and in some cases type of discontinuity, can also be obtained. Linear phased array transducers use an array of sound-producing elements to create an ultrasonic wave in a material that can be focused, steered or scanned along the length of the transducer by electronically triggering individual elements in the array to fire at specific time delay intervals. It is possible to improve the performance of the above-mentioned standard PAUT system by implementing a data acquisition method called full matrix capture (FMC) with a post-processing reconstruction algorithm known as total focusing method (TFM). Thus, FMC combined with TFM enables offline reconstruction of a more detailed image (with better spatial resolution, perspective, and defect definition) than a standard PAUT imaging method where all array elements create a unique wave front to form a beam with a fixed focus.

11.1.5.1 Summary of procedure

Star artefacts built from Stainless steel and Aluminium were tested using conventional UT (CUT) and phase array combination (PAUT-FMC/TFM) approaches respectively. Each section of the specimen was tested from the top and sides. These surfaces have as-built surface roughness. The procedure applied is explained below for each material.

Stainless Steel: A stainless steel star design S1 was tested using PAUT at EWI facilities. A linear scan with a normal beam, a linear scan with a beam angled at 10 degrees, and a sectorial (azimuthal) scan was investigated. A 1018 steel NAVSHIPS test block was used to standardize the gain. The NAVSHIPS test standard contains 1,19 mm (3/64 in) diameter side-drilled holes. The 6,35 mm (0,25 in) and the 44,45 mm (1,75 in) holes were used because they were closest to the range of depths represented in the sample.

Aluminium: Conventional UT(CUT) and PAUT-TFM method were used to test the aluminium star artefacts S1 and S2 designs. CUT was carried out at OKOS facilities while PAUT-TFM at TPAC amenities. For the UT test, a one linear probe acting as a transmitter/receiver to induce the longitudinal waves was used. The star artefact was immersed in a tank of water and scanned only from one side of its branches, from the top to the bottom of the star. The water path distance between the probe and the scanned surface of the artefact during the scan was 12,5 mm. Finally, the analogue gain was adjusted to 40 dB to acquire the data.

The digital gain can be subsequently adjusted on the reconstructed image (300 pixels × 400 pixels) offline. For the PAUT-TFM test, the transducer was 32 mm long and was composed of 128 transducers separated from each other by 0,25 mm (centre to centre). The steps followed for the TFM analysis were:

— first step: data acquisition with Full Matrix Capture (FMC);

— second step: data numerical post-processing (reconstruction) with Total Focusing Method (TFM).

11.1.5.2 Apparatus/settings

To inspect the stainless steel star a 32/128 channel Omniscan MX instrument with a 10 MHz, 128 elements, linear phased array transducer was used. The inspection was performed in air and the transducer was positioned from top to the bottom and the sides of the star as shown in Figure 45.

a) Top to bottom

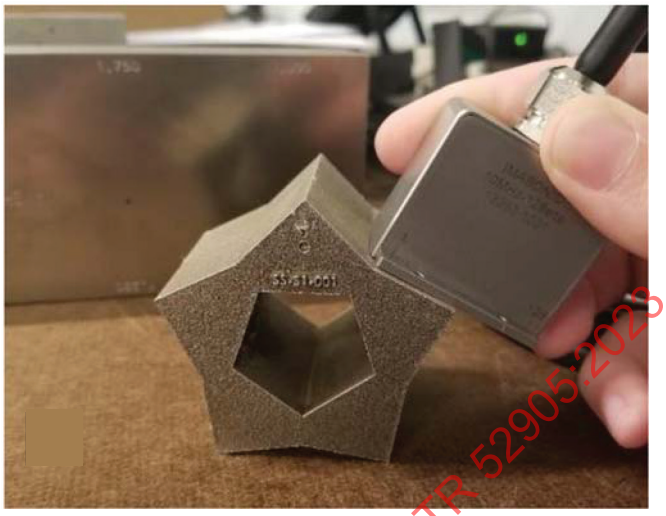

b) Sideways

NOTE For test at OKOS and TPAC only side inspection was performed.

Figure 45 — Position of the transducer during inspection at EWI

To inspect the aluminium star artefacts using PAUT-TFM, the OMPA instrument to acquire the data with a high rate (150 MB/s) was used. The probe is 32 mm long and was composed of 128 transducers separated from each other by 0,25 mm (centre to centre). It is shown in Figure 46a. For the conventional UT (water tank) a single transducer was operated as presented in Figure 46b. The characteristic and parameters of the ultrasonic test performed using conventional UT and PAUT are presented in Annex H.

a) Phase array

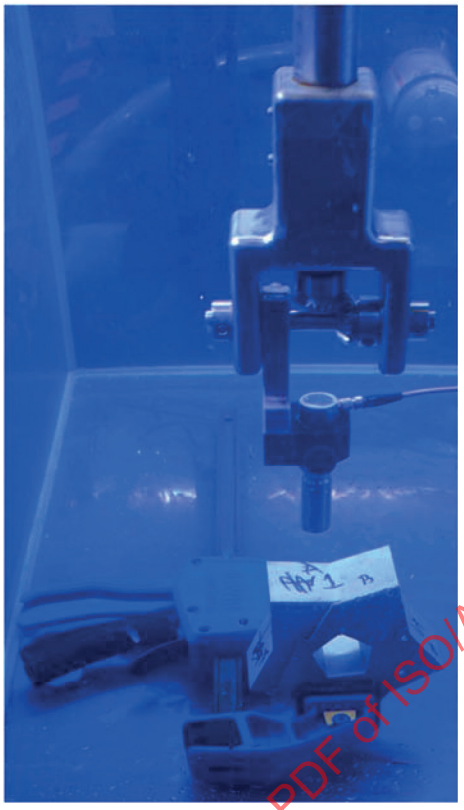

b) Conventional UT

NOTE The orientation of the star and position of the probe is shown in both cases.

Figure 46 — Set up for inspection of the aluminium start artefacts by phase array and conventional UT

11.1.5.3 Significance of data/interpretation of results

For the Stainless Steel star, the flaws were best detected when they were oriented parallel to the ultrasonic sensor because they reflected the most sound. Cylindrical flaws also reflected sound well because there is some surface area. Spherical flaws did not reflect sufficient sound to be detected because of the limited surface area available to reflect sound. The images of the CUT inspection performed is summarised in detail in H.2.1, and the finding are described as follows

— In region 1, one defect was detected at a depth of 11 mm using a 0° linearly swept beam, which corresponds to the second flaw from the top of the specimen. This flaw is perpendicular to the direction of the sound wave which is the ideal orientation for detection with ultrasonic inspection (See Figure H.1 a). Inspecting the specimen from the side with a linear beam at an angle of -10°, three defects were detected. Because of the proximity of two of the defects with the width of the probe, it is difficult to determine which one was detected (See Figure H.1 b).

— For region 2 containing vertical cylindrical defects varying diameters from 0,1 mm to 0,7 mm (Figure H.2 a), the inspection performed from the side with a linearly swept beam at an angle of -10° all the cylinders were detected (Figure H.2 b).

— No embedded flaws were detected in Region 3, which means that seeded spherical defects filled with powder or were not manufactured.

— Region 4 and region 5 defects (Figure H.3 a) were inspected simultaneously with a linear sweep of 0° from the top of the specimen. The 3,0 mm long cylinders (region 4) were better detected than the 2,0 mm defects close to the centre of the specimen with diameter greater than 0,3 mm. However,

the strength of the signal for each of these flaws does not directly correlate to the size of the defect because sound attenuates as it travels farther into a material. It seems the larger cylinders appear to have a weaker signal. Several focal lengths were used for this test being 15 mm the focal length selected for this scan (See Figure H.3 b).

For the star manufactured in aluminium, the images of the CUT inspection performed is summarised in detail in H.2.2, however, the finding using CUT is described as follows:

— Cylinders with different orientation (region 1) cannot be seen from sides labelled 1A and 2B (Figure H.4 a). However, the largest ones are visible for scans performed from side labelled as 3B (see Figure H.4 b).

— Vertical cylinders with different diameters (region 2) are visible form different sides except from side 1A due to cylinders with different orientations hidden them.

— Spheres in region 3 are not visible from different sides views.

— Most of the horizontal cylinders open at the inside face of the pentagon (region 5) are not visible form the all sides due to their location and diameter size. The larges one can be seen from the side labelled as 4A (Figure H.4 d).

For the inspection of the aluminium start using PAUT-TFM, the star artefacts version S1 and S2 were immersed in a tank of water acting as a coupling, and scanned only from one side of its sides from the top to the bottom of the star. The images collected are presented in detail in H.2.3. The main outcomes of this evaluation is summarised as follows:

Star artefact version S1:

— Three of the cylinders with different orientations can be seen from side 1A. The orientations of the other cylinders prevent detection (Figure H.5).

— Five vertical cylinders with different diameters can be detected from side 2A using the three optimized digital gains chosen to display the images. The cylinders with smaller diameters, down to 0,1 mm, can be detected with increased gain (Figure H.6 bottom images) at the expense of the reduced quality of the image (lower signal to noise ratio).

— Three of the spheres of different diameters can be seen from side 3A (Figure H.7).

— Three of the horizontal cylinders of different diameters (10 mm long) located on an outside edge of the star can be seen from side 4A (Figure H.8 a). Their position on the edge hides the others.

— Some horizontal cylinders of different diameters located on an inside edge of the star are seen from side 4A (Figure H.8 b). They are located on an edge and are short (2 mm long), so they are difficult to differentiate from the reflection of the edge.

— It does not seem that we can see the single cylinder manufactured by mistake.

Star artefact version S2:

— The horizontal cylinders open at the inside face of the pentagon (Region 1) are easier to see from side labelled as 5A when located inside the star artefact (Figure H.9). However, when are located outside the star artefact there are not visible at all. Four of them are seen in Figure H.10.

— All spheres can be seen in Region 3 from the side labelled 2A (Figure H.11). This means that defects down to 0,1 mm in diameter can be visualised.

— All vertical cylinders can be seen in Region 4 from the side labelled 3A (Figure H.12) similar in the S1 design by increasing the gain. This means that defects up to 0,1 mm in diameter can be detected.

— Six cylinders with different orientations were detected in Region 5 from side 4A (Figure H.13). Therefore, defects up to 0,2 mm in diameter in various orientations can be visualised.

The main findings for the ultrasonic test carried out both full size Stainless steel and Aluminium star artefacts are summarised in Table 28.

Table 28 — Summary of the smallest size of the defects detect on the stainless steel star by CUT and PAUT-TFM methods

Defects dimensions in millimetres

Design [a]	Defect region	Probe location	EWI[b]	TPAC[b]	
			Stainless steel	Aluminium	
			PAUT[c]	CUT[c]	PAUT-MFC/TFM[c]
S1	1	Top	One, horizontal	ND[d]	ND[d]
		Side	Two, ±45°	Inconclusive	Inconclusive
	2	Top	not specified	ND[d]	ND[d]
		Side	0,1	Inconclusive	0,1
	3	Top	ND[d]	ND[d]	ND[d]
		Side	ND[d]	Inconclusive	0,5
	4	Top	0,3	ND[d]	not detected
		Side	0,3	ND[d]	0,5
	5	Top	0,4	ND[d]	ND[d]
		Side	0,4	not specified	Inconclusive
S2	1	Side	NT[e]	NT[e]	Inconclusive
	2	Side	NT[e]	NT[e]	0,4
	3	Side	NT[e]	NT[e]	0,1
	4	Side	NT[e]	NT[e]	0,1
	5	Side	NT[e]	NT[e]	0,2

[a] The CAD files of the star artefact correspond to the preliminary version designed by MTC.

[b] The analysis were performed in one sample per each design at each centre.

[c] The nominal diameter size reported correspond to the feature detected by the technique used.

[d] ND stand for “Not detected”.

[e] NT stand for “Not tested”.

11.1.5.4 Comments/observations

The main conclusion for the phased array ultrasonic inspection performed are summarised as follows:

— PAUT in the stainless steel star can be used to detect subsurface embedded defects, but is influenced by flaw size, orientation, type and depth. When flaws are oriented in a way that reflects sound back to the receiver, this technique achieves a sensitivity of 0,1 mm in this material as seen in this study.

— This specimen is reasonably suited for ultrasonic inspection, but the sides of the star cause sound to be introduced into the material at an oblique angle. Electronic steering with a phased array transducer could accommodate this geometry in some cases, but a better specimen for inspection using conventional or phased array ultrasound may have flaws similar to this design. However be positioned perpendicular to the sensor so variations in flaw size and orientation could be better attributed to the technique’s strengths and limitation and not partially due to geometry.

For the inspection on the aluminium star using CUT and PAUT-FMC/TFM the following conclusions are obtained:

— Due to its high spatial resolution when used with FMC/TFM, the PAUT method reveals individual defects and even allows rough dimensional measurements. The interpretation of the images is easier than in CUT but is still not straight forward. However, like in CUT, the surface roughness did not prevent the part from being tested, and the size of the part was not an obstacle.

— Apart from the better resolution than in CUT, another real advantage of the PAUT-TFM methods is to be able to perform static inspection by steering the beam instead of scanning the probe. This is of particular interest for complex shapes that cannot be scanned.

11.1.6 Residual stress — RS (ILL)

The non-destructive determination of residual stresses within engineering components using laboratory equipment is limited to the surface (x-ray) or near surface regions (Barkhausen-noise) but with limited spatial resolution. Bulk stress investigations are often carried out using destructive methods. Examples are deep-hole drilling, slicing or the contour method. The destructive methods are based on the relaxation of stresses and therefore limit further materials investigations, and accepting the loss of an expensive, highly elaborated part.

Neutron stress determination conquers these shortcomings. It is a non-destructive technique, applicable to mock-ups as well as realistic sized engineering components. It allows mapping of stress fields from the bulk of the work piece to its surface with adjustable lateral resolution and providing the full stress tensor for each measuring point. The technique is based on diffraction at (poly-) crystalline material, comparable to x-ray diffraction, but provides much higher penetration. Neutron techniques are well suited for in-situ or in operando investigations, using even complex sample environment

SALSA, which stands for “Stress Analyser for Large Scaled engineering Applications”, is a stress diffractometer dedicated to engineering sciences and industrial R&D (Figure 47). SALSA provides a maximum of flexibility in terms of sample size and shape, allowing laterally resolved stress determination. The resolution is variable between 0,8 mm and 6 mm and allows stress mapping with penetration depths of about 60 mm in steel, 70 mm in titanium alloys, 40 mm in Nickel and 300 mm in aluminium.

It is also possible to obtain depth profiles from 40 µm below the surface into the bulk. This is applied to surface treatment investigations, comprising laser shock peening, induction hardening, spray coating etc.

11.1.6.1 Summary of procedure

In Figure I.1, the set up describes the fixed position of the gauge volume (GV: red point), and so the movement of the sample sited on the hexapod is necessary for the mapping of the region of interest (ROI). For each position, the Bragg-diffraction peak is recorded. The position of the peak is a precise measure of the lattice spacing of the crystallites within the GV that also allows phase-specific studies.

Then, stresses can be determined from the peak shift from a reference unstrained condition through Hooke’s law with the specific diffraction elastic constants. The strain component direction is defined by the scattering vector $\boldsymbol{q}$ in the bisector position of beam to detector. Hence, the sample would need to be oriented as many times (angle configurations) as components needed.

For the residual stress characterization at SALSA the region of the Ti6Al 4V star without artefacts was selected at two different heights: distance to the tip edge 5 mm and 17 mm, respectively (see Figure I.2). Three ROI within the thickness in the defect free corner were measured:

— Near surface entry scan from the bottom surface (0,6 mm × 2 mm × 0,6 mm) GV –until 2 mm in the bulk.

— Near surface entry scan from the top surface (0,6 mm × 2 mm × 0,6 mm) GV –until 2 mm in the bulk.

— Bulk scan (2 mm × 2 mm × 2 mm) GV from 1 mm from each surface

Note that the 2 mm for scans 1 and 2 were oriented in-plane with the scanning strategy, leaving the maximum resolution of 0,6 in height (building direction). An example of the set up and the scheme ROI’s and components is summarized in Figure 47. See all detailed for orientation and strain configurations in Figure I.2.

The procedure followed was focused on defining the optimum measuring parameters by performing multiple angle scans in order to: 1) select one reflexion and 2) select the strain component. Once it was determine, the bulk of the sample is scanned is carried out within the thickness out of the part then the reflexion position evolves and extracted peak profile of the reflection, which is accounted for further calculations. The Bragg's law and strain related to inter-planar spacing and peak position is used. The reflexion measured for the titanium is Ti (101) alpha + alpha' ($\alpha + \alpha'$).

The unstrained reference $\boldsymbol{d_0}$ is determined and pseudo strain correction is applied (to improve lateral resolution). Once these parameters were obtained the residual stresses in the in-planar direction are calculated using the stress conversion by Hooke's law. Here, the $\boldsymbol{d_0}$ unstrained reference was taken as the stable value in the middle of the thickness of the star, so everything reported is relative to that (even the sign compression/tension will depend on that).

11.1.6.2 Apparatus/settings used

The setup of the SALSA beam line is shown in Figure 47, white the parameters for residual stress analysis is shown in Table I.1. The instrument uses a monochromatic neutron beam and a Position Sensitive Detector (PSD), which covers 8° in 2θ at a typical distance of 1 m from the sample. The neutron beam is delivered via a double focusing monochromator composed of 39 silicon variably bent crystals. Using phase space focusing, it takes advantage of the beam divergence provided by the neutron guide and supplies the high resolution needed for strain determination.

A range of collimators is available with focal distance as small as 0,6 mm (FWHM) and a fixed distance to the gauge volume of 150 mm. These optical focusing system of collimators provide the most precise spatial resolution measurements, also reducing the background in comparison with slits. Therefore, they are particularly useful for high spatial resolution measurements near interfaces, surfaces or in coatings, since they give lower surface aberrations.

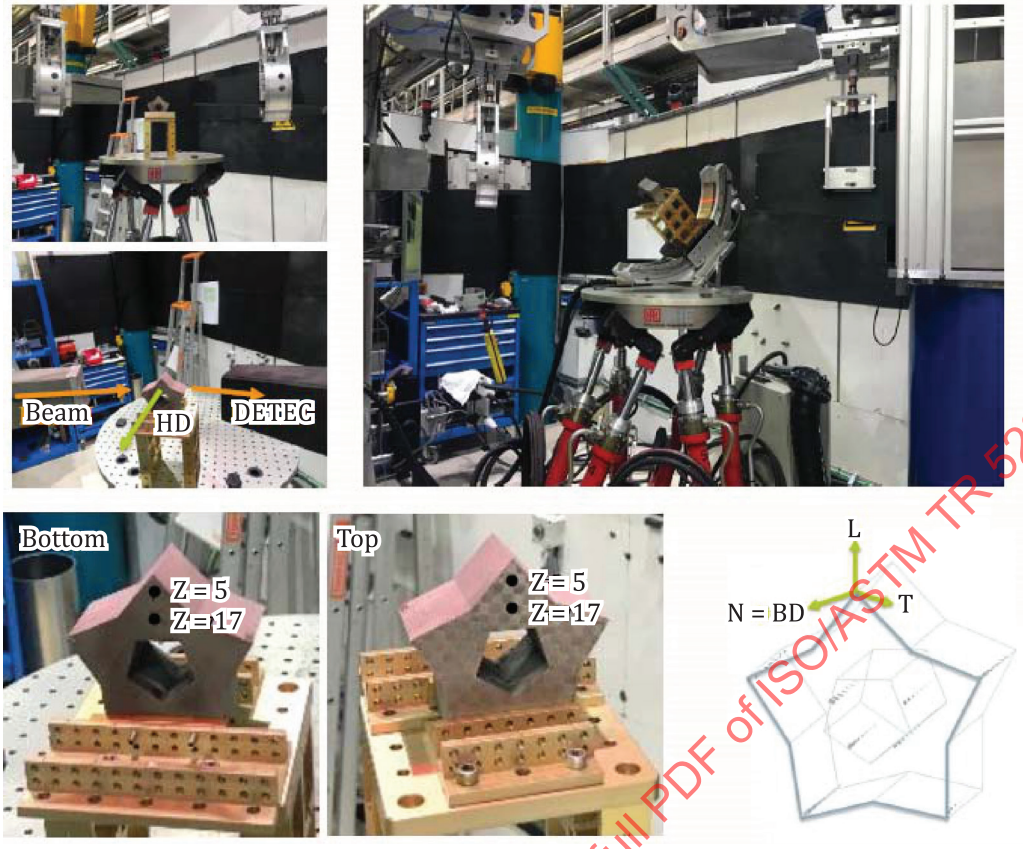

NOTE Bottom surface (near base plate) and top surface (finishing surface).

Figure 47 — ISO-Ti6Al4V demonstrator set up for residual stress characterization at SALSA. BD building direction, N normal component, L longitudinal, T transversal

11.1.6.3 Significance of data/interpretation of results

Strain tendencies of the three geometrical principal directions from the bottom (near previous base plate) to the top (finishing surface) are presented in Figure 48 a). Strain distributions from near surface and across the thickness were parabolic for the three components, positive for Longitudinal and Transverse and negative for Normal. All of them presented a plateau within the middle between 15 mm to 25 mm in the thickness, with an stable value of about −900 με for Transversal, −1 700 με for Longitudinal (compressive) and 4 000 με for Normal (tensile). Therefore, moderate and compressive microstrains values are observed within the printing plane (Longitudinal-Transverse), whereas in the building up direction (Normal) it reaches a tensile maxima within the bulk.

The gradient is sharper near the edge surfaces where the behaviour from tensile/compressive inverses for all components at around 4 mm from each surface. Indeed, there is a shift of local maximum values between bottom and top surfaces for all components as follows: 5 300 με vs 4 000 με for Transverse, 4 100 με vs 300 με for Longitudinal, and −3 100 με vs −1 500 με for Normal. Therefore, local maximum compressive/tensile values around 0,5 mm from surface are always reached in the region near the bottom surface (initially near base plate). Note that for these results the reference unstrained value was the same for all locations and angular conditions, which may be reconsidered near the surface after microscopy characterization. The presence of different phases and/or microstructural feature gradients may explain the bounces in the Normal component at those ROIs.

Similar parabolic trends are also visible in the stress values in Figure 48 b), where longitudinal and transverse are restricted between ±100 MPa and maximum Normal stress reaches around 500 MPa in tension in the middle region. As for the near surface region, maximum tensile values are reached for Transversal with 790 MPa vs 650 MPa bottom and top, and Longitudinal 600 MPa vs 550 MPa.

For the Normal component, it presents near 200 MPa tensile value at the first near surface location from both surfaces, changing abruptly to compressive −160 MPa and −60 MPa local minima at 1,2 mm from bottom and top surfaces, respectively. It can be remarked that besides the unstrained reference effect mentioned before, there is also an inherent anisotropy for different lattice reflections, particularly important in the plastic regime due to intergranular strains. This effect may lead to a certain overestimation of macroscopic residual stresses for the Ti (101). However, this last influence will not affect the tendency in Figure 48 b).

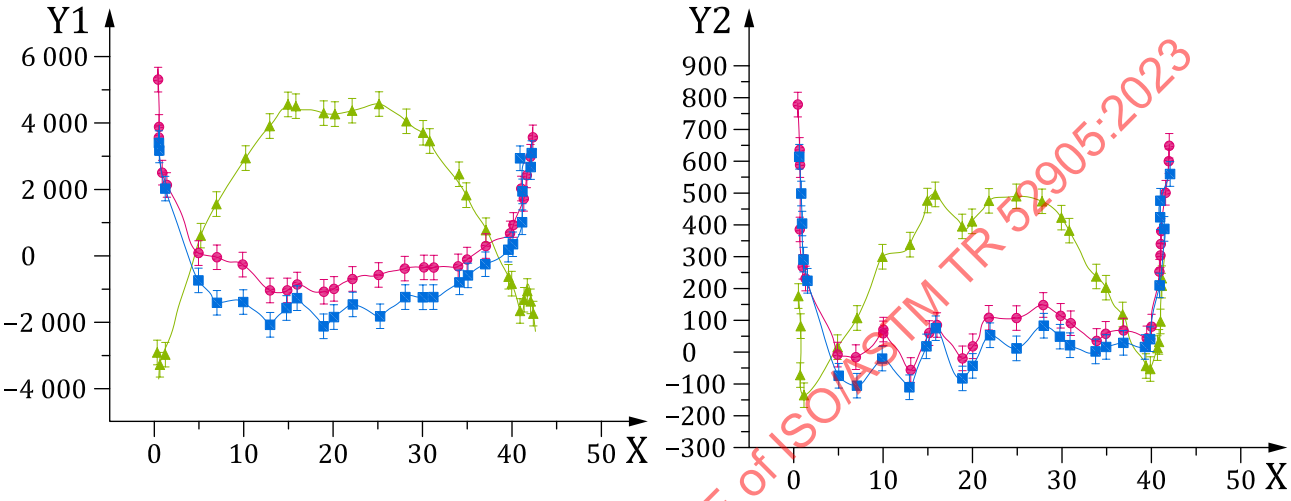

Key

X	position (mm)	X	position (mm)
Y1	microstrains	Y2	stress (MPa)
	5 mm long		5 mm long
	5 mm trans		5 mm trans
	5 mm norm		5 mm norm

a) strain for normal, longitudinal and transverse directions from the bottom surface (0 ref Position) towards top surface (42,6 mm). Errors ±300 με

b) related stress results. Errors ±50 MPa

Figure 48 — Strain tendencies of the three geometrical principal directions from the bottom (near previous base plate) to the top (finishing surface)

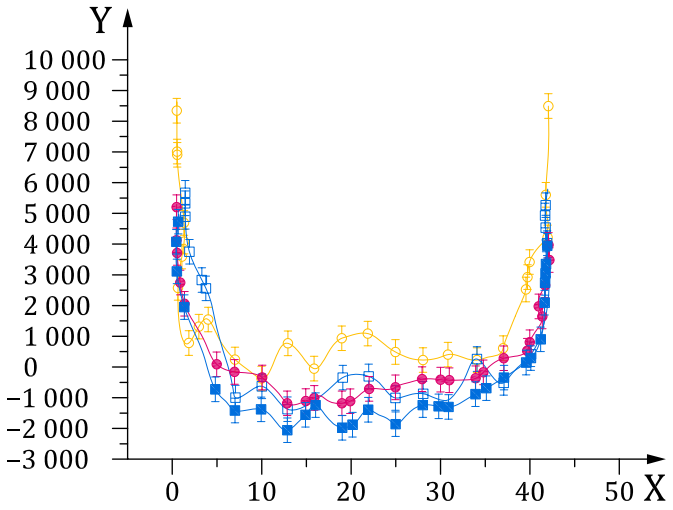

Key

X	position (mm)
Y	microstrains
	5 mm long
	5 mm trans
	17 mm long
	17 mm trans

Figure 49 — Strain distribution for longitudinal and transverse directions from bottom towards top surface for lines scans at 5 mm and 17 mm from the tip of the star sample (errors ±300 με)

For comparative purposes of the influence of the geometry, the strain distribution for a line at 17 mm from the tip is displayed in Figure 49 against the previous results for the line scan at 5 mm. A general rise of both longitudinal and transverse components around 1 000 με towards tensile values is observed. Furthermore, for transverse component at 17 mm from tip, the maximum near surface increases to more than 8 000 με in comparison with previous 5 000 με for 5 mm.

11.1.6.4 Comments/observations

The residual stress distribution has been investigated by means of neutron diffraction. The main outcome of the study are:

— Neutron diffraction enhances the visualization of strain gradients from the near surface into the bulk non-destructively.

— A parabolic and symmetric tendency of stress distribution is observed from bottom to finishing surfaces for all strain components, with a plateau within the middle of the bulk and an inversion of tensile/compressive at around 4,5 mm from top and from bottom surfaces.

— In-plane components were confined within the bulk to ±100 MPa, whereas in the building direction it was tensile 500 MPa.

— Near surface regions from 0,5 mm to 2 mm displayed an asymmetry of maximum values for both bottom and top surfaces, with higher strain values at the bottom region.

— In-plane components show an overall increase around 1 000 με towards tension at deeper positions from the tip of the star (z = 17), indicating the combined influence of geometry and printing strategy.

In conclusion, Ti6Al4V star artefact presents steep residual stress gradients from the near surface into the bulk (first 15 mm) even after detaching from base plate. They also change their compressive/tensile nature. Hence, a complete visualization of the strain gradient is recommended in thick AM components.

12 Defect built validation star artefact (Cut-off MTC)

The validation of the defects seeded in the star artefacts is described in this section. It would be used to assess the capabilities both the AM route and the NDT method. Two methods were used this approach could give information that confirm if the defects were built during the AM process. They are:

— XCT inspection approach;

— Metallography validation approach.

12.1 Summary of procedure by XCT

The analysis performed in the Inconel®[18] and Titanium star using both systems at MTC and GE power did not show any indication of the trapped powder defects (spheres and cylinders) in the star-shaped artefacts.

To establish if the system was not able to detect defects smaller than 0,2 mm diameter, cut ups of the sections seeded with spheres and cylinders containing trapped powder defects were carried out. The spheres containing trapped powder (region 5) and the vertical cylinders (region 1) were selected for this. Figure 50 shows the cut-up plan on the Inconel® star artefact 300A. The cut-up was carried out using wire EDM at the MTC. Figure 51 shows the sections created following the cut-up. Section 1 is the area in which it was intended to build/seed spheres with trapped powder, and section 2 the vertical cylinders.

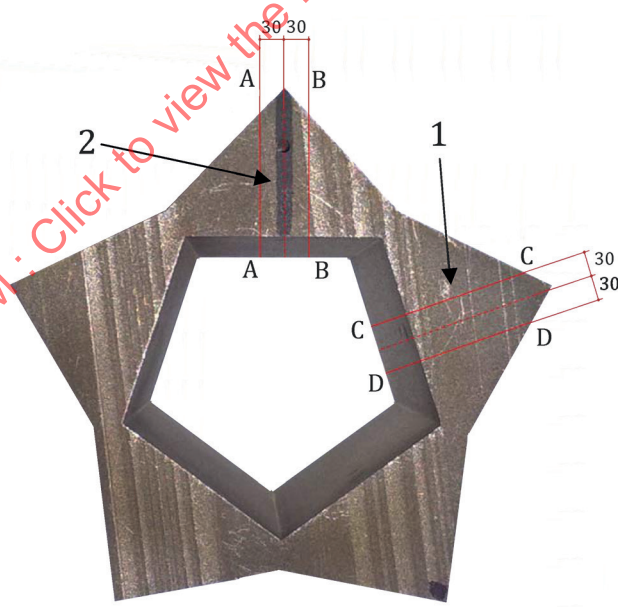

Key

1 section 1; contains the spheres containing trapped powders

2 section 2; contains the vertical cylinders

NOTE The solid red lines are the cutting lines for wire cut (EDM).

Figure 50 — Photo showing the cut-up plan on the Star 300A artefact

18) Inconel is an example of a suitable product available commercially. This information is given for the convenience of users of this document and does not constitute an endorsement by ISO of this product.

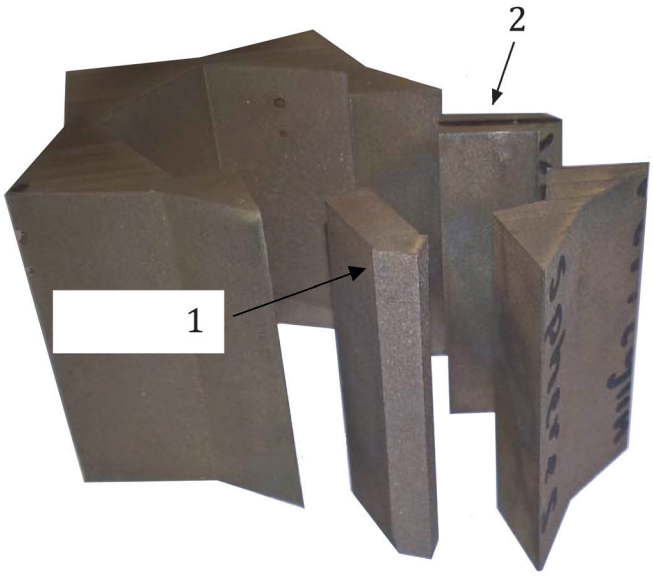

Key

1 section 1; contains the spheres containing trapped powders

2 section 2; contains the vertical cylinders

Figure 51 — Photo showing the Star 300A artefact after the cut-up

12.1.1 Apparatus

The cut-ups, Section 1 and Section 2 were inspected using XCT. This was carried out on a Nikon XTH 225 system at the MTC. The XCT parameters are shown in Table 29.

Table 29 — XCT parameters on Nikon XTH 225 for inspecting the cut-ups

XCT parameter	Nikon[a] value
Voltage (kV)	220
Current (µA)	140
Power (W)	128,5
Target	W
Filter (material/mm)	Tin/1
Exposure time (ms)	–
Image per projection	–
Number of projection	3141
Source-to-object distance (mm)	128,5
Source-to-detector distance (mm)	975,4
Magnification	–
Detector pixel (µm)	–
Voxel size (µm)	26
Focal spot size (µm)	200
[a] Nikon XT H-225 kV. System located at Tring in the UK.	

12.1.2 Significance of data/interpretation of results

Spheres with trapped powder: A total of seven spheres were expected to be in the Section 1 cut-up, based on the design shown in Figure 52. The spheres were in-line with a plane generated between the star tip and the centre of the star. The diameter of the spheres were 1,5 mm to 0,020 mm. A cross section through the tip (see box Right 1 view (a) in Figure 53) can reveal the spheres if they were present. However, the cross section view in Top 1 view (b) (in Figure 53) did not show any indication of the spheres.

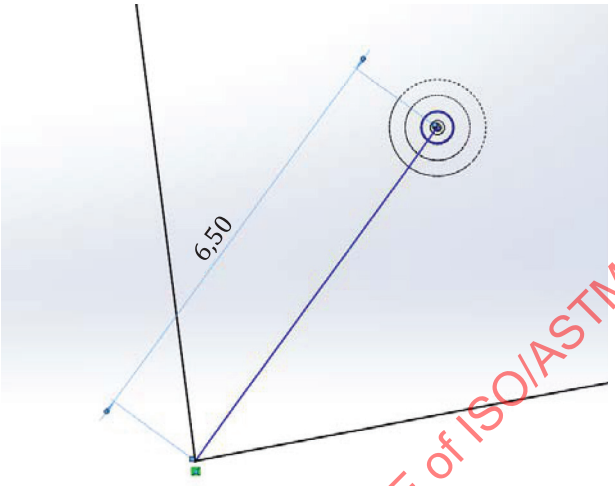

Figure 52 — Screen shot from the CAD model showing the distance from the centre of the sphere to the star tip is 6,5 mm

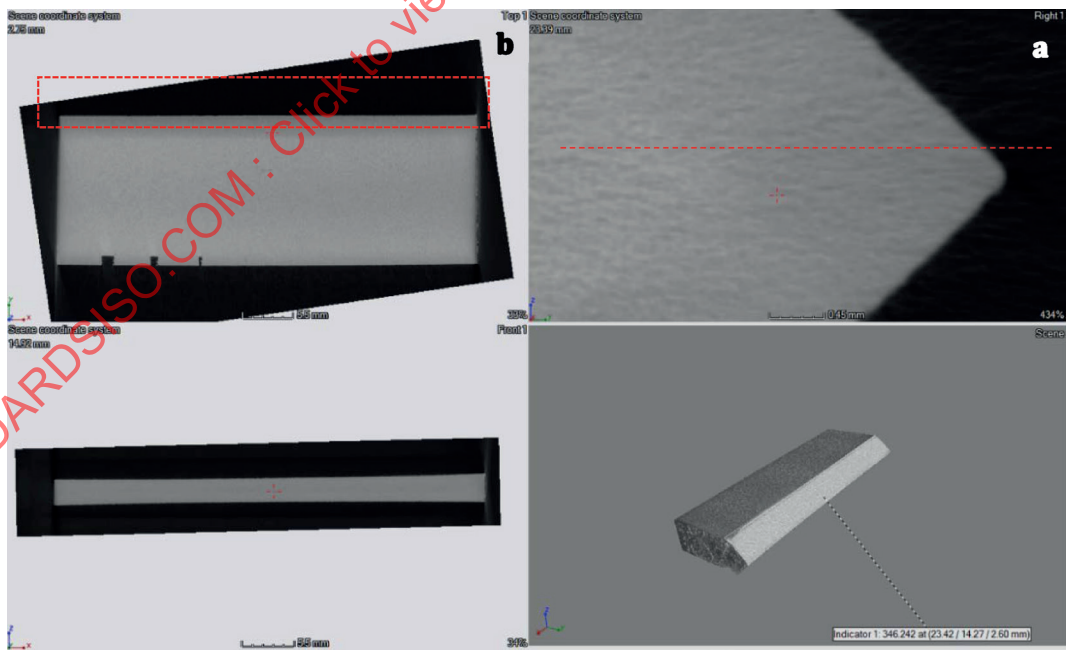

a The slice is indicated at the top right 1.

b The box in top left 1 indicates where the spheres with trapped powders are expected to be present.

Figure 53 — XCT image showing a slice through the tip

Further analysis was carried out by going through each slice in X, Y, and Z directions. A number of indications were found and they are shown in Figure 54 and Figure 55. In Figure 54, an indication was found close to the tip and approximately aligned with dashed line, where the spheres are expected to be present. It is very likely that this indication is a sphere with trapped powder.

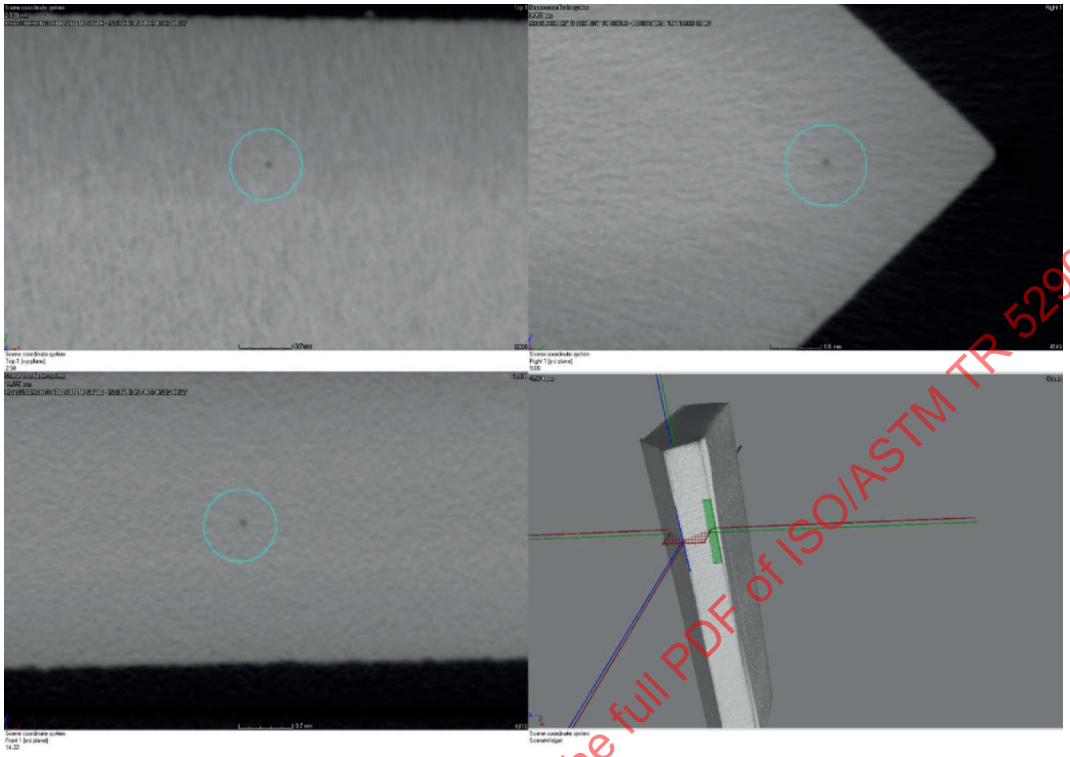

Figure 54 — XCT images showing an indication (Indication 1, in circle blue) that is likely to be a sphere containing trapped powder with size 0,2 mm diameter

Figure 55 shows two indications that are close to each other. Indication 2 lies far from the dashed line and therefore it is unlikely to be the spheres with the trapped powder. However, indication 3 is very close to the dashed line and could possibly be a real sphere with trapped powder.

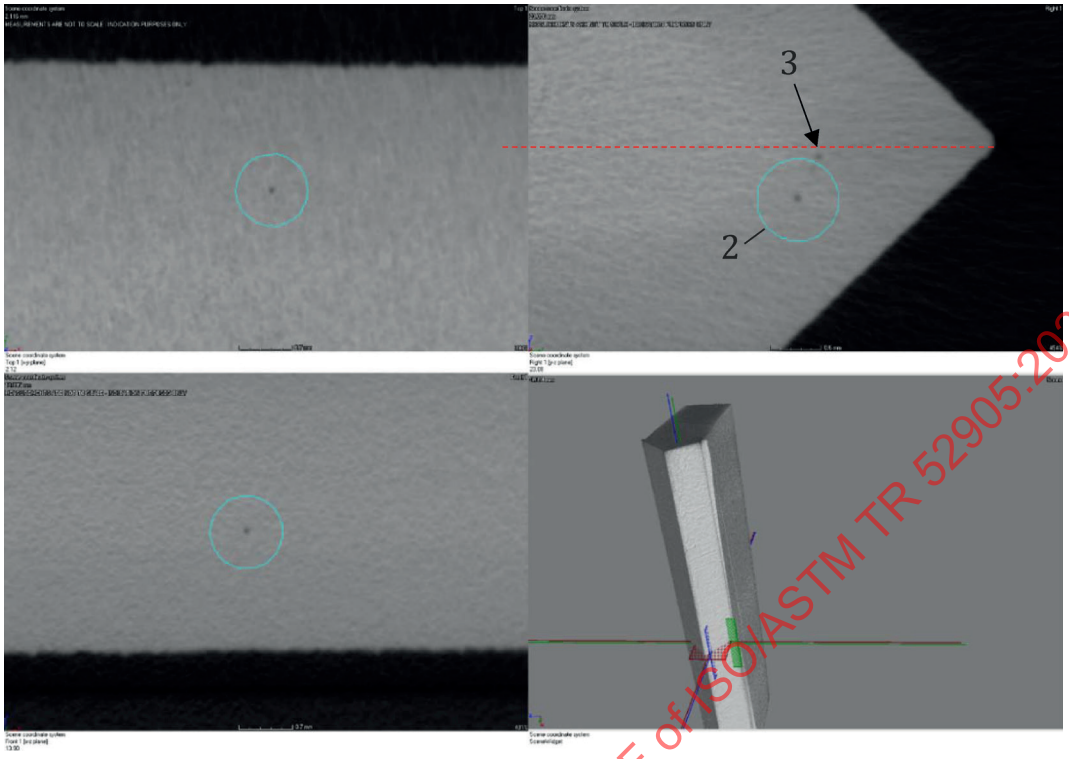

Figure 55 — XCT image showing indication 2 (in circle blue) and indication 3 (out circle blue)

Vertical cylinders: Figure 56 shows an XCT cross section image of the vertical cylinders in Section 2. The expected diameter of each cylinder is labelled above each cylinder. The three largest cylinders can be observed clearly on the image. There is a fine line from where ⌀ 0,2 mm cylinder's diameter is expected to start to the 0,2 mm cylinder's diameter. There is no indication of a cylinder present at where the cylinder with 0,2 mm diameter is expected.

Dimensions in millimetres

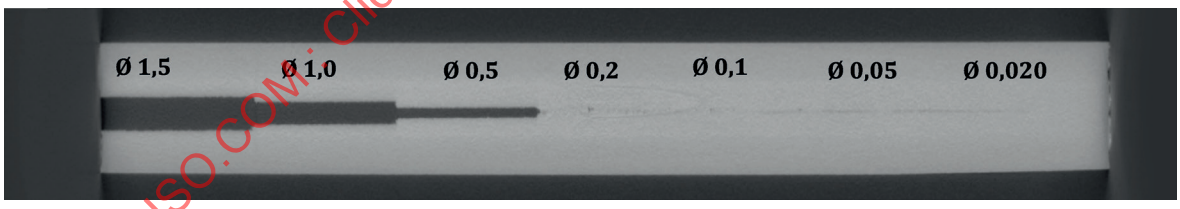

Figure 56 — XCT image showing the cross section through the vertical cylinders

Figure 57 shows a close up view of the cylinders with 0,5 mm and ⌀ 0,2 mm diameter. The 0,2 mm cylinder diameter does not have a consistent diameter and some sections are partially closed. In addition, the changes in the diameter from 0,5 mm to 0,2 mm diameter are not proportionate. The diameter of the 0,2 mm cylinder is smaller than expected and this extends to the 0,1 mm and 0,05 mm cylinder's diameter as shown in Figure 56. It indicates that defects under 0,2 mm diameter are unlikely or are too small to be made properly. In addition, it could illustrate that XCT system would be incapable to detect of detecting them.

Dimensions in millimetres

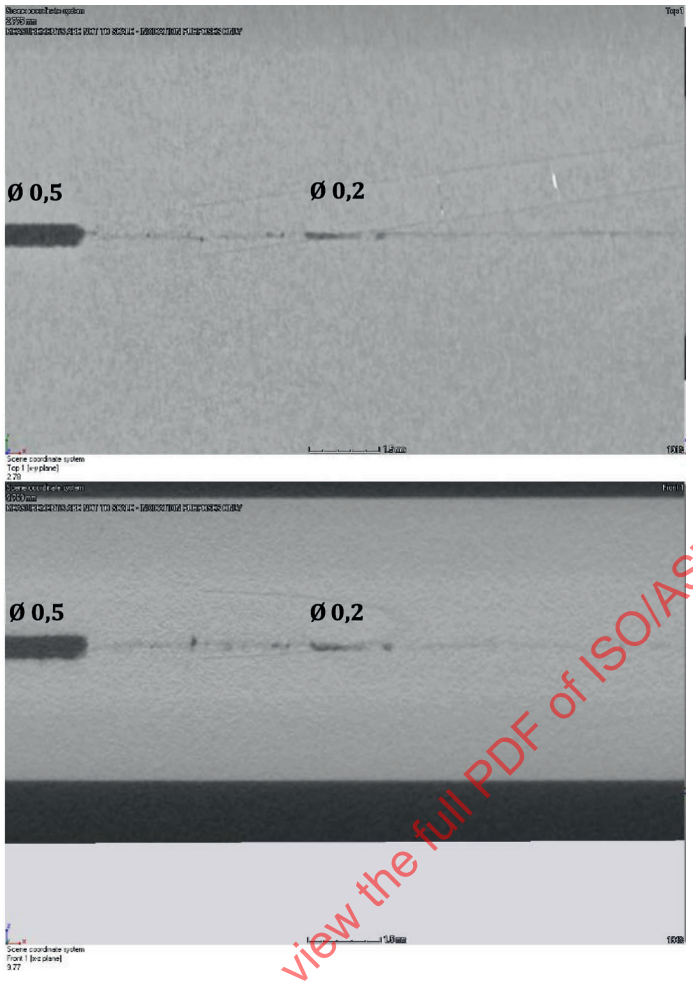

Figure 57 — XCT image showing the close up view of the 0,5 mm and 0,2 mm cylinder's diameter in Section 2

12.2 Summary of procedure by metallography

Star artefacts built from Hastelloy®[19] and Maraging steel were evaluated using conventional metallographic method including sectioning, mounting, grinding and final polishing as is indicated here. Three cut ups were performed for design S1corresponding to regions 2, 3, 4 and 5, while for design S2 two cut off, region 3 and region 4 were obtained (See Figure 58). The procedure applied for each material and region sectioned is described below:

— cut out samples — Buehler IsoMet high speed precision cutter;

— compression mounted - clear transoptic resin;

— marked and labelled samples;

— grinding down to the depth of the points of the stars using P120 SiC grinding;

— mild grinding to remove scratches and not lose the defects by P1200 grinding paper;

— ground using P4000 paper to remove large scratches;

— final polish using an Alumina suspension 0,05 µm;

19) Hastelloy is an example of a suitable product available commercially. This information is given for the convenience of users of this document and does not constitute an endorsement by ISO of this product.

— cleaned samples using Isopropanol;

— dry the samples and kept them on at desiccator for further process;

— analyse samples using an optical metallography microscopy.

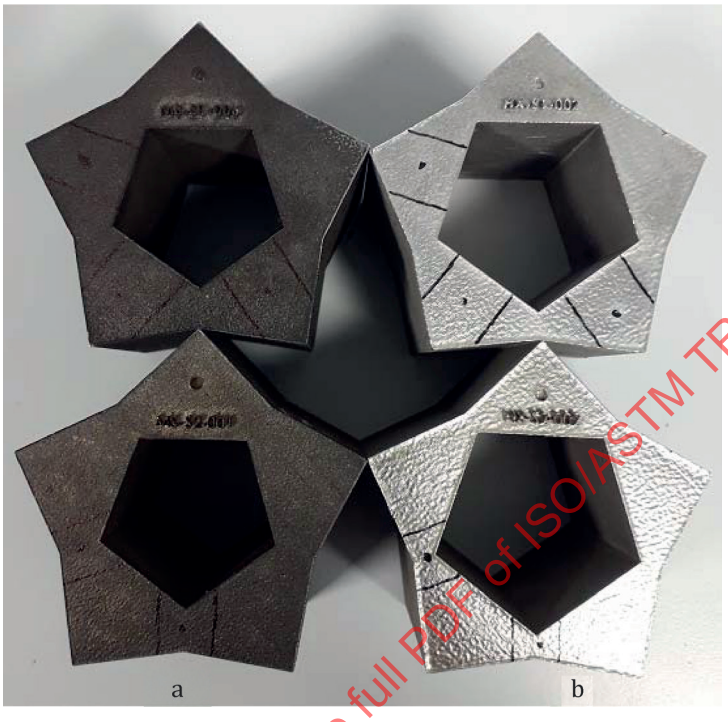

[a] Maranging steel.

[b] Hastelloy®.

NOTE The lines on the sample indicate the cut ups regions. Set Version S1 and S2 for Hastelloy® and Maraging steel were used for this comparison.

Figure 58 — Photo showing the set of samples used for the metallographic comparison

12.2.1 Apparatus

The cut-ups of the Hastelloy®[20] X and Maraging steel samples obtained via metallography preparation which were inspected using an optical metallographic microscope. The analysis was performed on a Zeiss imager M2m optical system, and each samples was evaluated on the regions of interest, measured and recorded accordingly. The measurement carried out at the ROI are summarised in Table 30.

12.2.2 Significance of data/Interpretation of results

The results of the metallography analysis performed on the star artefacts are summarised in Table 30, while examples of the metallography analysis are also shown in Figure 59.

20) Hastelloy is an example of a suitable product available commercially. This information is given for the convenience of users of this document and does not constitute an endorsement by ISO of this product.

Table 30 — Summary of the minimum dimension of the seeded defects measured by metallography analysis carry out in the star artefact design S1 and S2 in Hastelloy® and Maraging materials

Defect dimensions in millimetres

Design[a]	Defect region[b]	Defects size	
		Hastelloy®[c]	Maraging steel[c]
S0	NT[d]	NT[d]	NT[d]
S1	1	NT[d]	NT[d]
	2	0,3	0,1
	3	0,2	0,4
	4	0,4	0,2
	5	0,3	0,2
S2	1	NT[d]	NT[d]
	2	NT[d]	NT[d]
	3	0,4	0,2
	4	0,4	0,1
	5	NT[d]	NT[d]

[a] The star artefact correspond to the new design version S1 and S2 supplied by MTC.

[b] The analysis were performed in one sample per each region sectioned.

[c] The analysis were performed in one star artefact Hastelloy® and Maraging steel (design S1) and (design S2). The nominal features diameter size reported correspond to the average of the diameter detected using the set sample per each design.

[d] NT = Not tested.

The results showed that most of the seeded defects were successfully manufactured in the samples, however, the ones that were not found may be due to build limitations or were removed during the grinding stage. The smallest unconsolidated powder or trapped powder detected was between 0,2 mm to 0,4 mm in diameter. The smallest layer defect detected was between 0,2 mm to 0,4 mm in diameter. The smallest cross layer defect detected was 0,1 mm in diameter.

The metallography results for the two star artefacts showed the shape and dimensions of the artificial defects representing unconsolidated powder or trapped powder were not geometrical ideal as there were variations. It is not clear whether some of the missing defects were present during the built may have been eliminated during the metallography process. The validation performed through cut-ups and observation under microscope indicated that the artefacts did possess layer, cross layer defects and unconsolidated/trapped powder.

The analysis reported that the smallest defects detected was between 0,1 mm to 0,400 µm in diameter. However, it is assumed that some of the seeded defects were after the built but disappear or removed during the preparation process. It is stated based on the imagines of the areas where smallest indications clearly gave the idea that those are or were an artificial defect que was removed. The pictures in Figure 59 (a to d) shown the seeded defects detected via metallography microscope in the Hastelloy®[21] material in regions 2, 3, a and 5.

21) Hastelloy is an example of a suitable product available commercially. This information is given for the convenience of users of this document and does not constitute an endorsement by ISO of this product.

Diameter and length in millimetres

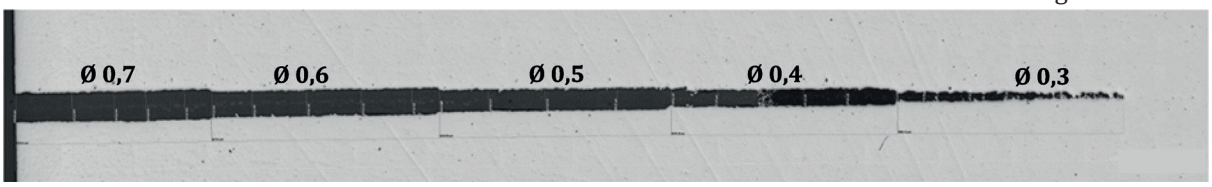

a) HX — S1 — Region 2. Five cylinders are detected

b) HX — S1 — Region 3. Five spheres detected, however, smallest dark indication is expected to be a seeded sphere 0,2 mm diameter

c) HX — S1 — Region 4. Five cylinders detected, however, smallest dark voids would indicated the presence of a seeded defect 0,2 mm

d) HX — S1 — Region 5. Five cylinders detected, however, smallest dark voids would indicated the presence of a seeded defect 0,2 mm

Figure 59 — Image of the HX region 2 version S1. Photo showing the set of samples used for the metallographic comparison

12.3 Comments/observations

— Two sections were cut-up from the Star 300A artefact labelled as Section 1, it was intended to possess spheres with trapped powder, and Section 2, vertical cylinders opening on one side. Both sections were inspected using the XCT system, Nikon XTH 225.

— Five indications were found in Section 1, near the area where the spheres are expected to be present. One indication, 0,2 mm diameter matched well with the expected description of the sphere, while the other four indications are likely to be real defects, but not necessarily the designed spheres.

— In Section 2, cylinders with diameter greater than 0,5 mm can be observed clearly in the XCT image. Cylinders smaller than 0,1 mm diameter were observed faintly in the XCT image. Based on their features, it is likely that they were not built correctly as some are partially closed.

— From the metallography analysis on the star artefacts version S1 and S2, cylinders with dimensions around 0,2 mm to 0,3 mm were detected and clearly indicate that the seeded defects were built. Also, the smallest size of the spheres were detected too.

— In overall, metallography analysis found that some defects not detected by XCT were found while in another cases occur the opposite. It could be indicated that metallography process preparation is helpful but it require special care to avoid bias the analysis.

13 NDT trials for à la carte artefact

Non-destructive inspection of the specific artefact built for these trials was carried out only by X-ray Computed Tomography, which is covered on this section.

13.1 Summary of procedure

The procedure to scanning the airfoil follows the same steps stated in 11.1.1.1. The inspection was carried out both concave (external and internal side) and convex (internal and external side). Figure 13 above illustrate the location of the point where holes were CAD seeded.

13.2 Apparatus

The XCT system used to inspect the air foil is the same used to inspect the star-shape reference in 11.1.1.2.

13.3 Significance of data/interpretation of results

The results of the XCT trials were performed by GE at their facilities in Zürich (Switzerland) for the generic airfoil version.

The XCT results showed that the artificial defects were successfully built. The smallest open surface defect detected was 0,1 mm in diameter, however, depending on location of the defect, this defect was not visible at some locations on the airfoil. Examples of the XCT image scan are presented from Figure 60 to Figure 63

Key

1 all 4 are visible
2 ⌀ 0,1 mm not visible
3 ⌀ 0,1 mm not visible
4 ⌀ 0,1 mm not visible
5 ⌀ 0,1 mm not visible

NOTE All defects are visible at one location while cylinders 0,1 mm diameter are not visible at the other locations.

Figure 60 — XCT image showing the horizontal cylinders outside concave side

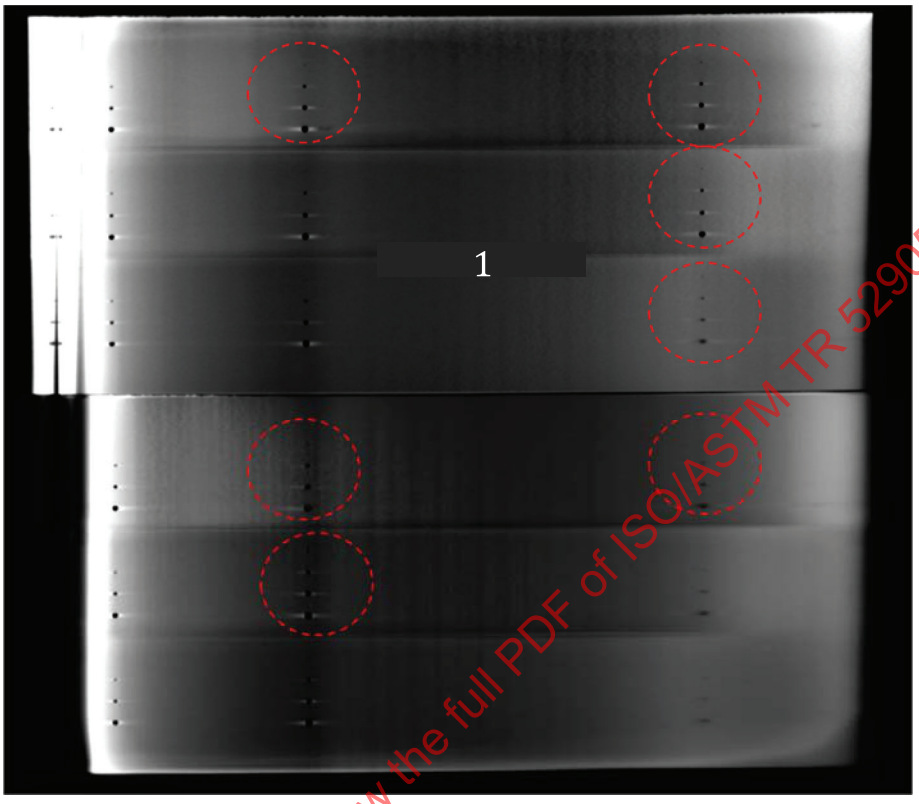

Key

1 all 4 are visible

NOTE All defects are visible a seven locations while holes with cylinders 0,1 mm diameter are not detectable at the other locations.

Figure 61 — XCT image showing the horizontal cylinders outside concave side

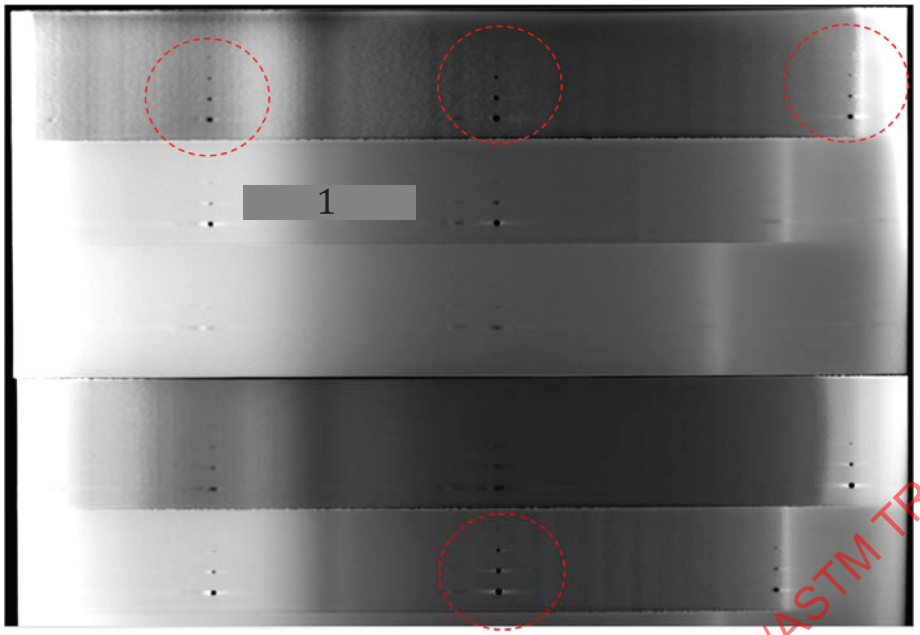

Key

1 all 4 are visible

NOTE All four size cylinders are visible a few locations, while cylinders with 0,1 mm diameter not detectable at the other locations.

Figure 62 — XCT image of air foil horizontal cylinders (layer defects) inside convex side

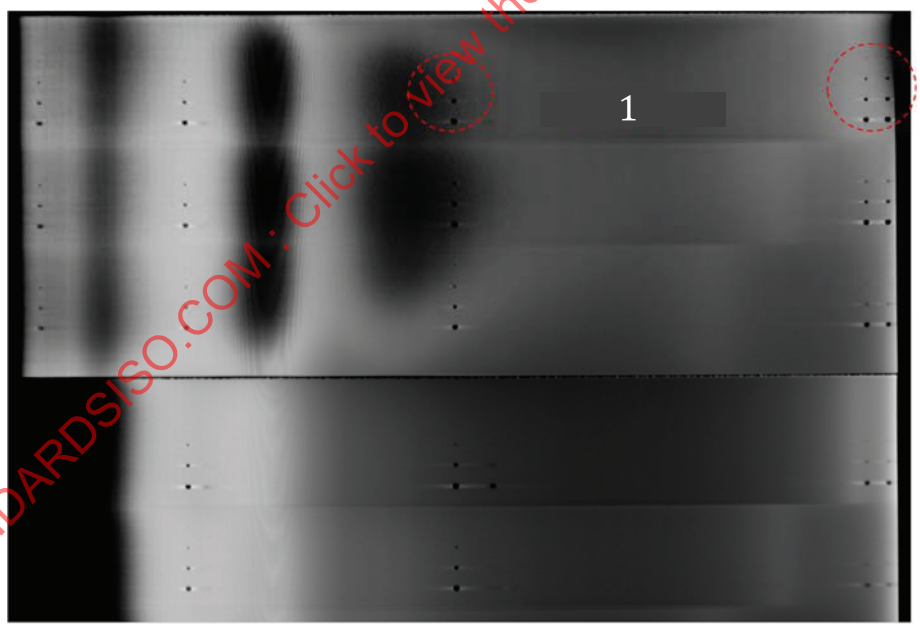

Key

1 all 4 are visible

NOTE All four size cylinders are visible a two locations, while cylinders with 0,1 mm diameter not detectable at the other locations.

Figure 63 — XCT image of air foil horizontal cylinders (layer defects) outside convex side

13.4 Comments/observations

The XCT inspection of the air foils was carried out by GE Power only. The results were shared with the MTC, and it was concluded that the majority of the defects (holes) on the air foils can be detected by XCT, except for the smallest holes (0,1 mm diameter) seeded on the part which it cannot be observed at a number of positions.

14 Summary of the trials findings by material

This section summarise of the analysis carried out by NDT technique on each material. The results presented from Table 31 to Table 37 reported the smallest defect detected per region and per set of samples tested which varied accordingly with the manufacturer or tester centre. For Hastelloy®[22] and Maraging steel a reference sample of the set is given for traceability purposes.

Table 31 — Summary of the smallest defects detected on the Hastelloy® star artefacts by NDT methods

Defect dimensions in millimetres

Built process		PBF[b]				
Design	Defect region	HX[b]				
		XCT[a]		TT[a]	PCRT[a]	NLR[a]
		ID	Defect			
S0	All	All	ND[c]	ND[c]	P[c]	ND[c]
S1	1	S1-005	All	ND[c]	F[c]	ND[c]
	2	S1-002	0,1	ND[c]		
	3	S1-001	0,4	ND[c]		
	4	S1-003	0,1	0,3		
	5	S1-004	0,2	0,3		
	Other	All	ND[c]	ND[c]		
S2	1	S2-001	0,1	ND[c]	F[c]	ND[c]
	2	S2-002	0,3	ND[c]		
	3	S2-005	0,1	ND[c]		
	4	S2-003	0,1	0,2		
	5	S2-002	All	0,2		
	Other	All	ND[c]	ND[c]		

[a] Abbreviations used: XCT = computed tomography, PCRT = process compensated resonance testing, NLR = non-linear acoustic resonance, TT = thermographic testing, UT = ultrasonic testing, PAUT = phase array ultrasonic testing, TFM = total focusing method, RS = residual stress.

[b] Material abbreviations used: HX = Hastelloy®, PBF = powder bed fusion.

[c] Abbreviations used for detection stage: DD = defects detected but not all, ND: not detected, NT = not tested, NS = not specified, P = pass, F = fail, Rp = reference point, C&P = cracks and porous

22) Hastelloy is an example of a suitable product available commercially. This information is given for the convenience of users of this document and does not constitute an endorsement by ISO of this product.

Table 32 — Summary of the smallest defects detected on the Maranging steel star artefacts by NDT methods

Defect dimensions in millimetres

Built process		PBF[b]				
		MS[b]				
Design	Defect region	XCT[a]		TT[a]	PCRT[a]	NLR[a]
		ID	Defect			
S0	All	All	ND[c]	ND[c]	P[c]	ND[c]
S1	1	S1-002	All	ND[c]	F[c]	ND[c]
	2	S1-001	0,1	ND[c]		
	3	S1-004	0,4	ND[c]		
	4	S1-003	0,2	0,3		
	5	S1-005	0,2	0,3		
	Other	All	ND[c]	ND[c]		
S2	1	S2-004	0,1	ND[c]	F[c]	ND[c]
	2	S1-003	0,1	ND[c]		
	3	S1-005	0,3	ND[c]		
	4	S2-002	0,1	0,2		
	5	S2-001	All	0,2		
	Other	All	ND[c]	ND[c]		

[a] Abbreviations used XCT = computed tomography, PCRT = process compensated resonance testing, NLR = non-linear acoustic resonance, TT = thermographic testing.

[b] Material abbreviations used: MS = maraging steel, PBF = powder bed fusion.

[c] Abbreviations used for detection stage: DD = Defects detected but not all, ND: not detected, NT = not tested, NS = not specified, P = pass, F = fail, Rp = reference point, C&P = cracks and porous.

Table 33 — Summary of the smallest defects detected on the stainless steel star artefacts by NDT methods

Defect dimensions in millimetres

Built process		PBF[b]	
		SS[b]	
Design	Defect region	XCT[a]	PAUT[a]
S0	All	NT[c]	NT[c]
S1	1	AD[c]	–
	2	0,1	0,1
	3	0,4	ND[c]
	4	0,2	0,3
	5	0,3	0,4
	Other	NS[c]	ND[c]

[a] Abbreviations used: XCT = computed tomography, PAUT = phased array.

[b] Material abbreviations used: SS = stainless steel, PBF = powder bed fusion.

[c] Abbreviations used for detection stage: AD = all detected, DD = defects detected but not all, ND: not detected, NT = not tested, NS = not specified, P = pass, F = fail, Rp = reference point, C&P = cracks and porous.

Table 33 *(continued)*

Built process		PBF[b]	
Design	Defect region	SS[b]	
		XCT[a]	PAUT[a]
S2	1	0,2	NT[c]
	2	0,2	
	3	0,3	
	4	0,1	
	5	DD[c]	
	Other	ND[c]	

[a] Abbreviations used: XCT = computed tomography, PAUT = phased array.

[b] Material abbreviations used: SS = stainless steel, PBF = powder bed fusion.

[c] Abbreviations used for detection stage: AD = all detected, DD = defects detected but not all, ND: not detected, NT = not tested, NS = not specified, P = pass, F = fail, Rp = reference point, C&P = cracks and porous.

Table 34 — Summary of the smallest defects detected on the Inconel®[23] star artefacts by NDT methods

Defect dimensions in millimetres

Built process		PBF[b]
Design	Defect region	IN[b]
		XCT[a]
S0	All	NT[c]
S1	1	0,2
	2	ND[c]
	3	Rp[c]
	4	0,2
	5	ND[c]
	Other	ND[c]
S2	1	0,2
	2	0,2
	3	Rp[c]
	4	0,2
	5	0,2
	Other	ND[c]

[a] Abbreviations used: XCT = computed tomography.

[b] Material abbreviations used: IN = Inconel, PBF = powder bed fusion.

[c] Abbreviations used for detection stage: DD = defects detected but not all, ND = not detected, NT = not tested, NS = not specified, P = pass, P = fail, Rp = reference point, C&P = cracks and porous.

23) Inconel is an example of a suitable product available commercially. This information is given for the convenience of users of this document and does not constitute an endorsement by ISO of this product.

Table 35 — Summary of the smallest defects detected on the Cobalt-Chrome star artefacts by NDT methods

Defect dimensions in millimetres

Built process		PBF[b]	
Design	Defect region	CoCr[b]	
		XCT[a]	SX[a]
S0	All	NT[c]	NT[c]
S1	1	NT[c]	NT[c]
	2		
	3		
	4		
	5		
	Other		
S2	1	0,3	0,2
	2	0,3	0,2
	3	0,5	0,2
	4	0,3	0,15
	5	DD[c]	DD[c]
	Other	ND[c]	ND[c]

[a] Abbreviations used: XCT = computed tomography, SX = synchrotron X-rays.

[b] Material abbreviations used: CoCr = cobalt-chrome, PBF = powder bed fusion.

[c] Abbreviations used for detection stage: DD = defects detected but not all, ND: not detected, NT = not tested, NS = not specified, P = pass, F = fail, Rp = reference point, C&P = cracks and porous.

Table 36 — Summary of the smallest defects detected on the aluminium star artefacts by NDT methods

Defect dimensions in millimetres

Built process		PBF[b]	
Design	Defect region	AL[b]	
		CUT[a]	PAUT[a]-TFM[a]
S0	All	NT[c]	NT[c]
S1	1	NS[c]	DD[c]
	2	NS[c]	0,1
	3	NS[c]	0,5
	4	NS[c]	0,5
	5	NS[c]	NS[c]
	Other	ND[c]	ND

[a] Abbreviations used: CUT = conventional ultrasonic testing, PAUT = phase array ultrasonic testing, TFM = total focusing method, AL = aluminium.

[b] Material abbreviations used: HX = Hastelloy®, PBF = powder bed fusion, EBM = electron beam melting.

[c] Abbreviations used for detection stage: DD = defects detected but not all, ND: not detected, NT = not tested, NS = not specified, P = pass, F = fail, Rp = reference point, C&P = cracks and porous.

Table 36 *(continued)*

Built process		PBF[b]	
Design	Defect region	AL[b]	
		CUT[a]	PAUT[a]-TFM[a]
S2	1	NT[c]	NS[c]
	2		0,4
	3		0,1
	4		0,1
	5		0,2
	Other		ND[c]

[a] Abbreviations used: CUT = conventional ultrasonic testing, PAUT = phase array ultrasonic testing, TFM = total focusing method, AL = aluminium.

[b] Material abbreviations used: HX = Hastelloy®, PBF = powder bed fusion, EBM = electron beam melting.

[c] Abbreviations used for detection stage: DD = defects detected but not all, ND: not detected, NT = not tested, NS = not specified, P = pass, F = fail, Rp = reference point, C&P = cracks and porous.

Table 37 — Summary of the smallest defects detected on the Ti6Al4V star artefacts by NDT methods

Defect dimensions in millimetres

Built process		PBF[b] & EBM[b]		
Design	Defect region	Ti6Al4V[b]		
		XCT[a]	SX[a]	NI[a]
S0	All	NT[c]	NT[c]	NT[c]
SP_{SLM}	1	–	0,1	0,2
	2	–	0,1	0,2
	3	–	0,1	0,2
	4	–	ND[c]	ND[c]
	5	–	ND[c]	ND[c]
	Other	–	C&P[c]	C&P[c]
SP_{EBM}	1	–	0,2	0,2
	2	–	0,2	0,2
	3	–	0,2	0,2
	4	–	ND[c]	ND[c]
	5	–	ND[c]	ND[c]
	Other	–	C&P[c]	C&P[c]

[a] Abbreviations used: XCT = computed tomography, SX = synchrotron X-rays, NI = neutron imaging, PAUT = phase array, TFM = total focusing method.

[b] Material abbreviations used: Ti64 = Ti6Al4V, PBF = powder bed fusion, EBM = electron beam melting.

[c] Abbreviations used for detection stage: DD = defects detected but not all, ND = not detected, NT = not tested, NS = not specified, P = pass, F = fail, Rp = reference point, C&P = cracks and porous.

15 Main conclusions

The main conclusion of this document, which include reviews carried out, potential NDT methods and trials are summarised as follows:

— **A review of the main causes and mode of failures** was carried out for DED and PBF process. Post built classification of the main defects was listed and samples given including a strategic for

classification of defects for AM as well as the capabilities and limitations of NDT methods for AM inspection.

— **In-process inspection** was reviewed and the main NDT approaches that offer most potential included Thermography, laser ultrasonic with laser line scanner as an additional option for metrology measurement.

— **A review of the currently NDT standards** for post-processing and in-process inspection in DED and PBF process was performed based on casting and welding standards. It was found that there are some similarities between defects from these two process with DED and PBF. From the defect type aspect, defects in DED can potentially be covered by current standards, however, for PBF some flaws are not included which are unique to AM including layer, cross layer, trapped powder and unconsolidated powder flaws. It was established that new developed standards are needed to assess this type of flaws.

— **The star and à la carte artefacts** were designed and built to cover those defects not included by current NDT standards, which are unique for additive process such as layer, cross layer and unconsolidated powder/trapped powder. The generic geometry star may be used as an initial NDT technique verification and could be applicable to relatively simple AM geometries, while the à la carte artefact shows the process to follow for more complex part applications. Both artefact designs were seeded with CAD simulate identified AM only defects to assess the capability of NDT methods.

— **Star artefacts trials** of selected NDT techniques provided the following conclusions:

  — In the following order, Synchrotron, XCT and Neutron methods offer the best resolution and detection capability, respectively. The three approaches were capable to detect smallest defects between 0,1 mm to 0,2 mm size being Synchrotron the technique that offer the finest resolution. In addition, synchrotron provides an excellent capability to detect partially filled spheres with powder.

  — Ultrasonic methods represented in these trials by conventional UT and PAUT shows limited capability. UT is limited to detect defects showing inconclusive results. PAUT shows capability to detect defects with size greater than 0,3 mm, however, when it is working in conjunction with FMC/TFM approach; it is able to detect 0,1 mm defects in some accessible locations.

  — Thermography test was able to detect open surfaces defects with sizes greater than 0,4 mm using flash thermography, however, when Step-heating method is used, it is capable to detect open surfaces defects not less than 0,2 mm diameter.

  — PCRT and RAM techniques are able to assess presence of defects on the samples inspected during the trials despite the smaller population used. The three different groups of full size parts for Hastelloy®[24] and Maraging steel were identified and are separated from each other as good parts or bad parts. The analysis carry out in the half-size star artefacts for Stainless Steel also shown PCRT and RAM capability for defect detection to differential good and bad parts.

  — NLR results were inconclusive for all the samples tested. It was concluded that either the samples do not exhibit significant nonlinear resonance features, or higher excitation levels are required. However, this method has shown some capability on a different geometry inspected in AMAZE project[21].

  — The residual stress distribution measured by ND in the star through its thickness shows a parabolic and symmetric tendency of stress distribution from bottom to top finishing surfaces for all strain components, with a plateau within the middle of the bulk and an inversion of

24) Hastelloy is an example of a suitable product available commercially. This information is given for the convenience of users of this document and does not constitute an endorsement by ISO of this product.

tensile/compressive at around 4,5 mm from top and from bottom surfaces. It demonstrated that high tensile strains are present near surface regions.

— **The XCT trials using the à la carte design** concluded that the majority of the defects (holes) on the airfoils can be detected by XCT, except for the smallest diameter holes (0,1 mm) seeded on the part which cannot be observed at a number of positions.

— **Defect build validation** using XCT method show that the area where the spheres are expected to be present one indication, 0,2 mm diameter matched well with the expected description of the sphere, while the other four indications are likely to be real defects, but not necessarily the designed spheres. Cylinders smaller than 0,1 mm diameter were observed faintly in the XCT image. Based on their features, it is likely that they were not built as some are partially closed.

— **Cut-ups and metallography build validation** analysis were carried out. The results clearly show that seeded defects with dimensions of 0,2 mm were visible under the optical microscope. Special attention is needed during metallography preparation to avoid impacting the results of the analysis, by removing the CAD seeded defects.

Annex A
(informative)

Causes and effects of defects in wire DED and PBF process

Table A.1 — Causes and effects of defects common in wire DED

Issue	Cause	Effect/defect on part
Metal transfer behaviour	Severe spatter generation	**Poor surface** quality in the as-deposited condition **Lack of geometrical accuracy**, possibly as a result of inconsistent stand-off distances Formation of deep and **continuous undercuts** at the toe of the welds between adjoining weld beads Bulk of the part may be compromised by **incomplete fusion** between weld beads
	Wire burn-back	Wire burn-back may severely affect the integrity of the part due to **incomplete fusion. Rough and rippled weld bead** surfaces with inconsistent cross-sectional profile.
Weld pool behaviour	Thermal cushioning effect (the front edge of the weld pool liquid grows ahead of the welding arc)	**Incomplete fusion** between the entire base metal surfaces and between adjoining weld beads. Weld string separation that will most probably result in **incomplete fusion** defects.
	Melt pool contraction/poor wetting and spreading	
	Continuous undercut along the string	**Incomplete fusion** all along the adjoining weld bead Local **incomplete fusion** Weld string separation that will most probably result in **incomplete fusion** defects
	Uneven weld pool liquid front (asymmetric)	**Reduced surface finish quality** **Incomplete fusion** defects, possibly due to weld string separation or undercut formation
	Excessively high weld pool depression	**Incomplete fusion** defects due to undercutting, humping, and porosity defects
	"Blow-holes"	**Incomplete fusion** Defects such as **holes, voids, undercuts**, etc.
Wire	Fouled wire	**Incomplete fusion** defects due to inconsistent wire feeding characteristics and variation in arc welding behaviour. Non-metallic **inclusions**, giving rise to variation of mechanical properties

Table A.2 — Causes and effects of defects common in powder bed fusion

Issue	Cause	Effect on/defect in part
Incomplete powder feed	— Powder run out — Poor powder flow properties, incl. bridging of powder in the hopper	Unconsolidated powder (large area)
"Drags" (lines) in the powder layer	— Agglomerated powder or contamination	Unconsolidated powder (localised area)
Poor fusing due to interruption to laser/EBM delivery	— Interruption to powder supply, optics systems errors (laser) or errors in data	Unconsolidated powder (large or small areas)

Table A.2 *(continued)*

Issue	Cause	Effect on/defect in part
Incorrect laser/EBM power	— Incorrect choice of parameters — Uncontrolled change in laser/EBM power	Over- or under-melted material
Layer shift	— SLM — scan head/optics problems — EBM — presence of electromagnetic interference — Build platform shift	Steps in part
Contamination of powder (Interstitials)	— New powder out of spec or degraded through reuse	Reduced mechanical properties (may get higher modulus but lower elongation)
Contamination of powder (Foreign body)	— Debris from AM or post processing equipment	Reduced mechanical properties (this risk can be eliminated completely)
Incorrect scaling/beam offset	— Scaling/offset factors are effected by part geometry, beam intensity and the density of the powder bed	Poor accuracy
Incorrect scan strategy	— Poor selection of parameters — Errors in beam delivery	Voids, unconsolidated powder
Gas-atomised powder particles	— Trapped gas bubbles	Pores
Poor localised layer surface quality	— Localised disturbance of melt pool — Lack of molten material feeding in localised area	Reduced wettability, pores
Development of high internal stress in some types of materials	— Heavily alloyed material or materials with a composition that cannot accommodate high residual stress	Cracking

Annex B
(informative)

Review of existing NDT standards for welding or casting for application of post build AM flaws

Table B.1 — Diagram showing the current NDT standards for welding (ISO 17635)

No	AM flaws on as-build parts	Similar flaw in weld (fusion) or casting	Manufacturing stage	Method	Welding or casting standards	Applicability to AM flaws
1	Void	Void	As-built	Radiography	ISO 17636-1, ISO 17636-2, ISO 10675-1, ISO 10675-2, EN 13068-3	Yes
			Post machined	Radiography	ISO 17636-1, ISO 17636-2, ISO 10675-1, ISO 10675-2, EN 13068-3, ISO 4993	Yes
				Ultrasonic	ISO 17640, ISO 23279, ISO 11666, ISO 10863, EN 15617, ISO 4992-1, ISO 4992-2	Depends on part external and internal geometry. Simple geometry is possible but complex geometry will have limited coverage and limited access for inspection.
2	Porosity	Porosity. A series on porosities joined in a line is also called wormholes or elongated cavities.	As-built	Radiography	ISO 17636-1, ISO 17636-2, ISO 10675-1, ISO 10675-2, EN 13068-3, ISO 4993	Yes
			Post machined	Radiography	ISO 17636-1, ISO 17636-2, ISO 10675-1, ISO 10675-2, EN 13068-3, ISO 4993	Yes
				Ultrasonic	ISO 17640, ISO 23279, ISO 11666, ISO 10863, EN 15617, ISO 4992-1, ISO 4992-2	Depends on part external and internal geometry. Simple geometry is possible but complex geometry will have limited coverage and limited access for inspection.

Table B.1 *(continued)*

No	AM flaws on as-build parts	Similar flaw in weld (fusion) or casting	Manufacturing stage	Method	Welding or casting standards	Applicability to AM flaws
3	Surface flaw (cracks, crater, voids, porosity) This excludes poor surface finish which can be covered by dimensional measurement (surface roughness).	Surface flaw including crack, void, inclusion, undercut, overlap, incomplete fusion, spatter, sagging, excess penetration, crater crack, incomplete root penetration, groove, excess weld metal. Steps in part.	As-built	Visual	ISO 17637, ISO 5817, ISO 10042, ISO 11971	Yes
				Penetrant	ISO 23277, ISO 3452-1, ISO 4987	Not applicable. As-built component have rough surface which is not suitable for penetrant inspection.
				Magnetic particle	ISO 17638, ISO 23277, ISO 4986	Not applicable. As-built component have rough surface which is not suitable for magnetic particle inspection.
			Post machined	Visual	ISO 17637, ISO 5817, ISO 10042, ISO 11971	Yes
				Penetrant	ISO 23277, ISO 3452-1, ISO 4987	Yes. It is likely that most surface flaws can be eliminated by machining the surface.
				Magnetic particle	ISO 17638, ISO 23277, ISO 4986	Yes for ferromagnetic materials. It is likely that most surface flaws can be eliminated by machining the surface.
4	Incomplete fusion (DED only)	Non-uniform weld bead and fusion characteristic	As-built	Visual	ISO 17637, ISO 5817, ISO 10042, ISO 11971	Applicable for external flaws only.
				Radiography	ISO 17636-1, ISO 17636-2, ISO 10675-1, ISO 10675-2, EN 13068-3, ISO 4993	In DED, direction of radiography beam is important to get a good coverage on the incomplete fusion flaws.
			Post machined	Visual	ISO 17637, ISO 5817, ISO 10042, ISO 11971	Applicable for external flaws only.
				Radiography	ISO 17636-1, ISO 17636-2, ISO 10675-1, ISO 10675-2, EN 13068-3, ISO 4993	In DED, direction of radiography beam is important to get a good coverage on the incomplete fusion flaws.
				Ultrasonic	ISO 17640, ISO 23279, ISO 11666, ISO 10863, EN 15617, ISO 4992-1, ISO 4992-2	Applicable for simple external and internal geometry. Complex geometry will have limitations.

Table B.1 *(continued)*

No	AM flaws on as-build parts	Similar flaw in weld (fusion) or casting	Manufacturing stage	Method	Welding or casting standards	Applicability to AM flaws
5	Undercuts at the toe of the welds between adjoining weld beads	Undercuts	As-built	Visual	ISO 17637, ISO 5817, ISO 10042, ISO 11971	Applicable for external flaws only.
				Radiography	ISO 17636-1, ISO 17636-2, ISO 10675-1, ISO 10675-2, EN 13068-3, ISO 4993	In DED, direction of radiography beam is important to get a good coverage on the flaws.
			Post machined	Visual	ISO 17637, ISO 5817, ISO 10042, ISO 11971	Applicable for external flaws only.
				Radiography	ISO 17636-1, ISO 17636-2, ISO 10675-1, ISO 10675-2, EN 13068-3, ISO 4993	In DED, direction of radiography beam is important to get a good coverage on the flaws.
				Ultrasonic	ISO 17640, ISO 23279, ISO 11666, ISO 10863, EN 15617, ISO 4992-1, ISO 4992-2	Applicable for simple external and internal geometry. Complex geometry will have limitations.
6	Inclusion in part (from contamination in powder or from wire feedstock)	Inclusion (slag, flux, oxide and metallic inclusion other than copper)	As-built	Radiography	ISO 17636-1, ISO 17636-2, ISO 10675-1, ISO 10675-2, EN 13068-3, ISO 4993	Inclusion of the same density to the part will be difficult to detect.
				Ultrasonic	ISO 17640, ISO 23279, ISO 11666, ISO 10863, EN 15617	Not possible due to surface roughness.
			Post machined	Radiography	ISO 17636-1, ISO 17636-2, ISO 10675-1, ISO 10675-2, EN 13068-3, ISO 4993	Inclusion of the same density to the part will be difficult to detect.
				Ultrasonic	ISO 17640, ISO 23279, ISO 11666, ISO 10863, EN 15617, ISO 4992-1, ISO 4992-2	Applicable for simple external and internal geometry. Complex geometry will have limitations.

Table B.1 *(continued)*

No	AM flaws on as-build parts	Similar flaw in weld (fusion) or casting	Manufacturing stage	Method	Welding or casting standards	Applicability to AM flaws
7	Non-uniform weld bead and fusion characteristic	Non-uniform weld bead	As-built	Visual	ISO 17637, ISO 5817, ISO 10042, ISO 11971	Applicable for external flaws only.
				Radiography	ISO 17636-1, ISO 17636-2, ISO 10675-1, ISO 10675-2, EN 13068-3, ISO 4993	Direction of radiography beam is important to get a good coverage on the flaws.
			Post machined	Visual	ISO 17637, ISO 5817, ISO 10042, ISO 11971	Applicable for external flaws only
				Radiography	ISO 17636-1, ISO 17636-2, ISO 10675-1, ISO 10675-2, EN 13068-3, ISO 4993	Direction of radiography beam is important to get a good coverage on the flaws.
				Ultrasonic	ISO 17640, ISO 23279, ISO 11666, ISO 10863, EN 15617, ISO 4992-1, ISO 4992-2	Applicable for simple external and internal geometry. Complex geometry will have limitations.
8	Unconsolidated powder	None	As-built	Radiography	None	New standard is required.
			Post machined	Radiography	None	New standard is required.
				Ultrasonic	None	New standard is required.
			Post machined	Radiography	None	New standard is required.
				Ultrasonic	None	New standard is required.
9	Cross layer	None	As-built	Visual	None	New standard is required.
				Radiography	None	New standard is required.
			Post machined	Visual	None	New standard is required.
				Radiographic	None	New standard is required.
				Ultrasonic	None	New standard is required.
10	Layer	None	As-built	Visual testing	None	New standard is required.
				Radiographic	None	New standard is required.
			Post machined	Visual	None	New standard is required.
				Radiographic	None	New standard is required.
				Ultrasonic	None	New standard is required.
11	Trapped powder	None	As-built	Radiography	None	New standard is required.
			Post machined	Ultrasonic	None	New standard is required.

Annex C
(informative)

Star artefacts using during the trials

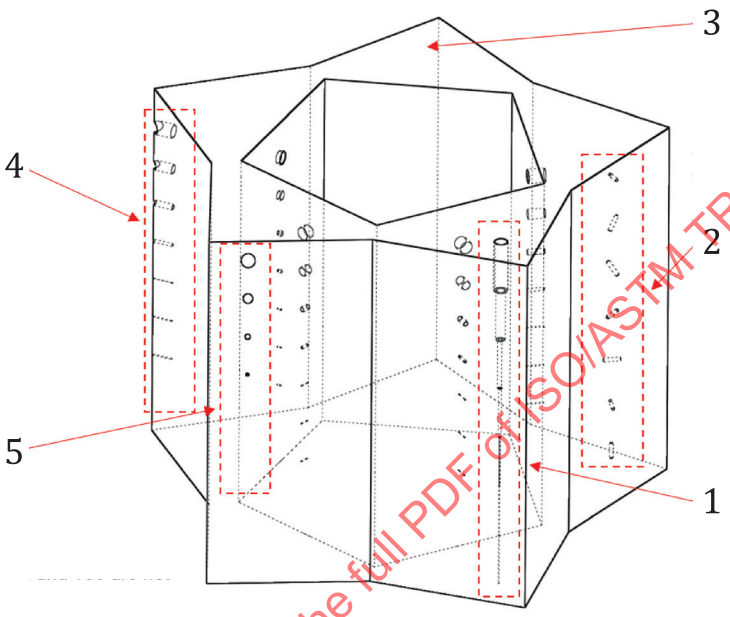

a)

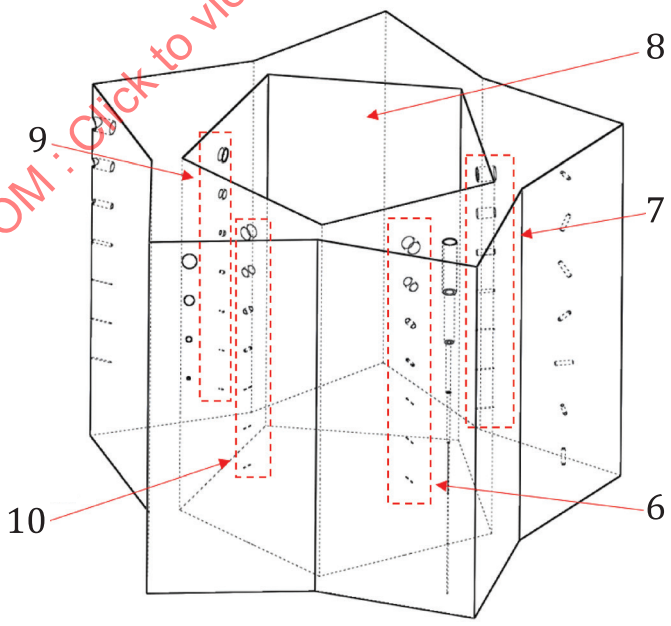

b)

Key

1 vertical cylinders, interconnected and open at both top and bottom (cross layer defects)
Length=6 400 µm
⌀ (µm)=20, 50, 100, 200, 500, 1 000, and 1 500.

2 cylinders in various orientations (unconsolidated/trapped powder)
length=200 µm
⌀ (µm)=300.

3 reference section (no seeded defects)

4 horizontal cylinders, open at the outside edge (layer defects)
length-2 000 µm
⌀ (µm)=20, 50, 100, 200, 500, 1 000, and 1 500.

5 spheres (voids/porosity, unconsolidated/trapped powder)
⌀ (µm)=20, 50, 100, 200, 500, 1 000, and 1 500
note that 20, 50, and 100 are not visible here.

6 horizontal cylinders (layer defects)
length=1 500 µm
⌀ (µm)=20, 50, 100, 200, 500, 1 000, and 1 500.

7 horizontal cylinders (layer defects)
length=2 000 µm
⌀ (µm)=20, 50, 100, 200, 500, 1 000, and 1 500.

8 reference section (no seeded defects)

9 horizontal cylinders (layer defects)
length=500 µm
⌀ (µm)=20, 50, 100, 200, 500, 1 000, and 1 500.

10 horizontal cylinders (layer defects)
length=1 000 µm
⌀ (µm)=20, 50, 100, 200, 500, 1 000, and 1 500.

Figure C.1 — Preliminary star artefact design

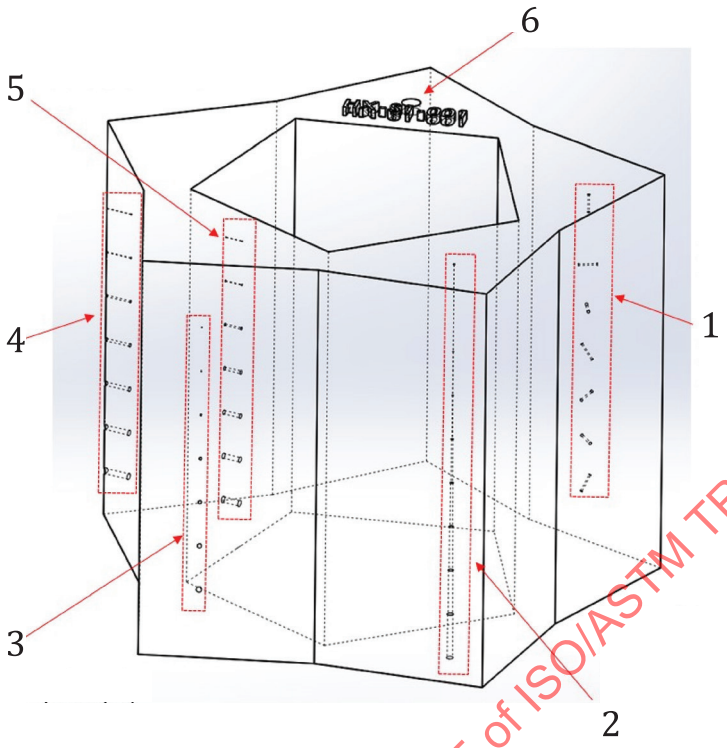

a)

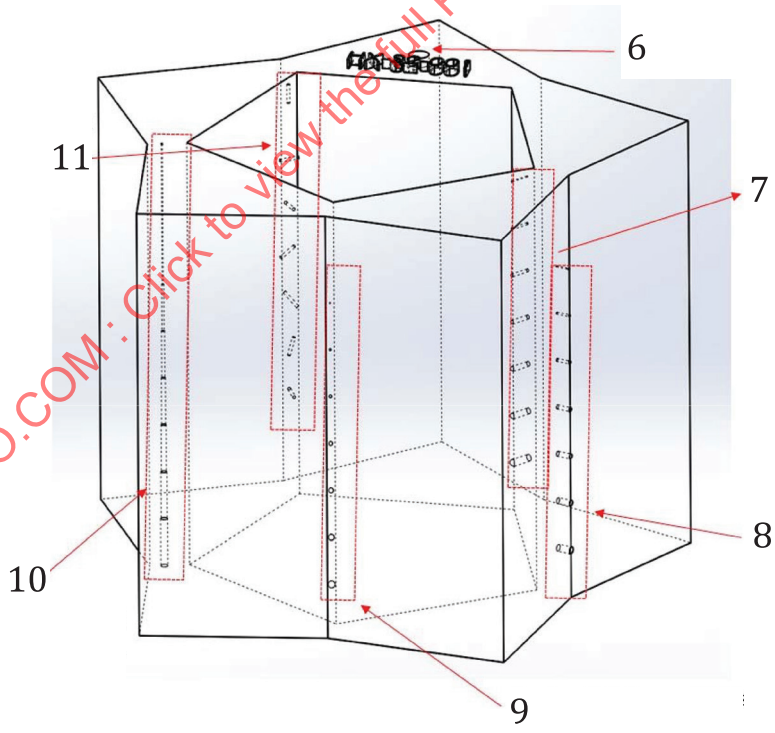

b)

Key

1 cylinders in various orientations (unconsolidated/trapped powder)
length (mm): 2,0
⌀ (mm): 0,3

2 vertical cylinders, interconnected and open at both top and bottom (cross layer defects)
length (mm): 5,0
⌀ (mm): 0,1, 0,2, 0,3, 0,4, 0,5, 0,6, and 0,7

3 spheres (voids/porosity, unconsolidated/trapped powder)
⌀ (mm): 0,1, 0,2, 0,3, 0,4, 0,5, 0,6, and 0,7

4 horizontal cylinders, open at the outside edge (layer defects)
length (mm): 3,0
⌀ (mm): 0,1, 0,2, 0,3, 0,4, 0,5, 0,6, and 0,7

5 horizontal cylinders, open at the inside edge (layer defects)
length (mm): 2,0
⌀ (mm): 0,1, 0,2, 0,3, 0,4, 0,5, 0,6, and 0,7

6 reference section- no seeded defects

7 horizontal cylinders, open at the inside edge (layer defects)
length (mm): 2 000
⌀ (mm): 0,1, 0,2, 0,3, 0,4, 0,5, 0,6, and 0,7

8 horizontal cylinders, open at the outside edge (layer defects)
length (mm): 2,5
⌀ (mm): 0,1, 0,2, 0,3, 0,4, 0,5, 0,6, and 0,7

9 spheres (voids/porosity, unconsolidated/trapped powder)
⌀ (mm): 0,1, 0,2, 0,3, 0,4, 0,5, 0,6, and 0,7

10 vertical cylinders, interconnected and open at both top and bottom (cross layer defects)
length (mm): 5,0
⌀ (mm): 0,1, 0,2, 0,3, 0,4, 0,5, 0,6, and 0,7

11 cylinders in various orientations (unconsolidated/trapped powder)
length (mm): 2,0
⌀ (mm): 0,3

Figure C.2 — Final design star artefacts used during the trials

Annex D
(informative)

Summary of star artefact manufacturing and NDT technologies for trials

Table D.1 — Summary of the samples builds including manufacturer, material, star type, size and quantity

No	Manufacturer	Material	AM process	Version	Size: F (full)/HF (half)	Qty
1	NIST/LNE	CoCr	PBF	S0	F	1
				S2	F	3
				S0	HF (defects/2 also)	1
				S2	HF (defects/2 also)	1
2	Zodiac Aerospace	AlSi10Mg	PBF	S1	F	1
				S2	F	1
3	NIST/LNE	Stainless steel 17-4	PBF	S0	F	2
				S1	F	2
				S2	F	2
				S0	HF	40
				S1	HF	8
				S2	HF	8
				S2	HF without defect in region 1	8
				S2	HF without defect in regions 1 and 2	8
				S2	HF without defect in regions 1, 2 and 3	8
				S2	HF without defect in regions 1, 2, 3 and 4	8
5	GE Power	Hastelloy®[25)]	LPBF	S0	F	5
				S1	F	7
				S2	F	5
6	Parker	Maranging Steel	LBPF	S0	F	5
				S1	F	6
				S2	F	5
				S0	F	1
				S2	F	1

NOTE.

S_{EB}: Star artefact manufactured by EB-PBF process

S_{LB}: Star artefact manufactured by L-PBF process

25) Hastelloy is an example of a suitable product available commercially. This information is given for the convenience of users of this document and does not constitute an endorsement by ISO of this product.

Table D.1 *(continued)*

No	Manufacturer	Material	AM process	Version	Size: F (full)/HF (half)	Qty
8	BAE System	Ti Cp	LBPF	S0	F	3
				S1	F	3
				S2	F	3
9	MTC	Ti6Al4V	EBM	S_{EB}	F	1
	UoB		LBPF	S_{LB}	F	1

NOTE.

S_{EB}: Star artefact manufactured by EB-PBF process

S_{LB}: Star artefact manufactured by L-PBF process

Table D.2 — Summary of the NDT (Material & NDE technologies), and company/Universities/ Research centre having performed the trials

Material	NDT Technologies	Research Centre/Company/University
Hastelloy®[26] X (HX)	XCT[a]	MTC, UK
	PAUT[c]	University of Bristol, UK
	PCRT[d]	Vibrant, Germany
	NLA[e]	Theta Tech, UK
	TT[f]	University of Bath, UK
Maraging steel (MS)	XCT[a]	MTC, UK
	PAUT[c]	University of Bristol, UK
	PCRT[d]	Vibrant, Germany
	NLA[e]	Theta Tech, UK
	TT[f]	University of Bath, UK
Cobalt Chrome (CoCr)	RAM[g]	NIST/LNE &TMS, USA/France
	XCT[a]	NIST/LNE, USA/France
	SX[b]	NIST/LNE & ESRF, USA/France
Stainless Steel 17-4 (SS)	XCT[a]	EWI, USA
	PAUT[c]	EWI, USA
	XCT[a] -Low Energy	ISS, Germany
	XCT[a]	MTC, UK
	RAM[g]	NIST/LNE & TMS, USA/France
	PCRT[d]	NIST/LNE & Vibrant, USA/France
Aluminium	XCT[a]	MTC, UK
	CUT/PAUT[j]	NIST/LNE & OKOS, USA/France
	PAUT[c] — TFM[k]	NIST/LNE & TPAC, USA/France
Titanium Cp	XCT[a]	MTC, UK
Ti6Al4V	SX[b] & NI[h]	ESRF, France & HBZ, Germany

26) Hastelloy is an example of a suitable product available commercially. This information is given for the convenience of users of this document and does not constitute an endorsement by ISO of this product.

Table D.2 *(continued)*

Material	NDT Technologies	Research Centre/Company/University
[a] X-Ray Computed Tomography		[g] Resonance Acoustic Method
[b] Synchrotron X-ray Tomography		[h] Neutron Imaging
[c] Phased Array Ultrasonic Testing		[i] Digital Radiography testing
[d] Process Compensated Resonance Testing		[j] Pulse/echo Ultrasonic Testing
[e] Nonlinear acoustic method		[k] Total Focus Matrix
[f] Thermography testing		

Annex E
(informative)

XCT parameters and XCT set up used for inspection and validation

E.1 Scan parameters for systems at EWI, MTC and GE

Table E.1 — XCT parameter for the 450 kV system at EWI, MTC and GE (De) on the final star design

XCT parameter	EWI [a] SS Value [a]	MTC [b] HX and MS Value [b]	MTC [b] IN718	GE [c] Co-Cr Value [c]
Voltage (kV)	300	340	TBC	450
Current (µA)	332	230		1,6
Power (W)	99,7	78,2		720
Target	W	W		TBI
Filter (material/mm)	Sn/5 mm	Cu/4 mm		Sn/1 mm Cu/1 mm
Exposure time (ms)	2 000	1 000		600
Image per projection	1	1		
Number of projection	3 141	3 500		1 080
Source-to-object distance (mm)	255,08	429,178		900
Source-to-detector distance (mm)	1 021,34	1 026,68		1 300
Magnification	4	2,39		1,44
Detector pixel (µm)	200	200		144
Voxel size (µm)	49,96	83,6		~100
Focal spot size (µm)	~100	~100		

[a] Nikon XT H-450 kV system high brilliant source. System located in the USA.

[b] Nikon XT H 450 kV system reflection target. System located in the UK.

[c] Nikon XT H 450 kV system reflection target. System located in Germany.

Table E.2 — XCT parameter for the 450 kV system at GE-UK on the final star design

XCT parameter	GE [a] HX Value [c]	GE [a] MS Value [c]	GE [b] HX Value [c]
Voltage (kV)	450	450	450
Current (µA)	1 500	1 500	1 100
Power (W)	675	675	495
Target	W	W	W
Filter (material/mm)	Sn/2,5	Sn/2,5	Sn/1,1, Brass/1,0
Exposure time (ms)	150	150	334

[a] Dyn|41 200 um

[b] Dyn|41| 100 um

Table E.2 *(continued)*

XCT parameter	GE [a] HX Value [c]	GE [a] MS Value [c]	GE [b] HX Value [c]
Voltage (kV)	450	450	450
Image per projection	10	10	10
Number of projection	1 200	1 200	2 250
Source-to-object distance (mm)	500	500	750
Source-to-detector distance (mm)	1 143	1 143	1 147
Magnification	2,29	2,29	1,53
Detector pixel (µm)	200	200	100
Voxel size (µm)	87,5	87,5	65,4
Focal spot size (µm)	400	400	400
[a] Dyn|41 200 um			
[b] Dyn|41| 100 um			

E.2 Scan set ups

E.2.1 MTC

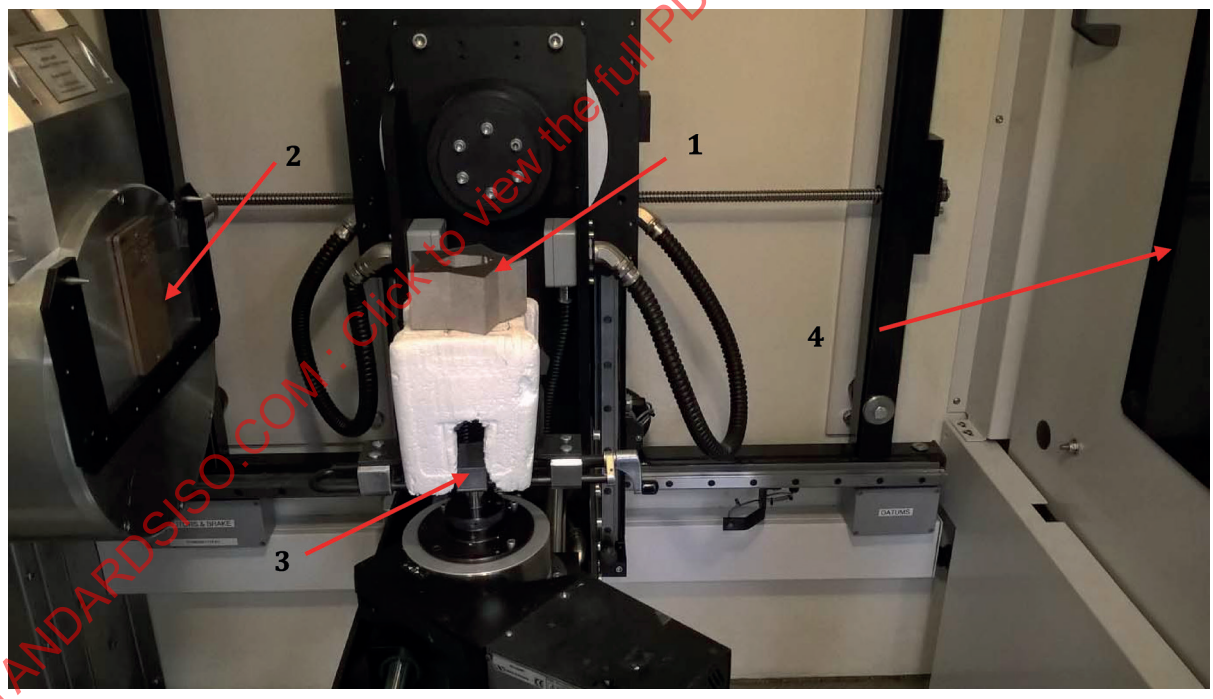

Key

1 star artefact
2 X-ray source
3 sample rotational table synchronised with the camera for 360° in the desired n° of steps
4 200 µm detector

Figure E.1 — XCT set up used for trials at the MTC

E.2.2 GE-UK

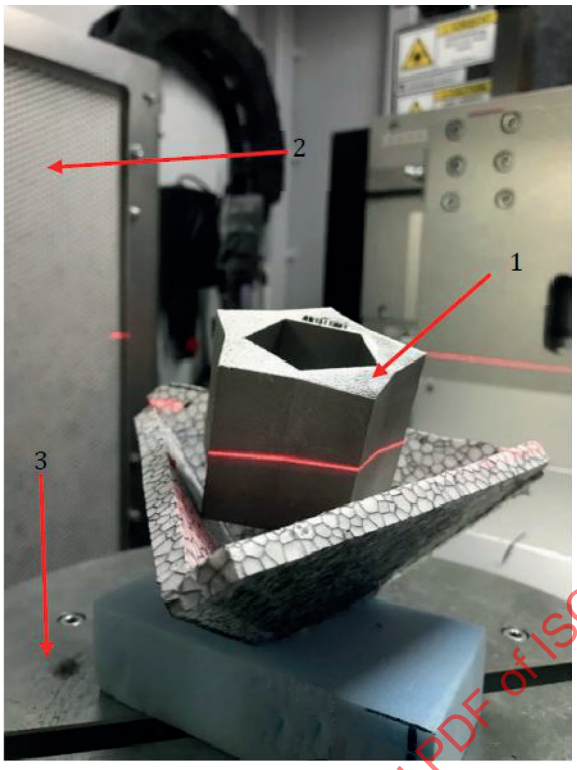

Key

1 star artefact

2 Dyn|41 200 um or 100 um detector behind scatter|correct grid

3 sample rotational table synchronised with the camera for 360° in the desired n° of steps

Figure E.2 — XCT set up used for trials at GE-UK

E.3 Scan results

E.3.1 MTC

Table E.3 — XCT assessment of the Hastelloy®[27] star artefact version S1

Design[a]	Region	Defect region	Defect value	HX-S1-001	HX-S1-002	HX-S1-003	HX-S1-004	HX-S1-005	HX-S1-006
S0	All	All	All	Not detected	Not detected	Not detected	Not detected	Not detected	Not detected
[a] The CAD file of the star artefact correspond to the new design version S0, S1 and S2 supplied by MTC.									

27) Hastelloy is an example of a suitable product available commercially. This information is given for the convenience of users of this document and does not constitute an endorsement by ISO of this product.

Table E.3 *(continued)*

Design[a]	Region	Defect region	Defect value	HX-S1-001	HX-S1-002	HX-S1-003	HX-S1-004	HX-S1-005	HX-S1-006
S1	1	Cylinders, length 2 mm, equal diameter = 0,30 mm, vary angle orientation	45°1st	Detected	Detected	Inconclusive	Detected	Detected	Detected
			45° 2nd	Detected	Detected	Detected	Inconclusive	Detected	Detected
			45° 3rd	Detected	Detected	Detected	Inconclusive	Detected	Detected
			45° 4th	Detected	Detected	Detected	Inconclusive	Detected	Detected
			horizontal (radial)	Detected	Detected	Detected	Detected	Detected	Detected
			horizontal (tangential)	Detected	Detected	Detected	Detected	Detected	Not detected
			vertical	Detected	Not detected	Detected	Detected	Detected	Detected
	2	Vertical cylinders, length 5 mm, vary ⌀	0,7	Detected	Detected	Detected	Detected	Detected	Detected
			0,6	Detected	Detected	Detected	Detected	Detected	Inconclusive
			0,5	Detected	Detected	Detected	Detected	Detected	Inconclusive
			0,4	Detected	Detected	Detected	Detected	Detected	Inconclusive
			0,3	Detected	Detected	Detected	Detected	Detected	Inconclusive
			0,2	Detected	Detected	Detected	Not detected	Detected	Not detected
			0,1	Detected	Detected	Not detected	Not detected	Detected	Not detected
	3	Spheres with trapped powder. Vary ⌀.	0,7	Detected	Detected	Detected	Detected	Detected	Detected
			0,6	Detected	Detected	Detected	Inconclusive	Detected	Detected
			0,5	Detected	Detected	Detected	Inconclusive	Detected	Inconclusive
			0,4	Detected	Detected	Inconclusive	Not detected	Inconclusive	Inconclusive
			0,3	Not detected	Not detected	Not detected	Not detected	Not detected	Inconclusive
			0,2	Not detected	Not detected	Not detected	Not detected	Not detected	Not detected
			0,1	Not detected	Not detected	Not detected	Not detected	Not detected	Not detected

[a] The CAD file of the star artefact correspond to the new design version S0, S1 and S2 supplied by MTC.

Table E.3 *(continued)*

Design[a]	Region	Defect region	Defect value	HX-S1-001	HX-S1-002	HX-S1-003	HX-S1-004	HX-S1-005	HX-S1-006
	4	Horizontal cylinders, from outside, length 3 mm, vary ⌀	0,7	Detected	Detected	Detected	Detected	Detected	Detected
			0,6	Detected	Detected	Detected	Detected	Detected	Detected
			0,5	Detected	Detected	Detected	Detected	Detected	Detected
			0,4	Detected	Detected	Detected	Detected	Detected	Detected
			0,3	Detected	Detected	Detected	Detected	Detected	Detected
			0,2	Not detected	Detected	Inconclusive	Inconclusive	Not detected	Not detected
			0,1	Not detected	Not detected	Not detected	Not detected	Not detected	Not detected
	5	Horizontal cylinders, length 2 mm, vary ⌀	0,7	Detected	Detected	Detected	Detected	Detected	Detected
			0,6	Detected	Detected	Detected	Detected	Detected	Detected
			0,5	Detected	Detected	Detected	Detected	Detected	Detected
			0,4	Detected	Detected	Detected	Detected	Detected	Detected
			0,3	Detected	Detected	Detected	Detected	Detected	Detected
			0,2	Not detected	Not detected	Not detected	Detected	Not detected	Not detected
			0,1	Not detected	Not detected	Not detected	Not detected	Not detected	Not detected

[a] The CAD file of the star artefact correspond to the new design version S0, S1 and S2 supplied by MTC.

Table E.4 — XCT assessment of the Hastelloy®[28] star artefact version S2

Design [a]	Region	Defect region	Defect value	HX-S2-001	HX-S2-002	HX-S2-003	HX-S2-004	HX-S2-005
S0	All	All	All	Not detected	Not detected	Not detected	Not detected	Not detected
	1	Horizontal cylinders, length 1,5 mm, vary ⌀	0,7	Detected	Detected	Detected	Detected	Detected
			0,6	Detected	Detected	Detected	Detected	Detected
			0,5	Detected	Detected	Detected	Detected	Detected
			0,4	Detected	Detected	Detected	Detected	Detected
			0,3	Detected	Detected	Detected	Detected	Detected
			0,2	Detected	Inconclusive	Not detected	Detected	Inconclusive
			0,1	Inconclusive	Not detected	Detected	Not detected	Not detected

[a] The CAD file of the star artefact correspond to the new design version S0, S1 and S2 supplied by MTC

28) Hastelloy is an example of a suitable product available commercially. This information is given for the convenience of users of this document and does not constitute an endorsement by ISO of this product.

Table E.4 *(continued)*

Design [a]	Region	Defect region	Defect value	HX-S2-001	HX-S2-002	HX-S2-003	HX-S2-004	HX-S2-005
S2	2	Horizontal cylinders, length 2,5 mm, vary ⌀	0,7	Detected	Detected	Detected	Detected	Detected
			0,6	Detected	Detected	Detected	Detected	Detected
			0,5	Detected	Detected	Detected	Detected	Detected
			0,4	Detected	Detected	Detected	Detected	Detected
			0,3	Detected	Detected	Detected	Detected	Detected
			0,2	Not detected	Not detected	Not detected	Not detected	Not detected
			0,1	Not detected	Not detected	Not detected	Not detected	Not detected
	3	Spheres with trapped powder. Vary ⌀.	0,7	Detected	Detected	Detected	Detected	Detected
			0,6	Detected	Detected	Detected	Detected	Detected
			0,5	Detected	Detected	Detected	Detected	Detected
			0,4	Detected	Detected	Detected	Detected	Detected
			0,3	Detected	Detected	Detected	Detected	Detected
			0,2	Inconclusive	Inconclusive	Inconclusive	Not detected	Detected
			0,1	Not detected	Not detected	Not detected	Not detected	Detected
	4	Vertical cylinders, length 5 mm, vary ⌀	0,7	Detected	Detected	Detected	Detected	Detected
			0,6	Detected	Detected	Detected	Detected	Detected
			0,5	Detected	Detected	Detected	Detected	Detected
			0,4	Detected	Detected	Detected	Detected	Detected
			0,3	Detected	Detected	Detected	Detected	Detected
			0,2	Inconclusive	Inconclusive	Inconclusive	Inconclusive	Inconclusive
			0,1	Inconclusive	Inconclusive	Inconclusive	Inconclusive	Not detected
	5	Cylinders, length 2 mm, equal diameter ⌀ = 0,30 mm, vary angle orientation	45° 1st	Detected	Detected	Detected	Detected	Detected
			45° 2nd	Detected	Detected	Detected	Detected	Detected
			45° 3rd	Detected	Detected	Detected	Detected	Detected
			45° 4th	Detected	Detected	Detected	Detected	Detected
			horizontal (radial)	Detected	Detected	Detected	Detected	Detected
			horizontal (tangential)	Detected	Inconclusive	Detected	Detected	Detected
			45° 1st	Not detected	Detected	Not detected	Not detected	Not detected

[a] The CAD file of the star artefact correspond to the new design version S0, S1 and S2 supplied by MTC

Table E.5 — XCT assessment of the Maranging steel star artefact version S1

Design [a]	Defect region	Defect value	MS-S1-001	MS-S1-002	MS-S1-003	MS-S1-004	MS-S1-005	MS-S1-006
S0	All	All	Not detected	Not detected	Not detected	Not detected	Not detected	Not detected

[a] The CAD file of the star artefact correspond to the new design version S0, S1 and S2 supplied by MTC.

Table E.5 *(continued)*

Design [a]	Defect region	Defect value	MS-S1-001	MS-S1-002	MS-S1-003	MS-S1-004	MS-S1-005	MS-S1-006
S1	Cylinders, length 2 mm, equal diameter ⌀ = 0,30 mm, vary angle orientation	45° 1st	Inconclusive	Detected	Detected	Detected	Detected	Inconclusive
		45° 2nd	Inconclusive	Inconclusive	Detected	Inconclusive	Inconclusive	Inconclusive
		45° 3rd	Inconclusive	Inconclusive	Detected	Detected	Detected	Inconclusive
		45° 4th	Detected	Detected	Detected	Inconclusive	Detected	Detected
		horizontal (radial)	Detected	Detected	Detected	Detected	Detected	Detected
		horizontal (tangential)	Detected	Detected	Detected	Detected	Detected	Detected
		vertical	Detected	Detected	Not detected	Detected	Inconclusive	Detected
	Vertical cylinders, length 5 mm, vary ⌀	0,7	Detected	Detected	Detected	Detected	Detected	Detected
		0,6	Detected	Detected	Detected	Detected	Detected	Detected
		0,5	Detected	Detected	Detected	Detected	Detected	Detected
		0,4	Detected	Detected	Detected	Detected	Detected	Detected
		0,3	Detected	Detected	Detected	Detected	Detected	Detected
		0,2	Detected	Inconclusive	Inconclusive	Inconclusive	Detected	Detected
		0,1	Detected	Not detected	Not detected	Not detected	Inconclusive	Inconclusive
	Spheres with trapped powder. Vary ⌀.	0,7	Inconclusive	Not detected	Detected	Inconclusive	Inconclusive	Inconclusive
		0,6	Detected	Not detected	Detected	Detected	Inconclusive	Inconclusive
		0,5	Not detected	Not detected	Detected	Inconclusive	Inconclusive	Inconclusive
		0,4	Not detected	Not detected	Not detected	Inconclusive		Inconclusive
		0,3	Not detected	Not detected	Not detected	Not detected	Not detected	Not detected
		0,2	Not detected	Not detected	Not detected	Not detected	Not detected	Not detected
		0,1	Not detected	Not detected	Not detected	Not detected	Not detected	Not detected
	Horizontal cylinders, from outside, length 3 mm, vary ⌀	0,7	Detected	Detected	Detected	Detected	Detected	Detected
		0,6	Detected	Detected	Detected	Detected	Detected	Detected
		0,5	Detected	Detected	Detected	Detected	Detected	Detected
		0,4	Detected	Detected	Detected	Detected	Detected	Detected
		0,3	Detected	Detected	Detected	Detected	Detected	Detected
		0,2	Detected	Detected	Detected	Detected	Detected	Detected
		0,1	Not detected	Not detected	Not detected	Not detected	Not detected	Not detected

[a] The CAD file of the star artefact correspond to the new design version S0, S1 and S2 supplied by MTC.

Table E.5 *(continued)*

Design [a]	Defect region	Defect value	MS-S1-001	MS-S1-002	MS-S1-003	MS-S1-004	MS-S1-005	MS-S1-006
	Horizontal cylinders, length 2 mm, vary ⌀	0,7	Detected	Detected	Detected	Detected	Detected	Detected
		0,6	Detected	Detected	Detected	Detected	Detected	Detected
		0,5	Detected	Detected	Detected	Detected	Detected	Detected
		0,4	Detected	Detected	Detected	Detected	Detected	Detected
		0,3	Detected	Detected	Detected	Detected	Detected	Detected
		0,2	Detected	Detected	Detected	Detected	Detected	Detected
		0,1	Not detected	Not detected	Not detected	Not detected	Not detected	Not detected

[a] The CAD file of the star artefact correspond to the new design version S0, S1 and S2 supplied by MTC.

Table E.6 — XCT assessment of the Maranging steel star artefact version S2

Design [a]	Region	Defect region	Defect value	MS-S2-001	MS-S2-002	M -S2-003	MS-S2-004	MS-S2-005
S0	All	All	All	Not detected	Not detected	Detected	Not detected	Not detected
S2	1	Horizontal cylinders, length 1,5 mm, vary ⌀	0,7	Detected	Detected	Detected	Detected	Detected
			0,6	Detected	Detected	Detected	Detected	Detected
			0,5	Detected	Detected	Detected	Detected	Detected
			0,4	Detected	Detected	Detected	Detected	Detected
			0,3	Detected	Detected	Detected	Detected	Detected
			0,2	Detected	Detected	Inconclusive	Detected	Detected
			0,1	Inconclusive	Detected	Detected	Inconclusive	Inconclusive
	2	Horizontal cylinders, length 2,5 mm, vary ⌀	0,7	Detected	Detected	Detected	Detected	Detected
			0,6	Detected	Detected	Detected	Detected	Detected
			0,5	Detected	Detected	Detected	Detected	Detected
			0,4	Detected	Detected	Detected	Detected	Detected
			0,3	Detected	Detected	Detected	Detected	Detected
			0,2	Detected	Detected	Inconclusive	Detected	Detected
			0,1	Not detected	Inconclusive	Detected	Not detected	Not detected
	3	Spheres with trapped powder. Vary ⌀.	0,7	Detected	Detected	Detected	Detected	Detected
			0,6	Detected	Detected	Detected	Detected	Detected
			0,5	Detected	Detected	Detected	Detected	Detected
			0,4	Detected	Detected	Not detected	Inconclusive	Detected
			0,3	Inconclusive	Inconclusive	Not detected	Not detected	Inconclusive
			0,2	Not detected	Not detected	Not detected	Not detected	Not detected
			0,1	Not detected	Not detected	Detected	Not detected	Not detected

[a] The CAD file of the star artefact correspond to the new design version S0, S1 and S2 supplied by MTC.

Table E.6 *(continued)*

Design [a]	Region	Defect region	Defect value	MS-S2-001	MS-S2-002	M -S2-003	MS-S2-004	MS-S2-005
	4	Vertical cylinders, length 5 mm, vary ⌀	0,7	Detected	Detected	Detected	Detected	Detected
			0,6	Detected	Detected	Detected	Detected	Detected
			0,5	Detected	Detected	Detected	Detected	Detected
			0,4	Detected	Detected	Detected	Detected	Detected
			0,3	Detected	Detected	Inconclusive	Detected	Detected
			0,2	Detected	Inconclusive	Inconclusive	Detected	Inconclusive
			0,1	Inconclusive	Inconclusive	Detected	Not detected	Not detected
	5	Cylinders, length 2 mm, equal diameter ⌀ = 0,3 mm, vary angle orientation	45° 1st	Detected	Detected	Detected	Detected	Detected
			45° 2nd	Detected	Detected	Detected	Detected	Detected
			45° 3rd	Detected	Detected	Detected	Detected	Detected
			45° 4th	Detected	Detected	Detected	Detected	Detected
			horizontal (radial)	Detected	Detected	Detected	Detected	Detected
			horizontal (tangential)	Inconclusive	Detected	Not detected	Not detected	Not detected
			45 deg 1st	Detected	Not detected	Detected	Not detected	Not detected

[a] The CAD file of the star artefact correspond to the new design version S0, S1 and S2 supplied by MTC.

E.3.2 EWI

Table E.7 — XCT assessment of the Stainless Steel star artefact version S1 and S2

Design [a]	Region	Defect region	Defect value	SS-S1-001
S0	All	All	All	Not tested
	1	Cylinders, length 2 mm, equal diameter ⌀ = 0,30 mm, vary angle orientation	45° 1st	Detected
			45° 2nd	Detected
			45° 3rd	Detected
			45° 4th	Detected
			horizontal (radial)	Detected
			horizontal (tangential)	Detected
			vertical	Detected

Design [a]	Region	Defect region	Defect value	SS-S2-001
S0	All	All	All	Not detected
	1	Horizontal cylinders, length 1,5 mm, vary ⌀	0,7	Detected
			0,6	Detected
			0,5	Detected
			0,4	Detected
			0,3	Detected
			0,2	Detected
			0,1	Inconclusive

[a] The CAD file of the star artefact correspond to the new design version S0, S1 and S2 supplied by MTC.